Title
ELECTRON MICROSCOPIC INVESTIGATIONS OF LUNG CELL RESPONSE TO PARTICULATE INSULT

Author
Finch, G.L.

Publication Date
1984-08-01

ELECTRON MICROSCOPIC INVESTIGATIONS OF LUNG CELL RESPONSE TO PARTICULATE INSULT

G.L. Finch
(Ph.D. Thesis)

August 1984

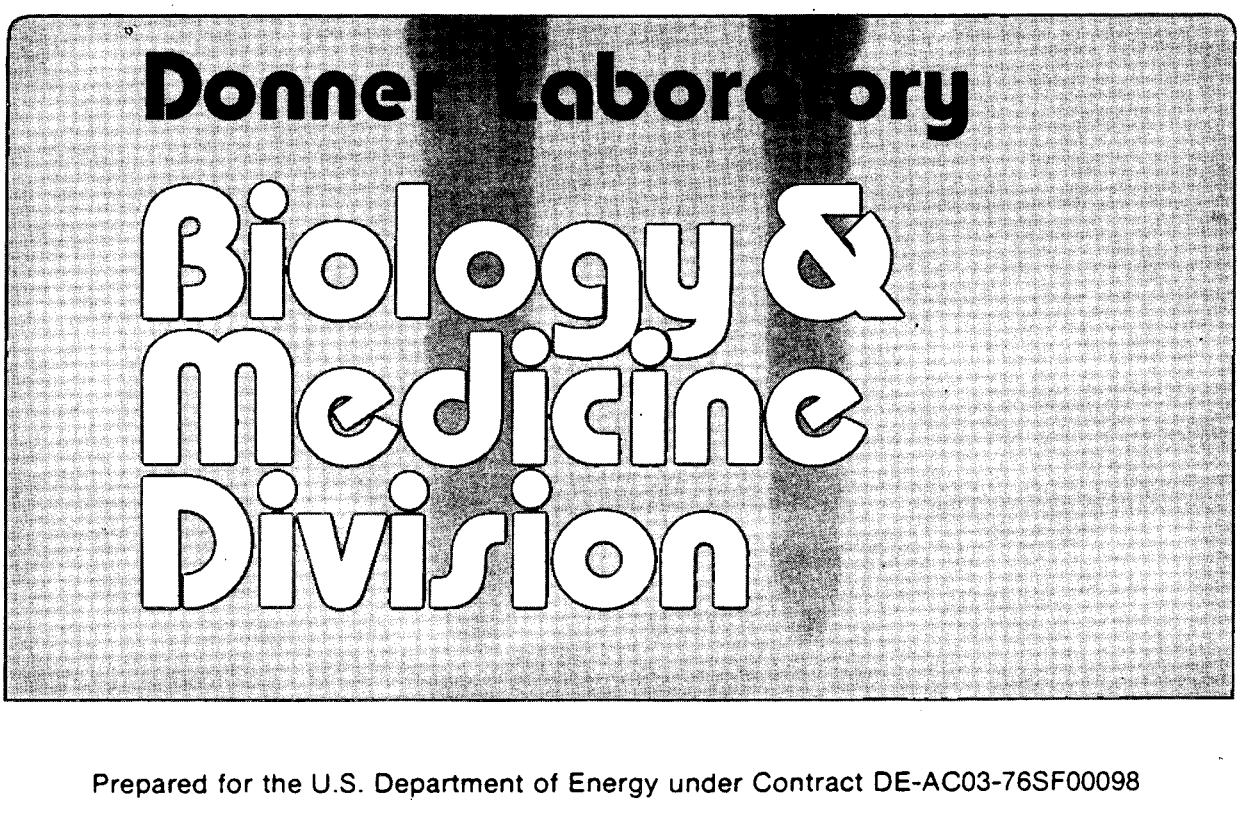

Prepared for the U.S. Department of Energy under Contract DE-AC03-76SF00098

DISCLAIMER

LBL-17218

ELECTRON MICROSCOPIC INVESTIGATIONS OF LUNG CELL RESPONSE TO PARTICULATE INSULT

Gregory Lee Finch

Ph.D. Thesis

Lawrence Berkeley Laboratory
University of California
Berkeley, California 94720

August 1984

TABLE OF CONTENTS

TABLE OF CONTENTS. iii

ABSTRACT vii

ACKNOWLEDGEMENTS ix

I. Introduction. 1

I.1. Pulmonary Deposition and Clearance. 1

I.2. Toxicologic Nature of Particulate Material. 5

I.3. Model Systems/Thesis Organization 9

II. In Vivo Responses to Instilled Particulate Material: Metabolism of $^{63}Ni_3S_2$. 11

II.1 Introduction. 12

II.2 Materials and Methods 14

II.2.A Exposure Techniques 14

II.2.B Tissue Collection and Analysis. 16

II.2.C Data Analysis 18

II.3 Results 19

II.3.A Clinical Symptoms. 19

II.3.B Free Lung Cell Response. 20

II.3.C Toxicokinetics of Instilled Particles. . . . 21

II.4 Discussion. 23

II.5 Tables and Figures. 31

III. Interactions Between Cultured Tracheal Explants and Nickel Subsulfide Particles. 45

III.1 Introduction 46

III.2 Materials and Methods. 53

III.2.A Culturing Techniques 53

III.2.B Microscopic Techniques 54

III.3 Results. 56

III.3.A Descriptive Morphology 56

III.3.B Quantitative Classification. 59

III.4 Discussion 63

III.5 Conclusions. 66

III.6 Tables and Figures 68

IV. In Vitro Analyses of Alveolar Macrophage Interactions with Respirable Particles. 84

IV.1 Introduction 85

IV.2 Materials and Methods. 90

IV.2.A Cell Collection 90

IV.2.B Particle Exposure 92

IV.2.C Viability Assay Techniques. 93

IV.2.D SEM Preparation 94

IV.2.E SEM Analysis. 95

IV.2.F Whole Cell Mount TEM. 98

IV.3 Results. 99

IV.3.A Qualitative Observations. 100

IV.3.B Quantitative Analyses 101

IV.3.C Whole Cell Mount TEM. 104

IV.3.D Methodological Considerations 106

IV.4 Discussion 107

IV.5 Tables and Figures 114

IV.6 Appendix: Statistical Methods 123

V. Morphological Studies of Frozen Hydrated Lung: Interactions Between Pulmonary Tissue and Respirable Particles 136

V.1 Introduction. 137

V.2 Materials and Methods 137

V.3 Results 140

V.3.A Lung Morphology: Frozen Hydrated and Freeze Dried 140

V.3.B Interactions Between Cells and Particles . . . 143

V.3.C Comments on Methodology. 144

V.4 Discussion. 145

V.4.A Frozen-Hydrated Lung Morphology. 145

V.4.B Particle Distribution. 147

V.4.C Frozen-Hydrated SEM Techniques 149

V.5 Figures 154

VI. Conclusions 162

VII. Bibliography. 168

VIII. Appendix: A Technique Permitting Correlative Microscopy (LM, SEM, TEM and HVEM) of Cultured Alveolar Macrophage Cells. A Short Technical Note 183

Gregory L. Finch
August, 1984
Ecology Group

ELECTRON MICROSCOPIC INVESTIGATIONS OF LUNG CELL RESPONSE TO PARTICULATE INSULT

ABSTRACT

The studies described herein provide quantitative morphological characterizations of the interactions between respirably-sized particles and lung tissues and cells. The differential effects of toxic versus nontoxic particulate materials administered at low doses and short time periods were examined. In vivo experiments on BALB/c mice investigated the pulmonary effects, clearance, and redistribution of intratracheally instilled Ni_3S_2 versus TiO_2. Nickel was cleared from the lungs more rapidly than Ti, resulting in a significantly lower lung burden after 3 and 7 days post-exposure. Nickel subsulfide instillation also resulted in an increase in lavageable polymorphonuclear leucocytes. The extent to which the intratracheal instillation route serves to model inhalation exposure was also evaluated.

Quantitative scanning electron microscopic (SEM) techniques were used to evaluate the effects of Ni_3S_2 on hamster tracheal explant sections maintained in tissue culture. A one hour exposure caused a rapid sloughing of differentiated columnar epithelial cells, followed by basal cell recolonization which led to the reappearance of essentially normal epithelium 7 days post-exposure. The clearance of particles from the lumenal surface was also described.

In vitro experiments were conducted on lavaged, cultured bovine alveolar macrophage cells (AM) exposed to Ni_3S_2, TiO_2, and glass beads (GB).

Correlative techniques were employed which permitted the examination of individual particle-exposed AM by vital dye staining light microscopy to determine viability, quantitative SEM to evaluate cell morphology and particle content, and whole cell mount transmission electron microscopy (TEM) to visualize AM internal ultrastructure. Many stages of AM cell disruption were described, including bleb formation and sloughing, cell rounding and the loss of normal surface architecture, degeneration of the external cell membrane, and complete cell degranulation. Quantitative examinations demonstrated that Ni_3S_2 and TiO_2, but not GB, particle content was correlated with AM alteration, and that Ni_3S_2 and TiO_2 internalization was correlated with cell death.

ACKNOWLEDGEMENTS

The research presented here was made possible by the assistance of many people. Dr. Jerry Fisher has provided guidance and support in all aspects of this work, and Dr. Tom Hayes has been helpful both with electron microscopy and in making his laboratory available to me. At Battelle Laboratory, Karen and Dan McNeill, Chuck Democko, Ming Chang, and Bruce Prentice were instrumental in various areas, including the toxicokinetic study, cell and organ culturing, and particle exposure. At the University of Vermont, Brooke Mossman and Lucy Jean kindly assisted with tracheal explant culturing and exposure. And at Donner Laboratory, Jacob Bastacky, Susan Klein, May McKoon, Jo Barr, Janet Lowe, Cliff Lai, and Greg Hook asissted with SEM and TEM observations, frozen-hydrated lung techniques, and cell culture techniques. Brian Knittel and Thomas Budinger kindly assisted in computerized data analysis. Diana Morris is to be thanked for her considerable word processing skills. My deepest thanks, however, go to Terry Finch, whose understanding and support helped me through arduous years of research, travel, and writing. This work was supported by the Director, Office of Energy Research, Office of Health and Environmental Research of the U.S. Department of Energy under Contract No. DE-AC03-76SF00098, the Electric Power Research Institute (RP-1639-2 and RP-1639-3), and the Battelle Columbus Memorial Laboratory.

I. INTRODUCTION

The lung is the primary target for inhaled pollutant-induced injury and a point of entry for exogenous material destined for transport to other organs. Pulmonary interactions with such materials can cause diseases such as fibrosis, emphysema, and cancer (Schlesinger, 1982). Although gaseous pollutants, such as SO_2, O_3, and NO_2, are generally agreed to cause lung damage, such materials are not considered here. The studies described herein are concerned with characterizing the pulmonary response to administered particulate material.

1. Pulmonary Deposition and Clearance

The effects of particulate matter on the pulmonary system are dependent on many factors, including the chemical and physical nature of inhaled material, the depth of penetration and fractional removal of specifically sized particles, sites of deposition and related physical clearance mechanisms, and translocation and excretion patterns of the inhaled particles (Stuart, 1973; Brain and Valberg, 1979). Models of particle deposition make approximations of the anatomical structure of the pulmonary system which is generally divided into three components; the nasopharynx or upper respiratory tract extending from the nose to the larnyx or epiglottis, the tracheobronchial compartment, consisting of the trachea and the bronchial tree distal to the terminal bronchioles, and the pulmonary or deep lung compartment, consisting of the respiratory bronchioles, alveolar ducts, and alveoli (Task Force on Lung Dynamics, 1966). Many factors influence aerosol deposition in

the lung, including the aerodynamic and physico-chemical properties of the aerosol, the activity state of an individual, and the anatomy of the respiratory tract. Major processes at work in particle deposition include (1) impaction, where inertial forces cause particles to cut across curving airstreams and impact on airway walls, (2) sedimentation, where gravitational forces acting on a particle cause it to settle out onto the lower surface of an airway, (3) diffusion, predominant with small particles, where Brownian motion causes a particle to move across airstreams to airway walls, and other mechanisms including interception, electrostatic charges, hygroscopicity, chemical reactivity, and gas-particle interactions (Stuart, 1973; Yeh et al., 1966; Brain and Valberg, 1979).

Once particles are deposited, clearance mechanisms begin removing particles from airway lumina. Older clearance models describe dust clearance in two ways depending on whether the dust is soluble or insoluble (Task Force on Lung Dynamics, 1966). Although solubility is very important, clearance is a highly variable process depending on both specific and nonspecific defense mechanisms, as well as sites of deposition, and thus simple clearance schemes cannot completely describe this phenomonon. Clearance models are discussed in many thorough reviews and briefly outlined here (Task Force on Lung Dynamics, 1966; Schlesinger, 1982; Casarett, 1972; Green et al., 1977; and Lauweryns and Baert, 1977). Models of pulmonary clearance include composites of cellular phagocytic activity, mucociliary transport, and the physico-chemical properties of the dust relating to dissolution

and translocation. Salient kinetic features include: (1) particles deposited on the ciliated epithelium will have clearance halftimes of minutes to hours due to mucociliary activity; (2) phagocyte ingestion and recruitment, in concert with mucociliary clearance, gives rise to a rapid clearance for nonciliated areas, with halftimes on the order of days, and (3) a slower, predominantly alveolar clearance phase dependent on many mechanisms, occurring through the lymphatic system, gastrointestinal system, and bloodstream, with or without cellular mediation.

Sites of particle deposition by inhalation appear to center at airpath branches (bifurcations), or at the interface between tidal and residual air, near transitions from terminal bronchioles and alveolar ducts (Lippmann et al., 1980). In vascular perfusion fixed mice and rats, Brody and Roe (1983) observed that for 5 different inhaled dusts significantly greater numbers of particles were deposited on alveolar duct bifurcations compared with adjacent surfaces, and also noted that few particles were seen in the alveoli. Holma (1969) and Sorokin and Brain (1975) observed similar deposition patterns, with the latter group reporting widespread, diffuse particles on alveolar lumina. Indirect evidence for increased deposition at the bronchiole/alveolar duct zone is provided by Plopper et al. (1983), who found that the focus on inhaled diesel exhaust induced lesions in cats was the region where alveolar ducts joined terminal conducting airways.

The multiple activities of alveolar macrophages (AM) are of great importance in pulmonary defense. This cell type has been extensively characterized in several reviews (Green et al., 1977; Hocking and Golde, 1979); AM are large, mononuclear phagocytes residing upon the alveolar epithelium, derived (at least in part) from circulating blood monocytes (Cline, 1975), with a wide variety of roles. Macrophages phagocytize particles for transport out of alveolar spaces, and are responsible for ingesting and destroying bacteria. Macrophages are involved in immune responses, and can interact with lymphocytes, polymorphonuclear neutrophils (PMN), other AM, and fibroblasts by secreting a variety of bioactive materials. Furthermore, elastolytic enzymes and oxygen radicals are secreted from AM and may play a role in the pathogenesis of emphysema (Cohen, 1979). Of interest in this work is the role of AM in response to administered particulate material. In vivo, AM function in the early phase of lung clearance by internalizing deposited particles then migrating towards the bronchial mucociliary escalator along airway surfaces and through alveolar pores of Kohn (Lauweryns and Baert, 1977; Sorokin and Brain, 1975; Ferin, 1982). This mechanism results in reduced numbers of extracellular particles in luminal spaces, which appear capable of reaching interstitial spaces (Lauweryns and Baert, 1977). Although AM may be recruited from the interstitium by poorly understood mechanisms, it appears that particle-laden AM are not capable of re-entering the interstitium by crossing the alveolar epithelium (Sorkin and Brain, 1975; and Lauweryns and Baert, 1977); however, this is disputed (Holt,

1980). Free particles which penetrate the epithelium can be phagocytized by interstitial macrophages which can in turn migrate to the lymphatic spaces (Lauweryns and Baert, 1977). Particle burdened AM have also been observed to migrate towards the pleura with resulting long-term particle accumulations (Holt, 1983; Green et al., 1977).

Cultured AM have been widely employed in studies of the cytotoxicity of various agents (Brody and Davis, 1982). The manner in which AM respond to various types of particulate matter may have a strong bearing on the resulting intact lung response, and are thus examined in Chapter IV of these studies.

2. Toxicologic Nature of Particulate Material

The toxicity of exogenous particulate material is dependent on many factors including intrinsic toxicity of constituent compounds, solubility, and crystalline form (Waters et al., 1975). The experiments contained in this work involve exposure of lung tissue and AM cells to nickel subsulfide (Ni_3S_2), titanium dioxide (TiO_2), and glass beads (GB). Although not widely dispersed throughout the environment (World Health Org., 1973), Ni_3S_2 apparently is the most potent known metallic carcinogen (Sunderman, 1977; 1981). Nickel subsulfide has been implicated in nickel-induced nasal cancers in workers (Sunderman, 1973) and in a variety of tumors in laboratory animals including muscle tumors (Sunderman et al., 1976, and Oskarsson et al., 1979), testicular sarcomas (Damjanov et al., 1978), ocular neoplasms (Albert et al., 1982), renal sarcomas (Sunderman et al., 1979), and tumors of the respiratory tract (Ottolenghi et al., 1974;

and Yarita and Nettesheim, 1978). Ottolenghi et al. (1974) exposed rats to Ni_3S_2 by inhalation and observed increased pulmonary tumors. Exposed animals had significantly lower body weights and lungs exhibited inflammatory reactions and occasionally appeared spotty and abscessed. Squamous metaplastic changes in bronchial epithelium occurred singly and at multiple foci. Similarly, Yarita and Nettesheim (1978) examined the progression of nickel subsulfide-induced carcinomas of respiratory tact epithelium using tracheal implants. Ni_3S_2 was toxic to differentiated mucociliary epithelium, causing focal necrosis and hyperplasia of undifferentiated cells as well as squamous metaplasia. Particles were evident within the connective tissue compartment within two weeks, and cellular infiltration to the submucosa increased over time. Tumors of both epithelial and submucosal cells resulted. The lethality of Ni_3S_2 administered by single and multiple intratracheal incubations to mice was described by Fisher et al. (1982). A single exposure of respirable-sized particles was more toxic than coarse particles, although enhanced toxicity of multiple intubations of coarse particles was observed.

The effects of Ni_3S_2 have also been investigated in vitro, and include morphological transformations as well as lethality in cultured hamster embryo cells (DiPaolo and Casto, 1979; Costa et al., 1979). Cells thus transformed were capable of producing malignant tumors following injection into nude mice (Costa et al., 1979). Finch et al. (1982) and Fisher et al. (1982) described the morphology of bovine AM exposed to Ni_3S_2 particles in vitro. The particles appeared to be

extremely cytotoxic to AM in that cells with particles suffered a loss of membrane integrity leading to complete cell lysis.

Interestingly, the physical form of administered nickel sulfides (Ni_3S_2, NiS) appears to play an important role in cellular uptake and resultant effect. Costa has described the increased phagocytosis and cell transforming activity of crystalline αNi_3S_2 and αNiS when compared with amorphous NiS (Costa and Molenhauer, 1980a, 1980b; Costa et al., 1981a, 1981b).

Titanium dioxide has been widely considered to represent an inert, insoluble, non-fibrogenic nuisance dust (World Health Org., 1982). The in vitro and in vivo solubility of TiO_2 is extremely low (Ferin, 1976), and excluding the gastrointestinal tract, essentially no TiO_2 has found in various tissues (heart, blood, liver, kidney and spleen) of the rat following inhalation exposure (Ferin, 1971b, 1976). Following instillation of quartz and TiO_2 to rats, Sykes et al. (1982) characterized TiO_2 as non-fibrogenic in that both extracellular levels of lactate dehydrogenase (a marker for cell damage) and numbers of infiltrating polymorphonuclear neutrophils (PMN) returned to control levels, whereas with quartz, these indicators remained high, thus constituting an inflammatory response. Dale (1973) instilled large doses of dusts into rabbit lungs and found TiO_2 was inert compared with quartz in that early pathological changes in all treated animals were reversed over time in TiO_2-treated animals. Rylander et al. (1979) exposed guinea pigs to aerosols of TiO_2, SiO_2, and MnO_2 and found that TiO_2 alone failed to induce an

inflammatory response and was characterized by normal numbers of macrophages and PMN. Rats were exposed to TiO_2 by intubation with similar results (Wozniak et al., 1976); no evidence of fibrosis was observed after 3 months. Also, Christie et al. (1963) observed no weight change or pulmonary pathological responses compared with controls following long-term inhalation exposure to low concentrations of TiO_2. Hunt et al. (1981) investigated the hemolytic potential and effect on alveolar macrophage viability of various materials in vitro. Titanium dioxide had the lowest bioreactivity in either test system when compared with chrysotile asbestos or a variety of calcium silicates. Zitting and Skytta (1979), however, did observe in vitro TiO_2 hemolytic behavior dependent on crystalline form; in vivo, TiO_2 failed to increase proline hydroxylase levels in rats. In TiO_2-intubated hamsters, Stenback et al. (1976) observed focal sites of inflammation, although doses used (15 instillations, 3 mg TiO_2 each) were much higher than in this study. Titanium dioxide was relatively inert compared with silica, fly ash, or silicic acid in assays evaluating rabbit AM viability and ATP levels, and colony survival in Chinese Hamster Ovary cell cultures (Garrett et al., 1981). Although TiO_2 may not be completely inert when administered to biological systems, it is clear from this brief review that TiO_2 exerts fewer and less severe alterations to normal cell or tissue function when compared to many compounds, particularly Ni_3S_2.

Therfore, in these experiments TiO_2 is used as a negative control particle against which reactions to administered Ni_3S_2 can be judged.

3. Model Systems/Thesis Organization

The following chapters describe studies undertaken to elucidate various mechanisms at work in lung/particle interactions. The unifying feature of this research is that low doses of toxic versus non-toxic materials were administered in single exposures. The responses of intact animals, organs, or cells were then characterized at various times post-exposure. Chapter II involves the in vivo exposure of whole lung to radiolabelled $^{63}Ni_3S_2$ and TiO_2 using the method of intratracheal instillation in the BALB/C mouse. At various times post-exposure several parameters describing organism response were examined. Pulmonary lavage effluents were examined for alveolar macrophage (AM) and polymorphonuclear leucocyte (PMN) number, viability, and particle uptake. Toxicokinetic data were obtained for lung, kidney, gastrointestinal tract, and blood compartments following tissue digestion and isotope level determinations using liquid scintillation counting techniques. Clinical effects, the nature of the inflammatory response and the redistribution and elimination of radiolabelled Ni were characterized in the intact mouse, and the more rapid clearance of Ni_3S_2 versus TiO_2 from lungs was described.

Chapter III involves a technique with both in vivo and in vitro characteristics. Hamster trachea were excised, sectioned, cultured, then exposed to Ni_3S_2 in vitro. The morphological responses at

various timepoints were assessed using scanning electron microscopy (SEM). An early sloughing of the normal columnar epithelium was followed by colonization of the luminal surface with presumptive basal cells at first, followed by the regeneration of apparently normal epithlium by seven days.

Chapter IV examines the in vitro interactions between AM cells and particles (Ni_3S_2, TiO_2, and glass beads) using light microscopy and both scanning and transmission electron microscopy. A morphological classification system was employed to rigorously describe AM lavaged from Ni_3S_2-intubated mice. Also, a culturing technique was developed permitting individual cell viability determination coupled with subsequent SEM,, TEM, and x-ray microanalysis on the same AM populations. Various aspects of cell/particle interactions and AM response were characterized.

The distribution of Fe_2O_3 particles administered by instillation is examined in Chapter V. Inflated frozen hydrated mouse lungs were examined using low temperature SEM techniques. Various aspects of pulmonary architecture were identified and correlated with lung morphology as revealed by conventional SEM techniques, and particles were located both intra- and extracellularly. Techniques employed omitted many of the steps employed in conventional EM preparations and decreased the chances of particle translocation and/or washout.

CHAPTER II

IN VIVO PULMONARY RESPONSES TO INSTILLED PARTICULATE MATERIAL: METABOLISM OF $^{63}Ni_3S_2$

II.1 INTRODUCTION

This study examines the pulmonary effects and clearance of a toxic, carcinogenic particulate, nickel subsulfide (Ni_3S_2), versus a more inert material, titanium dioxide (TiO_2). Nickel subsulfide exposure results in respiratory tumors in experimental animals (Ottolenghi et al., 1974; and Yarita and Nettesheim, 1978) and has been implicated in nickel-induced nasal tumors in refinery workers (Sunderman, 1973). Fisher et al. (1982) found that a respirably-sized fraction of Ni_3S_2 administered by intratracheal instillation was toxic to mice, with a median lethal dose of 4 mg/kg; furthermore, Ni_3S_2 was cytotoxic to alveolar macrophages (AM) in vitro. Titanium dioxide is widely thought to be relatively inert (World Health Organization, 1982), and is used in these experiments as an inert nuisance dust with low pulmonary solubility (Ferin, 1976).

Intratracheal instillation techniques, described by Ho and Furst (1973) and Fisher et al. (1982), were employed to deliver low doses of respirably-sized particles into mouse lungs in this study. Particle instillation is widely used in toxicologic studies for various reasons including ease of exposure, low cost (compared to inhalation), and the ability to administer doses in short periods of time (Brain et al., 1976). The extent to which instillation accurately models inhalation exposure has been questioned. Criticisms include differences in deposition, possible mechanical damage to the trachea by the intubation tube, and potential alterations to the pulmonary fluid balance (Watson et al, 1969). Nonuniformity of particle deposition has been observed

by many researchers using instillation; Brain et al. (1976) and Kennedy and Little (1974) found that the dose was concentrated in basal versus apical portions of lung lobes, with heavy focal deposits, and suggested that the distribution of particles may be determined in part by the redistribution of the carrier fluid. Watson et al. (1969) similarly observed that lead chromate particles penetrated "deeper" into the lung, but noted that clearance kinetics were similar from 7 to 20 hours post-exposure for instillation when compared with the inhalation exposure route. Similar findings were reported by other researchers. Ferin and Feldstein (1978) instilled rats with a wide range of TiO_2 doses (ca 0.3-300 mg/kg) and examined pulmonary clearance between 1 and 25 days post-exposure. For low doses, clearance rates were similar for the instillation versus inhalation techniques; however, clearance prior to the first day post-exposure was not considered. It appears that the use of low particulate doses is essential to avoid overloading clearance processes; LaBelle and Brieger (1961) concluded that doses greater than about 5 mg/kg to rats were necessary to alter or block lung clearance mechanisms.

The experiments described herein examine early pulmonary clearance and biological effects of low doses (0.5 mg/kg) of instilled Ni_3S_2 versus TiO_2. A rapid clearance phase is widely attributed to mucociliary action coupled with phagocyte ingestion and emigration through the airways (Green et al., 1976). Subsequent clearance routes may strongly depend on particle solubility, in that soluble compounds may be translocated throughout the organism (Task Force and Lung

Dynamics, 1966). Also, differential expressions of toxic effects may be mediated (at least in part) through the alveolar macrophage (Brody and Davis, 1982). In addition to deleterious effects of particles on AM cells, as described in Chapter IV of this work, AM are important in immune and inflammatory processes in the lung (Hunninghake et al., 1979). Inflammatory responses are characterized by an influx of polymorphonuclear leukocytes (PMN) into the lung, usually peaking after a few days, and are a common result of exposure to cytotoxic particles such as quartz (Sykes et al., 1982; Moores et al., 1980) and asbestos (Dodson et al., 1983).

II.2 MATERIALS AND METHODS

II.2.A Exposure Techniques

Strain BALB/C BYJ male mice were obtained at 7 and 8 weeks of age (Jackson Laboratories, Bar Harbor, ME) and immunized against Sendai virus by intraperitoneal injection of killed virus (Sendai Vaccine, M.A. Bioproducts, Walkersville, MD). Animals were multiply housed in polycarbonate cages, with water and Purina rodent chow provided ad libitum, for a two week quarrantine period, then weight randomized (mean of 25.7 to 27.7 gm per group) into groups of three.

Animals were exposed to test particles using an intratracheal instillation technique described by Ho and Furst (1973). Sterile Ca^{++}- and Mg^{++}- free phosphate buffered saline (PBS, Grand Island Biological Co., GIBCO, Grand Island, NY) was used to suspend and deliver TiO_2, Ni_3S_2, and $^{63}Ni_3S_2$ as described below. TiO_2 (Alfa Products, Danvers, MA) was ground and settled to yield a VMD = 1.57 μm

and σ_g = 2.3; Ni_3S_2 (INCO Co., Mississanga, Ontario) was separated into a fine fraction, VMD = 1.83 μm, σ_g = 2.3; and $^{63}Ni_3S_2$ (synthesized by New England Nuclear Co., Boston, MA) was provided at a VMD = 1.65 μm, σ_g = 1.83, with a specific activity of 0.254 mCi/mg. Appropriate size fractions were obtained by settling in an Andreason pipet as described by Fisher et al. (1982). Particulate doses used were 11.8 μg per mouse delivered in 20 μl PBS (equivalent to a $^{63}Ni_3S_2$ dose of 3 μCi per mouse). Particles were weighed using a Sartorius microbalance (Westbury, NY) in a negative pressure glove box; each dosing suspension was prepared within two hours of use then sonicated for 10 minutes. A Gilson pipetman (P-200D, West Coast Scientific, Oakland, CA) was calibrated by delivering 20 μl boluses of PBS to tared glass fiber filters. Control animals received 20 μl of PBS.

For dose administration, animals were anesthesized using Metofane (Methoxyflurane, Pitman-Moore, Inc., Washington Crossing, NJ) until the onset of slow, deep breathing, then held upright with fiberoptics illuminating the buccal cavity. Particle suspensions were vortexed, then the dose withdrawn using the micropipet with a 1 inch sterile 23 ga. blunt needle (Monoject, Sherwood Medical, St. Louis, MO) slightly bent to deliver the dose at the first bifurcation distal to the vocal cords. Animals were held upright for ca. 30 seconds until coughing ceased then placed in a recovery cage for several minutes. Recovery was complete within 5 minutes and animals displayed no immediately evident ill effects.

II.2.B Sample Collection and Analysis

Animal sacrifices were performed at 15 minute, 1, 5, and 20 hour, and 3 and 7 day periods post-exposure. Bronchopulmonary lavage was performed on three animals from each group (PBS, TiO_2, and Ni_3S_2) at each time period. Following cervical dislocation, the trachea was cannulated with a 23 ga. blunt needle (Monoject), sutured in place, then the lungs washed with ice-cold PBS (GIBCO) by introducing 1 ml PBS, waiting 1 minute, then withdrawing the lavage effluent into a 3 cc tuberculin syringe (Becton-Dickinson Co., Rutherford, NJ). Lavage was continued until 5 ml of lavage fluid was obtained; fluids were held on ice in 15 ml centrifuge tubes until a cell pellet was obtained by centrifugation (300 x g, IEC Centra-7, International Equipment Co., Needham Hts., MA). The pellet thus obtained was resuspended in 0.5 ml Eagle's minimal essential medium (GIBCO), mixed, then seeded into a hemacytometer (American Optical, Buffalo, NY) for lavage cell count. Viability was determined by nuclear exclusion of 0.4 percent trypan blue dye (GIBCO), and a differential count was performed after staining with Wright's stain (Sigma Chemicals, St. Louis, MO) following techniques described by Fisher et al. (1978). The remainder of the cell suspension was fixed with 2.3 percent glutaraldehyde for scanning electron microscopy (SEM).

Tissue samples were obtained from TiO_2 and $^{63}Ni_3S_2$ exposed animals (3 per group) at each time point. For TiO_2, animals were killed by cervical dislocation, weighed, then lungs and trachea (distal to the larynx) excised. The heart, excess musculature, and

connective tissue was trimmed off, the lungs were blotted dry, weighed, and frozen in acid-washed porcelin crucibles. For analysis, lungs were ashed, fused with 0.25 gm potassium pyrosulfate, dissolved in concentrated nitric acid (all reagents spectroscopically pure), then Ti was determined using inductively-coupled argon plasma (ICAP) spectroscopy with identically treated standards.

For $^{63}Ni_3S_2$ tissues, animals were anesthesized using Metofane, weighed, then blood was obtained by cardiac puncture with heparinized 25 ga. needles (Monoject) in 1 ml tuberculin syringes (Becton-Dickinson). Animals were opened and the following tissues were excised, blotted dry, and weighed: lungs and trachea (distal to larynx), gastrointestinal tract (GI) including esophagus, stomach, and intestines, and the kidneys. Tissues were frozen in individual scintillation vials until dissolution was initiated by complete mincing then removal of duplicate aliquots for dissolution using 0.2 ml $HClO_4$, 0.4 ml H_2O_2, and 0.1 ml HNO_3 in an 80°C water bath for at least 4 hours (modification to technique described by Valentine and Fisher, 1983; Smith and Hackley, 1968). After cooling to room temperature, 10 ml of scintillation cocktail was added, consisting of 4 g Omnifluor (New England Nuclear), 500 ml toluene, and 500 ml 2-ethoxyethanol to make 1 liter of scintillant. Samples were counted in a Searle Mk. III liquid scintillation counter after a few hours of dark adaptation. Counting standards were prepared in triplicate and consisted of 100 percent, 10 percent and 1 percent of the original instillation

dose spiked into either empty vials or untreated lungs and treated identically to the tissues as described above.

II.2.C Data Analysis. To assess possible differences between sample means, the Welch approximation (for unknown, unequal variances) to the Student's t-test was used (Remington and Schork, 1970).

Hypothesis: no significant difference; $\bar{X}_1 - \bar{X}_2 = 0$.

Test static:
$$t = \frac{\bar{X}_1 - \bar{X}_2}{\sqrt{\frac{S_1^2}{n_1} + \frac{S_2^2}{n_2}}}$$

with

$$df = \frac{\left(\frac{S_1^2}{n_1} + \frac{S_2^2}{n_2}\right)^2}{\frac{\left(\frac{S_1^2}{n_1}\right)^2}{n_1+1} + \frac{\left(\frac{S_2^2}{n_2}\right)^2}{n_2+1}} - 2 \text{ degrees of freedom}$$

Critical test statistic $t_c = t_{0.95;df}$ for one-sided 95 percent confidence level.

Radiotracer data were analyzed using a two compartment model. Mean values and standard deviations from each timepoint were computer fitted using a biexponential fitting program (OFIT program, PDP 11 Computer, kindly provided by B. Knittel and T. Budinger, Donner Laboratory) of the form $y = A_1 \exp(-k_1 t) + A_2 \exp(-k_2 t)$. TiO_2 and $^{63}Ni_3S_2$ lung burdens are expressed as the percentage of dose administered. Kidney and gastrointestinal tract data are presented as counts per minute (CPM)/gm wet tissue, and blood levels as CPM/ml blood.

II.3 RESULTS

II.3.A Clinical Symptoms

The instilled dose was well-tolerated by the animals at early timepoints. In all cases, mice were awake and exhibited no apparent ill effects within 5 minutes of dose administration. PBS and TiO_2-instilled mice appeared normal throughout the course of the study. Ni_3S_2-instilled animals appeared lethargic and had rough haircoats approximately 2 or 3 days after dose administration, with an improved appearance over the next few days.

Pulmonary hemorraging resulted from Ni_3S_2 administration and was most evident at 3 days post-exposure. The lavage effluent appeared reddish and numerous erythrocytes were present in the cell pellet. Furthermore, blood was evident in lungs excised from Ni_3S_2-instilled animals at 3 days post-exposure, but not at earlier timeperiods. When present, blood infiltration was most pronounced apically in the immediate vicinity where lobar bronchi entered lung lobes. No bleeding in the lungs of PBS or TiO_2-instilled animals was observed.

The poor appearance of Ni_3S_2-instilled mice 2 to 3 days post-exposure corresponded to a decrease of body weight (Table II.1, Figure II.1). When compared with weight at the time of instillation, Ni_3S_2-exposed mice lost weight at both 3 days (-1.48 ± 1.72 gm) and 7 days (-1.00 ± 1.94 gm), but not 20 hours (0.51 ± 0.64 gm). In contrast, TiO_2 and PBS-exposed animals exhibited nearly identical weight gains, which at 3 and 7 days were significantly greater ($p < 0.01$) when compared with Ni_3S_2 treated mice.

The organ weights of particle-instilled mice are presented in Table II.2. Lung weights were obtained for $^{63}Ni_3S_2$, TiO_2, PBS-exposed, and untreated controls; GI tract and kidney weights were obtained only for $^{63}Ni_3S_2$-dosed animals. For each dosage group, lung weights appear elevated above untreated animals at 15 minute and 1 hour periods, returning to untreated levels after 5 hours, possibly reflecting the distribution of the instillation fluid. However, this difference is not statistically significant ($p > 0.05$). $^{63}Ni_3S_2$-exposed lungs show a slight increase at 3 days (again not significant), possibly corresponding to an influx of edema fluids or inflammatory cells. Kidney weights were variable and displayed no clear trends; weights were highest at the beginning (15 min) and end (3 and 7 days) of the study. Gastrointestinal tract weights were approximately constant throughout the study except for the 20 hour and 3 day time-points, which were slightly depressed (not significantly, $p > 0.05$). Since stomach and intestinal contents were included in the G.I. tract, this decrease may reflect a decreased food consumption by sick animals.

II.3.B Free Lung Cell Response

The recovery of lavageable cells from intubated mice is presented in Table II.3 and Figure II.2. At early timepoints the total cell yield is comparable with untreated controls for all three dosage groups (PBS, TiO_2, and Ni_3S_2). After 5 to 20 hours, an increase in free cells is evident, with all three treatment groups yielding significantly more ($p < 0.05$) cells than untreated mice 7 days

post-exposure. Differential effects of Ni_3S_2 versus TiO_2 are evident when compared with PBS-instilled mice; whereas cell yield is similar for TiO_2 versus PBS treatment throughout the study, Ni_3S_2-instilled mice yield significantly more ($p < 0.05$) cells at 3 and 7 days post-exposure compared with PBS. The viability of lavaged cells, as determined by light microscopic evaluation of nuclear trypan blue dye exclusion, is presented in Table II.4. In all cases, cell viabilities are greater than 93 percent, and there are no significant differences between groups instilled with Ni_3S_2, TiO_2 or PBS, or untreated controls.

Light microscopic analyses of Wrights-stained lavaged-cell smears revealed that AM were the predominant cell type obtained in all groups, occurring with a 96 percent or greater incidence, except for Ni_3S_2-instilled animals (see Table II.5 and Figure II.3). Lymphocytes and other cell types (primarily epithelial cells) were observed infrequently (3 percent or less) and exhibited no apparent trends. The percentage of PMN, however, was significantly increased in certain Ni_3S_2-dosed groups as shown graphically in Figure II.3. The influx of PMN appeared greatest at 20 hours and 3 days post-exposure, with decreased although still elevated levels 7 days post-exposure.

II.3.C Toxicokinetics of Instilled Particles

In particle-exposed mouse lungs, a rapid early phase of clearance was followed by a more gradual phase (see Table II.6 and Figures II.4 and II.5). Upon instillation, bubbles often formed at the larynx then

rose up into the buccal cavity. Such bubbles surely carried particles out of the respiratory tract; 15 minutes after instillation, TiO_2 and $^{63}Ni_3S_2$-instilled mice retained only 66 and 75 percent of the administered dose, respectively. A biexponential curve fitting program was applied to the data at 15 minutes and later; calculated clearance halflives were 0.5 and 462 hours for Ti, and 2.0 and 119 hours for ^{63}Ni. The longer-term clearance rate constants were significantly different ($p < 0.05$) for ^{63}Ni versus Ti. At 3 and 7 days post-exposure, significantly less ^{63}Ni was present in the lungs compared with Ti ($p < 0.05$).

Appropriate standards were prepared and analyzed for both $^{63}Ni_3S_2$ and TiO_2-exposed lungs. For $^{63}Ni_3S_2$, triplicate dosage samples were added to either empty vials or vials containing unexposed lungs. After digestion, aliquots were taken and there were no differences in activity between the two groups (spiked lungs had $X \pm SD$ of $1.94 \pm 0.164 \times 10^6$ CPM, empty vials had $1.91 \pm 0.189 \times 10^6$ CPM), therefore the groups were pooled, thus constituting the 100 percent dosage activity . Ten and one percent dilutions were made in triplicate from the 100 percent dosage standards; measured activity was $1.68 \pm 0.23 \times 10^5$ and $1.70 \pm 0.05 \times 10^4$ CPM for the 10 and 1 percent dosage standards, respectively, verifying that counting efficiency was essentially linear throughout the measured range. For TiO_2, triplicate dosages were spiked to excised mouse lungs; furthermore, PBS-exposed lungs were analyzed for Ti content. Interestingly,

background Ti levels were observed in PBS-intubated mice (2.90 ± 0.37 μg Ti for PBS-dosed mice, n=5). This Ti burden was subtracted from all TiO_2-exposed animals, and standard deviations were added in quadrature. The 100 percent TiO_2 dose was observed to be 11.1 ± 1.78 μg TiO_2 per mouse, slightly less than the calculated dose of 11.8 μg/mouse.

Gastrointestinal tract and kidney ^{63}Ni burdens are shown in Figures II.6 and II.7, respectively. Values are given in terms of CPM/gm wet tissue. Halftimes of the two clearance phases were 1.8 and 32.7 hours for the GI tract, and 5.5 and 93.0 hours for the kidneys. For collected blood, samples were refrigerated until centrifugation was carried out. In most samples, varying degrees of hemolysis occurred, making segregation of cells and plasma impossible. Aliquots for digestion were taken from the top of samples and are therefore referred to here as blood plasma, even though some contamination from hemolyzed red blood cells occurred. The clearance of ^{63}Ni from blood plasma is shown in Figure II.8; halftimes of 1.3 and 121 hours were observed. Thus, it appears that the longer phase of clearance halftime was similar for lungs (119 hours), kidneys (93 hours), and blood (121 hours), with no differences significant at the $p < 0.05$ level.

II.4 DISCUSSION

Although TiO_2 has generally been considered to be inert and nontoxic (World Health Organization, 1982), several research groups have noted biological effects resulting from TiO_2 administration.

Moores et al. (1980) instilled rats with 5 mg TiO_2 (ca. 20 mg/kg) and observed a transient increase of lavageable PMN. Similar effects were noted by Sykes et al. (1982), who administered 5 mg TiO_2 to rats (12 mg/kg). Significantly more PMN were recovered by lavage at 1 day post-exposure when compared to saline-instilled controls; at seven days, PMN numbers returned to control levels. Stenback et al. (1976) administered 3 mg TiO_2 once per week for 15 weeks to hamsters and observed some pulmonary inflammation and chronic interstitial fibrosis. However, Wozniak et al. (1976) instilled rats with 50 mg TiO_2 and observed no fibrosis after 3 months. In the literature cited above, the TiO_2 doses used were at least an order of magnitude greater than used here. We administered approximately 0.5 mg/kg TiO_2 to mice and observed effects indistinguishable from PBS-dosed controls. Thus, although internalized TiO_2 particles can exert toxic effects on cultured AM (see Chapter IV), acute effects on the intact mouse appear negligible at the low doses used here. This is in contrast to Ni_3S_2; acute effects included a decrease in animal body weight at 3 and 7 days, significant at the $p < 0.05$ level, the recovery of blood in lavage fluids, and a significant increase in the number of lavaged cells and PMN cells at 3 and 7 days post-exposure. These results are in agreement with those of Valentine and Fisher (1983).

Although the intratracheal instillation exposure technique has been considered to deliver a quantifiably accurate dosage (Brain et al., 1976), we find that a significant portion of the dose is

rapidly cleared within 15 minutes (25 and 34 percent of the instilled dose for Ni_3S_2 and TiO_2, respectively). Even with slow (duration of 5 to 10 seconds) instillation of a 20 µl suspension to an upright, deep-breathing anesthesized animal, induced coughing which persisted for several seconds frequently resulted in the formation of bubbles emanating from the larynx and moving upwards to the buccal cavity. In studies using high doses of Fe_2O_3 (2 mg/mouse, or 80 mg/kg; described in Chapter V), similar effects were observed in mice deeply anesthesized with ether or pentobarbital. Furthermore, the bubbles formed had the rust color of Fe_2O_3 particles, and reddish particle deposits were evident in the buccal cavity when bubbles burst. Similar observations were made by Goldstein et al. (1962) using colored suspensions. Here, the relatively high does of $^{63}Ni_3S_2$ recovered from the gastrointestinal tract at short timepoints post-exposure (20 and 25 percent of the instilled dose at 15 min. and 1 hour, respectively) suggests that particles cleared in this manner are rapidly swallowed. Thus, it appears that the instilled dose is not identical to the dose delivered to the lungs, and furthermore, an extremely rapid clearance route operating within a minute (dependent on the instilled fluid) exists for instillation which is not available to particles introduced to the pulmonary system by inhalation.

Other researchers have commented on rapid losses of material following particle instillation. Goldstein et al. (1962) instilled rats with 50 mg quartz and reported some regurgitation of the

innoculum resulting in a dose recovery of 82 percent from animals "killed immediately". Watson et al. (1969b) determined that 79 percent of a 170 μg dose of ceramic particles remained in the lungs of rats one hour after particle instillation. Ferin and Ulehlova (1959; cited in Goldstein et al., 1962) observed a 68 percent retention of a 70 mg bolus of instilled quartz shortly after dose administration. Finally, Grandjean et al. (1956) administered 50 mg quartz by instillation to rats and recovered only 39 percent of the dose 5 minutes post-instillation. While it is clear that quality of dosing technique as well as quantity of fluid carrier can influence dose deposition in the lung, it is equally apparent that rapid elimination of administered particles can occur through regurgitation of instilled suspensions.

Studies on the pulmonary clearance and translocation of intratracheally-instilled ^{63}Ni-containing compounds have found that solubility plays an important role in routes of Ni elimination. English et al. (1981) observed that soluble forms such as $NiCl_2$ are more rapidly mobilized from the lung compared with the more insoluble NiO, are more rapidly translocated to other tissues at short periods post-exposure, and are excreted primarily in the urine. For NiO, approximately 40, 21 and 17 percent of the instilled dose remained in the lungs after 2 hours, 3 days, and 7 days, respectively. In the case of $NiCl_2$, only 26 percent was present after 2 hours, 2 percent after 3 days, and 1 percent after 7 days. Initial dose retentions are lower than we report here, and may reflect differences in dosing

techniques. English et al. (1981) concluded that ^{63}Ni solubilization was required before translocation from the lungs to other organs could occur. Clary (1975) also reported a rapid transport of $NiCl_2$ from the lung following instillation. After 6 hours, more ^{63}Ni was found in the kidneys than lungs. After 3 days, only 10 percent of the original dose was still in the lungs, with 75 percent having been excreted in the urine. Similarly, Carvalho and Ziemer (1982) report a rapid clearance of $^{63}NiCl_2$ from the lungs, with 72, 24, 9 and 2 percent of the instilled dose present at 35 minutes, 1, 3, and 7 days post-exposure, respectively. The authors comment on the importance of using low doses to avoid overloading potential lung Ni binding sites. This point was also stressed by Charles et al. (1978), who observed an initial clearance halftime of approximately 4.3 hrs for $^{63}NiCl_2$-instilled rat lungs.

In these studies, we report that ^{63}Ni is rapidly translocated from the lungs into various body compartments. As mentioned above, a substantial portion of the initial dose is located in the GI tract (20, 25 and 8 percent at 15 min., 1, and 5 hours, respectively). This activity most probably reflects the presence of particulate $^{63}Ni_3S_2$ cleared by bubble transport during dosing and a rapid phase of clearance thereafter by mucociliary action coupled with swallowing; Valentine and Fisher (1983) suggest that high fecal elimination rates observed during the initial 12 hours of their study may largely represent particulate $^{63}Ni_3S_2$. Here we report that the GI tract

^{63}Ni content peaks at 1 hour post-exposure. It therefore appears that a significant amount of clearance from the lung to the GI tract occurs between the 15 minute and 1 hour timepoints, and that this accumulation over the 15 minute level is not balanced by excretion. Significant clearance from the GI is seen only after a few hours, with clearance halftimes of 1.9 and 32.7 hours. The increase in radiolabelled Ni observed from 15 minutes to 1 hour postexposure is indirect evidence that ^{63}Ni is not rapidly mobilized from the gut by mechanisms other than fecal excretion, and that the feces may indeed be the primary clearance route for Ni deposited in the GI tract. The sharp decrease in GI tract ^{63}Ni levels observed here for later timepoints is in agreement with the results of Valentine and Fisher (1983), who report a sharp decrease in ^{63}Ni fecal content after an initial 12 hour period.

Radiolabelled Ni was also observed in the kidneys and in blood shortly after exposure in the current study; levels peaked 1 hour post-exposure. At 1 hour and later times, clearance halftimes of 5.5 and 93 hours were observed for kidney, and 1.3 and 121 hours for blood plasma. Halftimes for the later clearance phases are similar to that of lung, in agreement with the findings of Valentine and Fisher (1983). Since Ni is apparently poorly absorbed through the GI tract (Ho and Furst, 1975; Kasprzak and Sunderman, 1979), the most likely mechanism to account for rapid Ni mobilization is solubilization in the lung followed by transport through the blood (English et al.,

1981). Solubilized Ni has been shown to bind to serum albumin and ultrafiltrable ligands (Soestbergen and Sunderman Jr., 1972; Kasprzak and Sunderman, Jr., 1979). Although occasionally considered to be insoluble, perhaps because of its low solubility in water, Ni_3S_2 dissolution is enhanced in the presence of serum proteins and O_2 (Kasprzak and Sunderman, Jr., 1977), conditions which are likely to exist in the lung.

In conclusion, this study has shown that intratracheally instilled Ni_3S_2 exerts acute toxic effects to mice. Blood was recovered from the lungs during lavage; other effects included increased PMN cell levels, body weight decreases, and a clinically sick condition. These effects were in contrast to TiO_2-instilled animals, which appeared similar to PBS-control mice. The clearance of instilled particles from the lungs was examined for both Ni_3S_2 and TiO_2-exposed mice. Some particles were rapidly cleared to the GI tract within 15 minutes; this clearance was nonspecific for Ni or Ti and appeared to be an artifact of the exposure technique. However, we report that significanty less Ni is present compared with TiO_2 in mouse lungs at 3 and 7 days post-exposure ($p < 0.05$), with a factor of three difference in halflife of the later clearance phase, also significantly different at the $p < 0.05$ level. Various aspects of the metabolism of ^{63}Ni were examined; much of the early Ni lung burden was cleared to the GI tract, and Ni levels in the kidney and blood

peaked at one hour. Longer term clearance rate constants were similar for lung, kidney, and blood, and are consistent with the hypothesis that ^{63}Ni is solubilized in the lung then transported through the blood.

Table II.1. ANIMAL BODY WEIGHT CHANGES FOLLOWING INTRATRACHEAL INSTILLATION[a]

Instilled Agent[b]		Time Post-instillation 20 hr.	3 day	7 day
PBS	$\bar{X}$	+0.32	+0.48[c]	+0.82[c]
	S	.63	.31	.49
	n	4	5	8
TiO_2	$\bar{X}$	+0.42	+0.37[d]	+0.89[d]
	S	.78	.80	.82
	n	9	9	10
Ni_3S_2	$\bar{X}$	+0.51	-1.48[c,d]	-1.0[c,d]
	S	.64	1.72	1.94
	n	7	10	9

a Mean and standard deviations of differences between body weights (grams) at time of sacrific vs. time of instillation; n equals number of animals per group.

b TiO_2 and Ni_3S_2 dose used was 11.8 µg/mouse, delivered in 20 µl phosphate buffered saline.

c,d Within each time group, means with the same superscript are different at the $p < 0.01$ level.

Table II.2. SELECTED ORGAN WEIGHTS FOLLOWING INTRATRACHEAL INSTILLATION

Compound[a]	Time Post-Instillation	Organ Weight[b] Lung	G.I. Tract	Kidneys
UTC	—	.226 ± .032	—	—
PBS	15 min	.247 ± .024	—	—
	7 day	.219 ± .013	—	—
TiO_2	15 min	.265 ± .008	—	—
	1 hr	.259 ± .036	—	—
	5 hr	.226 ± .029	—	—
	20 hr	.240 ± .040	—	—
	3 day	.213 ± .019	—	—
	7 day	.198 ± .014	—	—
$^{63}Ni_3S_2$	15 min	.255 ± .033	3.67 ± 0.21	.483 ± .039
	1 hr	.254 ± .066	3.38 ± 0.02	.412 ± .021
	5 hr	.216 ± .003	3.66 ± 0.22	.417 ± .020
	20 hr	.210 ± .008	3.16 ± 0.35	.397 ± .020
	3 day	.239 ± .032	3.15 ± 0.68	.457 ± .029
	7 day	.222 ± .037	3.71 ± 0.75	.514 ± .028

a TiO_2 and $^{63}Ni_3S_2$ dose used was 11.8 µg/mouse, delivered in 20 µl PBS, UTC = untreated controls.

b Mean ± standard deviation, in grams. Lungs included all lobes plus trachea distal to the larynx; G.I. tract included esophagus, stomach, and intestines; both kidneys pooled.

Table II.3. TOTAL CELL YIELD FROM BRONCHOPULMONARY LAVAGE OF PARTICLE-INSTILLED MICE[a]

Time post-Instillation	UTC[b]	Administered Agent[c]		
		PBS	TiO_2	Ni_3S_2
15 min.	2.59 ± 1.05	3.13 ± 0.18	2.52 ± 0.57	1.96 ± 1.50
1 hr.		3.18 ± 0.18	2.58 ± 1.12	2.15 ± 0.64
5 hr.		3.71 ± 0.83	2.63 ± 0.48	3.22 ± 0.91
20 hr		4.57 ± 2.05	4.19 ± 0.83	4.52 ± 2.16
3 day		4.27 ± 1.23	3.28 ± 0.89	6.80 ± 1.53[d,e]
7 day		4.39 ± 0.76[e]	4.81 ± 1.84[e]	6.55 ± 0.90[d,e]

a Based on a sample n = 3 except n = 2 for PBS 1 hr, TiO_2 20 hr.

b UTC = untreated controls (n = 3) lavaged pre-study

c All figures represent mean ± standard deivation x 10^5

d Cell yields with this superscript are significantly greater ($p < 0.05$) than PBS-instilled mice at the same timepoint.

e Cell yields with this superscript are significantly greater ($p < 0.05$) than untreated control mice.

Table II.4. VIABILITY[a] OF CELLS OBTAINED FROM BRONCHOPULMONARY LAVAGE ON PARTICLE-INSTILLED MICE

Time post-Instillation	UTC[b] x ± S.D.	Administered Agent[c] PBS x ± S.D.	TiO_2 x ± S.D.	Ni_3S_2 x ± S.D.
15 min	95.8 ± 0.8	95.2 ± 3.0	97.0 ± 1.0	97.0 ± 0.5
1 hr		96.2 ± 3.2	96.7 ± 1.6	94.3 ± 3.1
5 hr		96.8 ± 0.3	95.8 ± 1.3	95.6 ± 2.7
20 hr		98.2 ± 0.6	94.8 ± 2.6	97.0 ± 1.8
3 day		95.7 ± 1.3	95.9 ± 1.4	93.5 ± 3.9
7 day		98.0 ± 1.0	96.8 ± 0.8	96.2 ± 1.5

a Determined by trypan blue dye nuclear exclusion.

b UTC = untreated control mice (n=3) lavaged pre-study.

c All figures represent mean percentage ± standard error

Table II.5. CELL TYPES OBTAINED FROM BRONCHOPULMONARY LAVAGE OF PARTICLE-INSTILLED MICE[a]

Exposure; time post-exposure		Alveolar Macrophages x ± SD (%)	Lymphocytes x ± SD (%)	PMN x ± SD (%)	Other types[b] x ± SD (%)
UTC[c]		97.3 ± 1.5	2.7 ± 1.5	0	0
PBS	15 min	99.0 ± 1.7	0.7 ± 1.2	0.3 ± 0.6	0
	1 hr	98.5 ± 0.7	0.5 ± 0.7	0.5 ± 0.7	0.5 ± 0.7
	5 hr	98.7 ± 0.6	1.3 ± 0.6	0	0
	20 hr	97.7 ± 0.6	1.3 ± 1.5	0.3 ± 0.6	0.7 ± 0.6
	3 d	98.3 ± 1.5	0.3 ± 0.6	0.3 ± 0.6	1.0 ± 1.0
	7 d	98.0 ± 1.0	0	1.0 ± 0.0	1.0 ± 1.0
TiO_2	15 min	98.3 ± 1.5	1.0 ± 1.0	0	0.7 ± 1.2
	1 hr	98.0 ± 1.0	0.3 ± 0.6	0.3 ± 0.6	1.3 ± 0.6
	5 hr	98.3 ± 1.5	0.7 ± 0.6	0	1.0 ± 1.0
	20 hr	97.7 ± 2.5	0	2.0 ± 2.0	0.3 ± 0.6
	3 d	96.7 ± 2.3	0.7 ± 0.6	1.0 ± 1.0	1.7 ± 1.5
	7 d	96.7 ± 2.1	0.3 ± 0.6	1.3 ± 0.6	1.7 ± 2.1
Ni_3S_2	15 min	98.3 ± 0.6	0.3 ± 0.6	0.7 ± 0.6	0.7 ± 0.6
	1 hr	99.3 ± 0.6	0	0.7 ± 0.6	0
	5 hr	94.0 ± 4.6	1.0 ± 1.0	2.0 ± 1.7	3.0 ± 3.6
	20 hr	79.3 ± 8.7	1.7 ± 2.9	19.0 ± 11.5	0
	3 d	80.3 ± 5.7	0.7 ± 1.2	18.3 ± 4.2	0.7 ± 0.6
	7 d	87.0 ± 1.7	1.0 ± 1.0	11.0 ± 2.6	1.0 ± 1.0

a 100 cells per animal counted after Wright's differential stain. N = 3 for all groups except PBS 1 hour where n = 2.

b Other cell types were primarily epithelial cells.

c UTC = untreated control mice (n = 3) lavaged pre-study.

Table II.6. NICKEL AND TITANIUM LUNG BURDEN AT VARIOUS TIMES AFTER INSTILLATION[a]

Time Post-Exposure[b]	Ti Burden[c] (%) x ± SD	^{63}Ni Burden[d] (%) x ± SD
15 min.	65.5 ± 10.3	74.9 ± 4.8
1 hr	57.0 ± 5.0	67.9 ± 6.3
5 hr	50.4 ± 21.1	56.8 ± 6.5
20 hr	50.6 ± 7.6	47.6 ± 7.6
3 day	46.8 ± 7.2[e]	35.0 ± 3.8[e]
7 day	40.1 ± 7.6[f]	20.5 ± 4.6[f]
Spiked Dose	100 ± 16.0 (11.1 µg Ti)	100 ± 8.0 (1.92 x 10^6 CPM)
PBS-dosed	(2.90 ± 0.37 µg Ti)	

a Instillation of calculated 11.8 µg dose in 20 µl PBS. Percentage contents were ratioed to spiked lung dose.

b Time from instillation to sacrifice. For spiked dose samples, lungs were excised, placed in crucibles or scintillation vials, then the dose was administered to the crucible. PBS-dosed animals were given 20 µl of PBS alone.

c Analysis by ICAP. N = 3 per group except for 3 day where N = 2 and PBS dosed animals where N = 5. The mean Ti level in PBS-dosed animals was subtracted from TiO_2-treated groups, and standard deviations were added in quadrature.

d Analysis by liquid scintillation counting. N = 3 per group except for 20 hour where N = 2. Percentages ratioed to the zero hour spiked dose. Duplicate aliquots averaged for each sample.

e,f Values with the same superscript are significantly different ($p < 0.05$, Student's t-test).

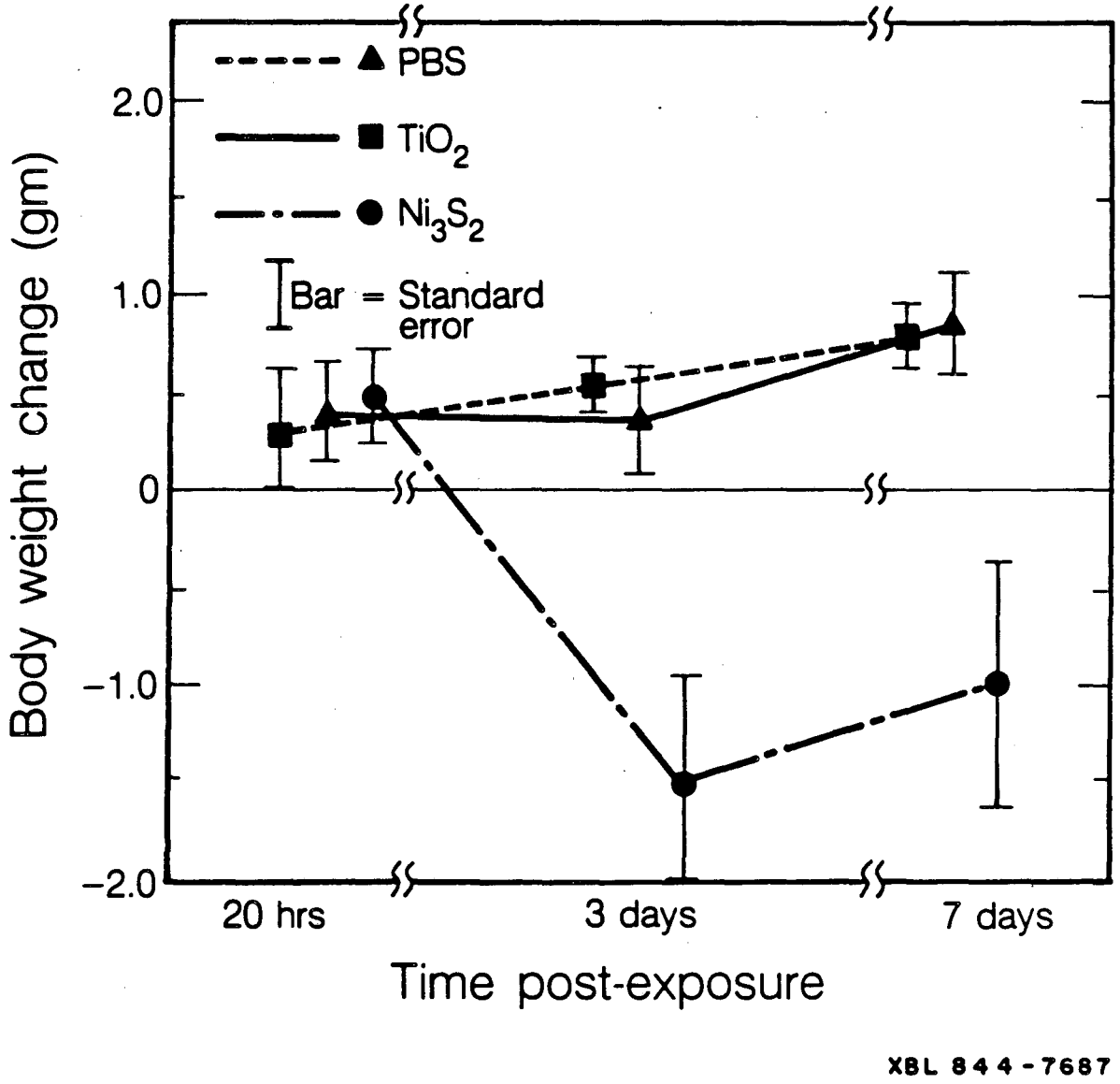

Figure II.1. Body weight changes at 20 hours, and 3 and 7 days post-exposure, in groups of Ni_3S_2, TiO_2, and PBS-instilled mice.

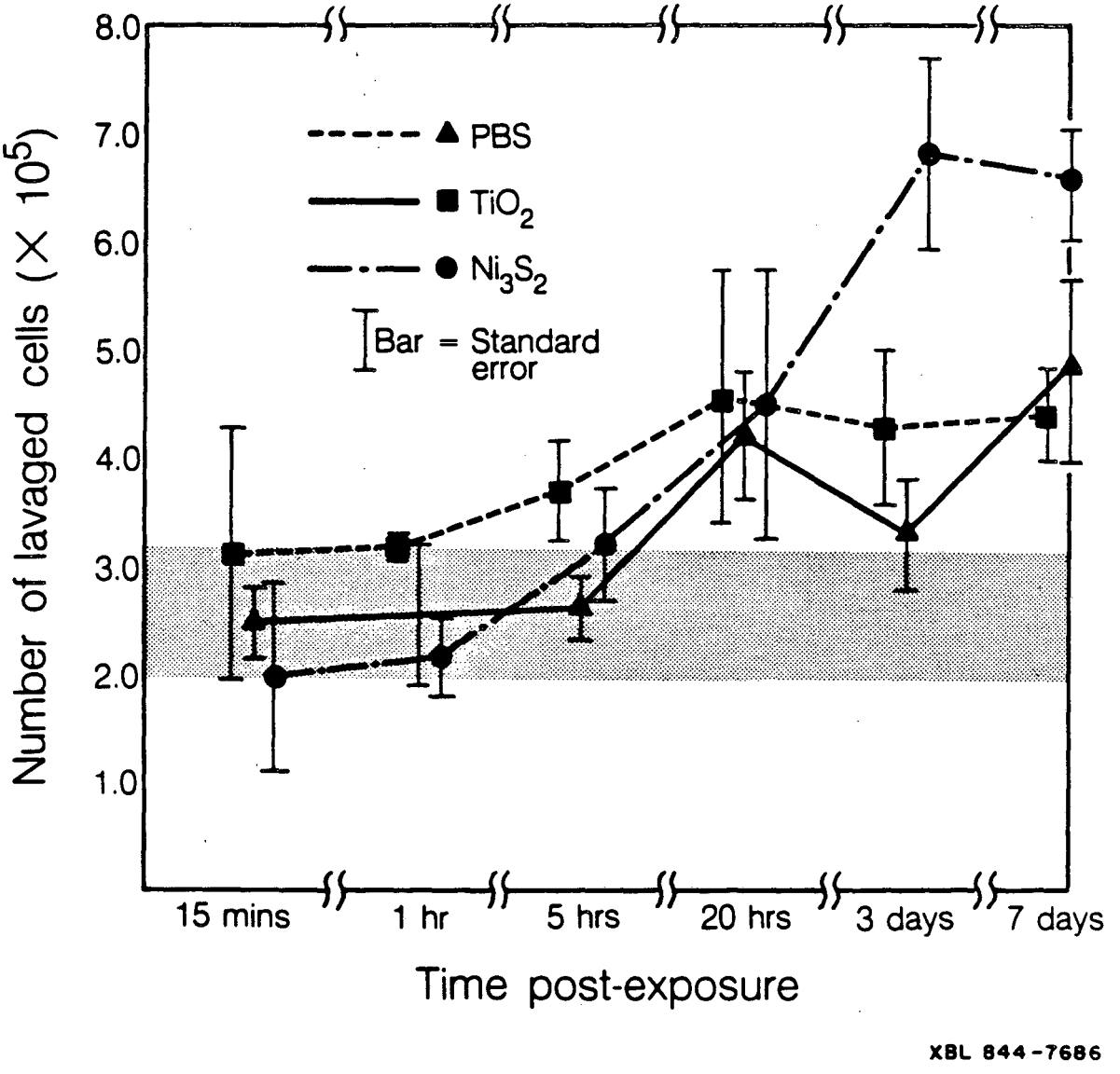

Figure II.2. Number of lavaged cells (all cell types) recovered from Ni_3S_2, TiO_2, and PBS-instilled mice at various timepoints post-exposure. Shaded area indicates number of cells recovered from untreated controls (mean ± standard error).

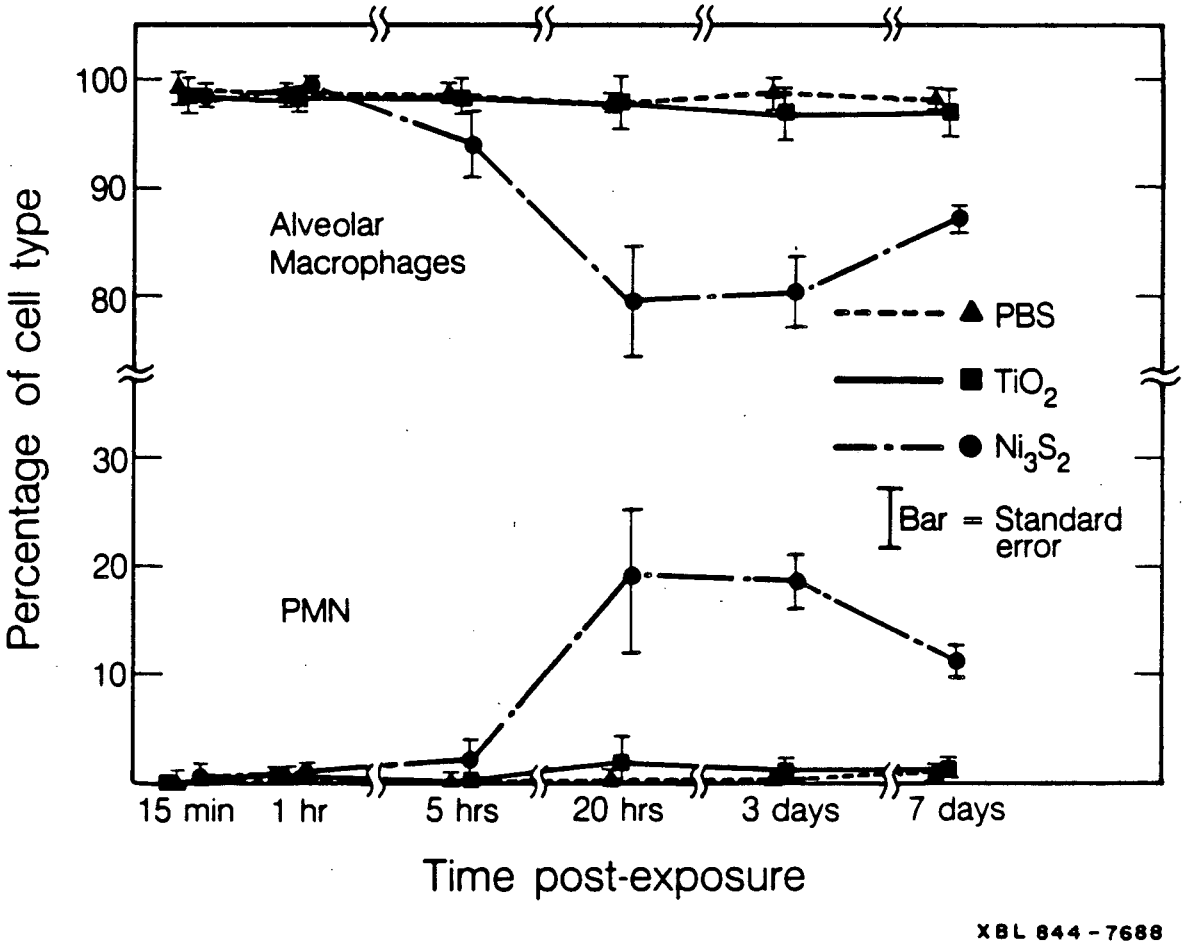

Figure II.3. Percentage of alveolar macrophage and polymorphonuclear leucocytes recovered from Ni_3S_2, TiO_2, and PBS-instilled mice at various times post-exposure, determined from Wright's stained cell smears.

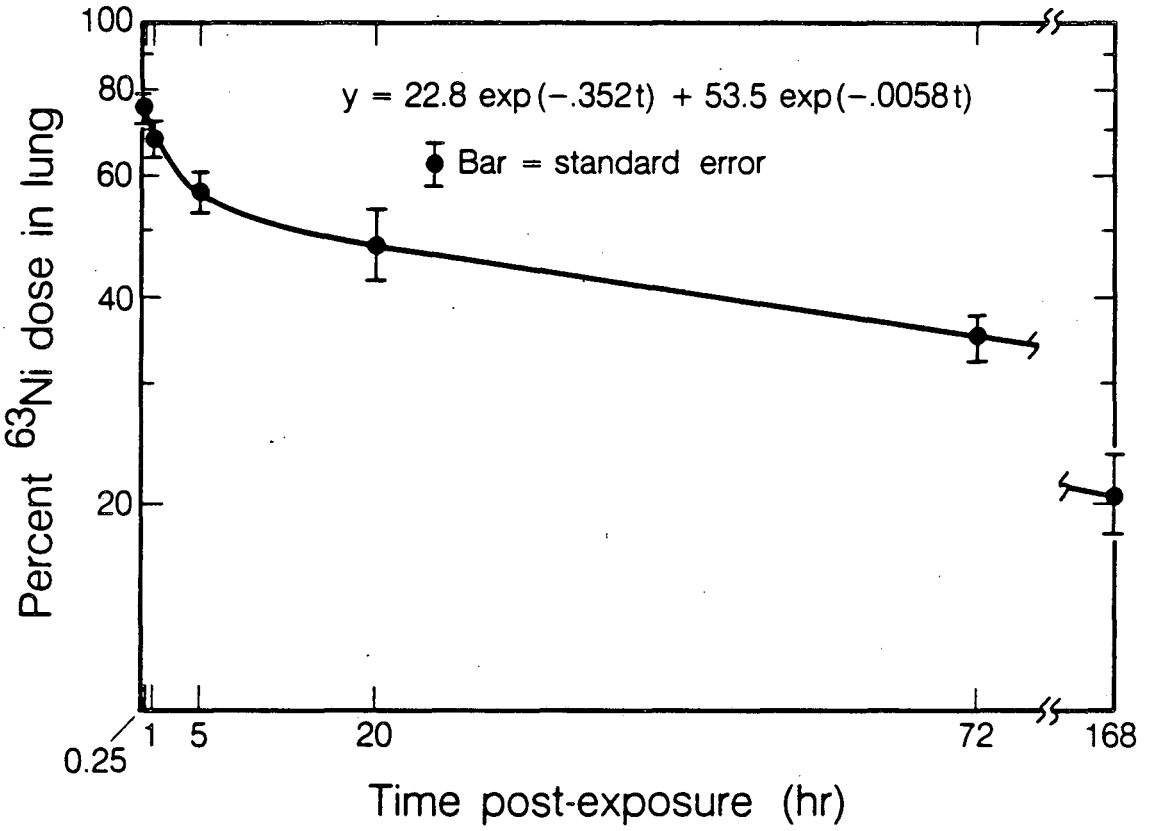

Figure II.4. Percentage of ^{63}Ni remaining in mouse lungs and trachea at various times after Ni_3S_2 instillation; a biexponential fitted line and equation is also shown.

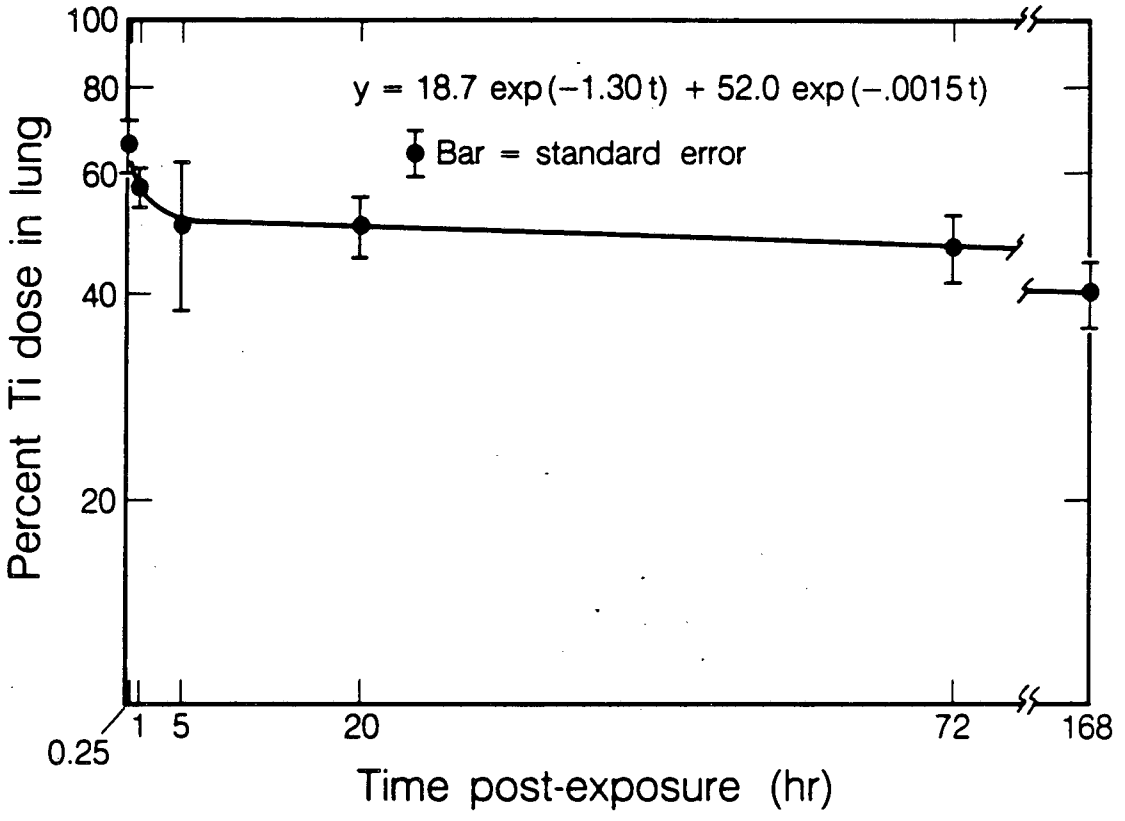

Figure II.5. Percentage of Ti remaining in mouse lungs and trachea at various times after TiO_2 exposure, with fitted biexponential line and equation.

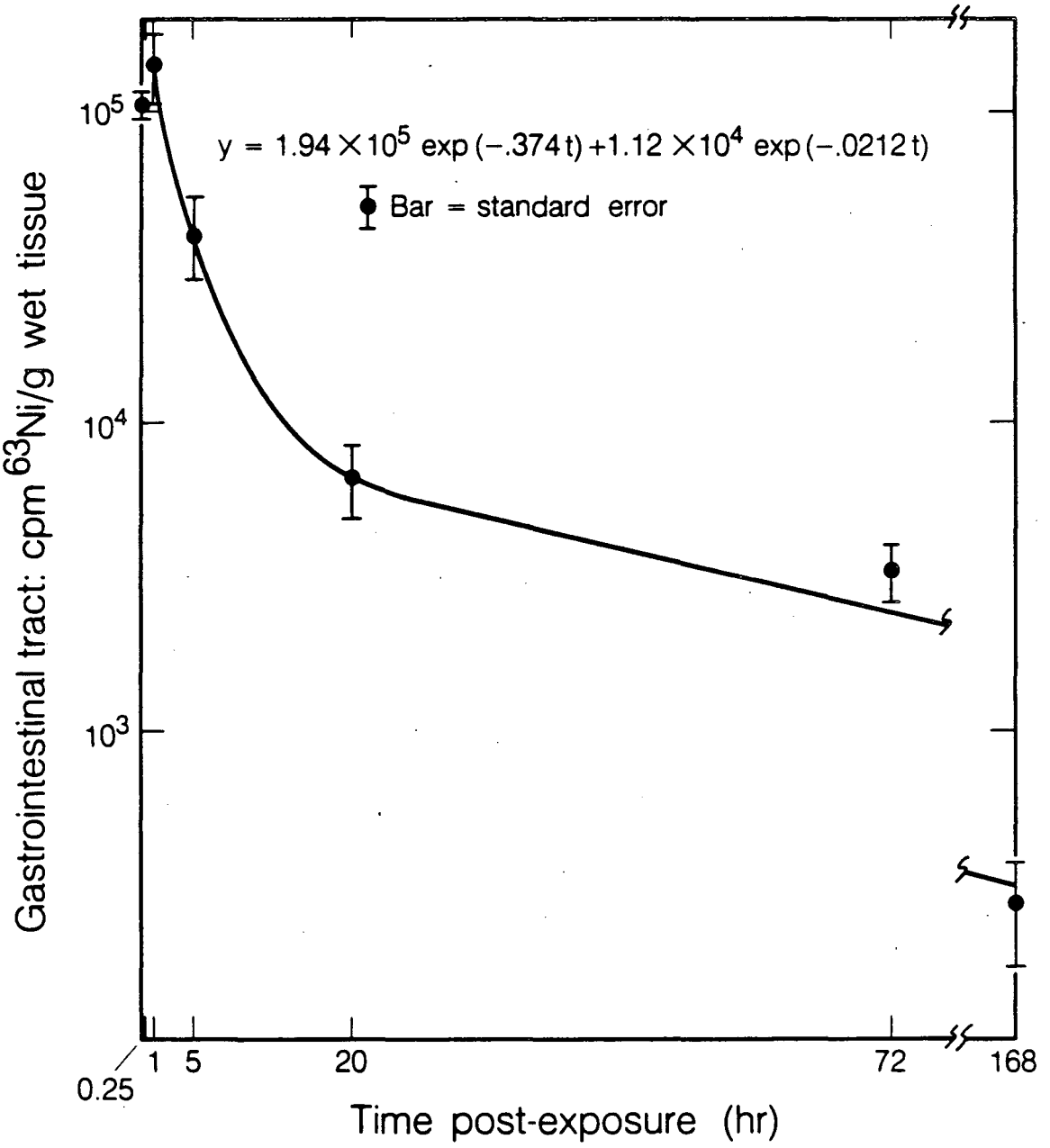

Figure II.6. ^{63}Ni activity (cpm) in the gastrointestinal tract following $^{63}Ni_3S_2$ instillation; the fitted biexponential line is for one hour and later timepoints.

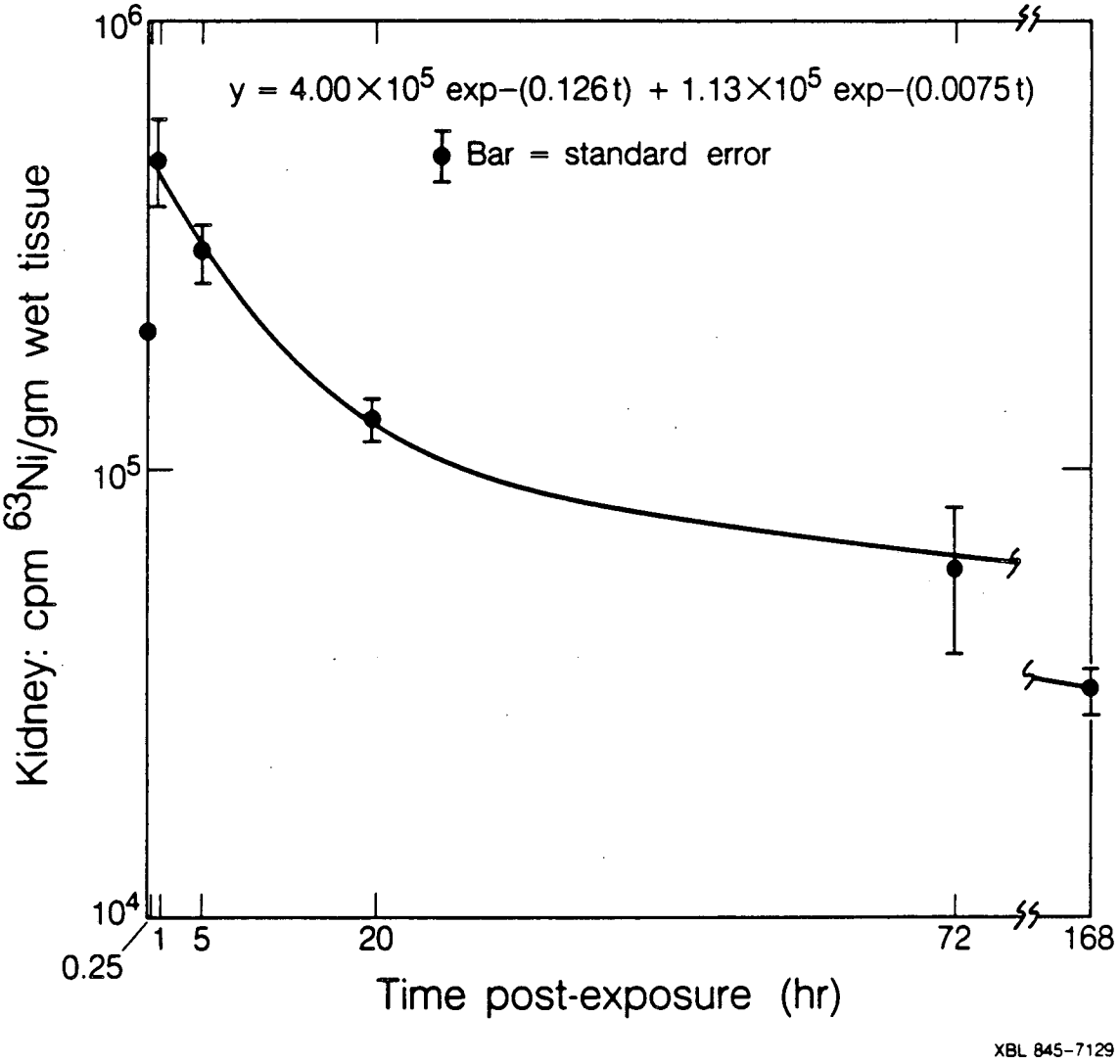

Figure II.7. ^{63}Ni activity (cpm) in the kidneys after $^{63}Ni_3S_2$ instillation; the fitted biexponential line is for one hour and later timepoints.

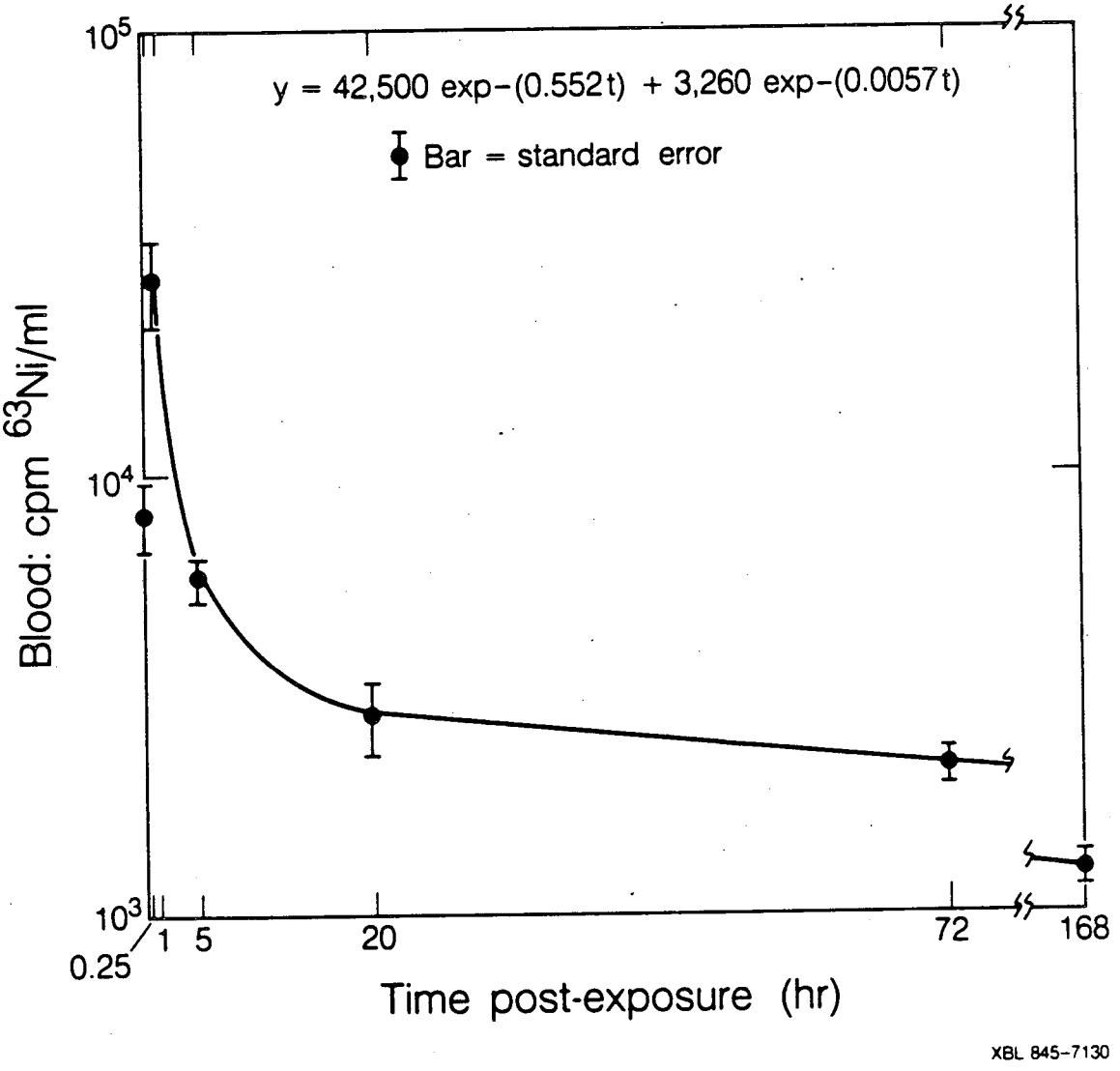

Figure II.8. ^{63}Ni activity (cpm) in blood plasma after $^{63}Ni_3S_2$ instillation; the fitted biexponential line is for one hour and later timepoints.

CHAPTER III

INTERACTIONS BETWEEN CULTURED TRACHEAL EXPLANTS AND NICKEL SUBSULFIDE PARTICLES

III.1. INTRODUCTION

In recent years research has focussed on the use of tracheal explant cultures to model the interaction of particles with the upper respiratory tract mucosa. Tracheas can be easily excised, sectioned, and maintained in tissue culture up to several months provided that culture medium is changed every three days (Collier, 1980). Hamsters are commonly used because of their tracheal size and ability to tolerate *in vitro* conditions (Gabridge et al., 1979). Although this system generally excludes factors involving immune and inflammatory responses (Lane et al., 1976), the easy manipulation of the culture environment allows many toxicologic endpoints besides morphological alteration to be examined. For example, ciliary beat frequency can be measured using light microscopy and has been shown to be reduced after exposure to agents such as cadmium (Adalis et al., 1977) and volcanic ash (Schiff et al., 1981). Also, cellular synthesis of various macromolecules can be examined using autoradiography, and rapidly dividing cell populations have been characterized by increased protein and DNA synthesis (Lane et al., 1976). An additional feature of this system is that normal epithelial morphology and response to external agents is similar when *in vitro* explants are compared with *in vivo* tracheas (Schiff et al., 1981; Schiff et al., 1979).

The trachea consists of a hollow tube reinforced by rings of cartilage containing chondrocytes. Above this is the connective tissue compartment consisting largely of interwoven collagenous and

elastic fibers with occasional submucosal cells, lymphatics, and glands which open to the lumenal surface. Atop this lies a basement membrane then a normally pseudostratified, columnar epithelium consisting of ciliated, nonciliated and basal cells. Basal cells are those cells sitting upon the basement membrane but not reaching the lumen, and nonciliated cells are of several types including mucous, brush, and other minor cell types (Weiss and Greep, 1977). The ciliated and nonciliated cells work in concert to produce and transport a mucus blanket upwards along the luminal surface; it is this transport which is largely responsible for clearing particles deposited in the upper respiratory tract. However, this normal epithelium appears to be quite sensitive in its response to a variety of agents including mechanical damage and exposure to noxious gasses and particles. A general pattern of cell sloughing and regeneration is commonly observed in the literature. In this study, we describe the morphology of epithelial response to administered nickel subsulfide (Ni_3S_2) particles over time using scanning electron microscopy (SEM). Ni_3S_2 is a potent cytoxic agent and probable carcinogen (Fisher et al., 1982; Sunderman, 1981) that dramatically affects explant morphology at very low doses, as shall be shown. In order to understand these effects in light of the literature, we first undertake to examine the results of other researchers in this field.

The epithelial surface of cultured explants apparently reacts to external stimuli rapidly. Mossman et al. (1978) observed prominent cytoplasmic protuberances forming atop mucin-secreting cells within 5

minutes after exposure to administered carbon particles. This response occurred with several different types and sizes of carbon particles, and may be related to the observed hypersecretion of mucin within 15 minutes after exposure to asbestos (Mossman et al., 1980). Within 1 hour, particles were observed at the margins of explants (presumably by mucociliary action) and trapped within clumps of cilia and at the surfaces of non-ciliated cells. Marginal accumulations of asbestos have also been observed following exposure (Woodworth et al., 1983). Although ciliated cells were not observed to form protuberances, this cell type was the first to slough from the epithelium, occurring within 3 hours post-exposure (Mossman et al., 1979). Desquamation of nonciliated cells was observed less frequently or later at lower doses (4 or 8 mg/ml). This general pattern of initial ciliated cell sloughing is confirmed by other researchers. Kennedy and Allen (1979) observed desquamation of individual ciliated, but not nonciliated, columnar cells after exposure of rabbit explants to cigarette smoke residues. Upon further exposure both cell types were observed to slough. The earliest identifiable change post-exposure appeared to be the rupture of junctional complexes at the apical ends of columnar cells, leading to the physical separation of adjacent cells. Also, Schiff et al. (1981b) reported that focal desquamation of ciliated cells was observed after exposure of hamster tracheal explants to a respirable fraction of volcanic ash. This appears to correspond with the in vivo situation; Asmundsson et al (1973) observed some loss of

cilia, and vacuolization and degeneration of ciliated cells after exposure of hamsters to SO_2.

Focal desquamation of cells can apparently lead to a general sloughing of columnar epithelium if the challenge is sufficient. This exposes both basal cells and basement membrane when basal cells are sparse. Frequently, remnant necrotic columnar cells are present. This complete desquamation can be the result of exposure to a wide range of insults. The early events in sloughing described above lead to complete desquamation in a variety of rodent species after exposure to carbon particles (Mossman et al., 1978), asbestos (Mossman et al., 1977, 1980, and 1981), carbon particles with and without H_2SO_4 mist (Schiff et al., 1979), $BaSO_4$ particles administered *in vivo* to rats (Stirling and Patrick, 1980), fly ash (Schiff et al., 1981), volcanic ash (Schiff et al., 1981b), cigarette smoke (Dalbey et al., 1980), and smoke residues (Kennedy and Allen, 1979). Excluding the effects of various physicochemical forms, the extent and severity of particle-induced damage is probably related to the amount of added material. Mossman et al. (1978) noted that high loadings (>40 mg/ml) of carbon particles produced complete necrosis of the tracheal epithelium, whereas lower doses caused a less severe pattern of cell sloughing. Schiff et al. (1981) noted that epithelial changes became more pronounced and extensive with higher concentrations of fly ash or longer exposures, and in studies using administered carbon particles, this research group noted effects similar but less extensive to those obtained by Mossman et al. (1978) with lower carbon doses (Schiff et al., 1979).

Basal cells are rarely affected at this stage and can be seen by SEM to form a network of elongated, interconnecting cells residing upon the basement membrane. This morphology was described by Schiff et al. (1981b) after exposure of hamster trachea to volcanic ash, by Kennedy and Allen (1979) after exposure of rabbit trachea to cigarette smoke residues and by Gordon and Lane (1976) after mechanical damage to rat trachea in vivo. Basal cells are generally flattened and elongated at this stage thus distinguishing themselves from residual columnar cells which project higher into the lumen. This stage does not persist; basal cell replacement occurs rapidly to replace the denuded mucosal surface. Basal cell hyperplasia was observed within 24 hours after hamster tracheal explant exposure to asbestos (Mossman et al., 1977); cells took up radiolabelled thymidine and contained accumulations of mitochondria. Cells of similar appearance undergoing cell division were observed within 24 hours after mechanical injury and progressed to form a stratified epithelium of polygonal and flattened cells (McDowell et al., 1979). A significant increase in basal cell number was observed by Frank (1980) within two days after exposure to amosite asbestos. However, Gordon and Lane (1976) find that the onset of basal cell hyperplasia following mechanical injury in vivo in rats is much sooner, on the order of hours. These researchers find that the basement membrane is covered with flattened basal cells by 4 hours post-injury, and that by 6 hours, intercellular junctions are present and early evidence of stratification is observed.

Basal cell replacement can result in a variety of types of renewed epithelium. Since basal cells can serve as precursors to the more differentiated columnar cells, relatively normal renewed epithelia may result. Schiff et al. (1979) observed new growth of ciliated cells within 2 days after exposure to H_2SO_4 and carbon particles both in vivo and in vitro. With carbon particles only, epithelial morphology was indistinguishable from controls. Also, after sloughing of the mucociliary epithelium following mechanical injury, Gordon and Lane (1976) observed ciliated cells in marginal areas of regenerating areas as early as 6 hours after damage, although in similar experiments, McDowell et al (1979) found that regeneration was not complete until 4 days post-injury.

With chronic exposure to particles, basal cell hyperplasia may lead to the formation of squamous metaplasia. The surface alterations characterizing squamous metaplasia have been widely described (Schiff et al., 1981, 1981b and Woodworth et al., 1983). Ciliated cells are absent and nonciliated cells are flattened with microvilli covering the luminal surface. Cell profiles are generally polygonal and outlined by borders of microvilli. Cell sizes are heterogeneous and frequently large and small cells are interspersed. As squamous metaplasia progresses keratin may accumulate and stratification of the epithelium is marked.

The results of particle exposure to tracheal explants have been generally discussed above. Particles appear able to enter and cross the epithelial barrier. Epithelial cells can ingest particles after

in vivo exposure (Sorokin and Brain, 1975) and also in the tracheal explant model. Both asbestos and Fe_2O_3 particles were observed within mucosal and submucosal spaces by Mossman and Craighead (1979). In studies with carbon particles, this group observed that particles were phagocytized by hyperplastic basal cells and were transported within one week post-exposure across the basement membrane, where particles accumulated in mesenchymal cells (Mossman et al., 1977). Asbestos fibers have also been found within epithelial cells (Mossman et al., 1977b). Fibers were found inside and projecting from sloughing cells, were observed inside phagolysosomes of proliferating basal cells, and were subsequently found inside submucosal cells. Basal cells were also observed proliferating around extracellular particles near the basement membrane. Ciliated cells also appear capable of phagocytizing short fibers (Woodwoth et al., 1983). The authors conclude that particles may penetrate the mucosal surface both intra- and extra-cellularly (Mossman et al., 1977b; and Woodworth et al., 1983). It appears clear that interactions of the epithelium with particles are related to particle size and morphology as well as dose. Mossman et al. (1978) exposed explants to a small (0.5-1.0 μm) and large (15-30 μm) size range of carbon particles and found that smaller particles were able to reach the submucosa. Particles were phagocytized by hyperplastic basal cells and transported to the basal lamina where particle accumulations were observed. Also, small particles were observed within cells in the submucosa. In contrast, large particles remained at the luminal surface and were frequently

associated with hyperplastic basal cells and areas of squamous metaplasia. Similar observations have been made with asbestos fibers. Short fibers penetrated epithelial cells whereas long fibers were more likely to be found at the luminal surface or cleared to the edges of explants (Mossman et al., 1977; Woodworth et al., 1983). Schiff et al. (1981b) also observed particle size dependent responses in cultured explants. Large (MMAD = 7.7 μm) volcanic ash particles produced extensive desquamation, whereas with small (MMAD = 1.6 μm) ash particles the response was less severe.

III.2 MATERIALS AND METHODS

III.2.A Culture Techniques

The experimental procedures used to examine explant morphology are described in Figure III.1. Male Golden Syrian hamsters at 4 to 6 weeks of age were sacrificed and tracheas harvested as described by Mossman and Craighead (1975). After shaving the neck region the skin and musculature was removed from the tracheal area using sterile techniques. The trachea was cut proximally from the first bifurcation and distally from the larynx then transferred to a Petri dish containing Hank's balanced salt solution containing Ca^{++} and Mg^{++} (HBSS, Grand Island Biological Co., Grand Island, N.Y.) with 50 ug/ml gentamycin and 20 units/ml mycostatin (GIBCO). After cutting lengthwise along the tracheal discontinuity, trachea were cut longitudinally at every second ring then cut in half into semi-sections. Each piece was then transferred to a 35 mm Petri dish containing 0.5 ml culture

medium consisting of minimal essential medium (MEM, GIBCO) supplemented with 1 μg/ml insulin, 0.1 μg/ml hydrocortisone, 50 μg/ml gentamycin, and 20 units/ml mycostatin (all GIBCO).

Nickel subsulfide (Inco Metals, Canada, VMD = 1.83 μm, σ_g = 2.3, as prepared by Fisher et al., 1982) was weighed into sterile injection vials; culture medium was added to yield a 20 μg/ml dosage then vials were sonicated for 10 minutes. Suspensions were prepared immediately before use to decrease solubilization of the compound into the medium. Vials were vortexed immediately before dose withdrawal. For each plate, the culture medium was removed then 2 ml of either fresh or Ni_3S_2-added medium at 37°C was added to completely immerse tracheal sections. Cultures were returned to the incubator for one hour then explants were transferred to a fresh dish with fresh medium, except for the 0 minute timepoint which was immediately rinsed and fixed. The Ni_3S_2 dosage used was 20 μg/ml; experimental timepoints employed are shown in Table III.1. Calculations indicated that vortexing of the Ni_3S_2-laden medium was sufficient to keep the coarsest particles in suspension until seeded into the dishes, and that the one hour exposure was sufficient to allow gravity settling of at least 98 percent of the particles onto the explant luminal surfaces.

III.2.B Microscopic Techniques

After exposure, explant sections were fixed in one of two different manners. For light microscopic histopathology, two sections per group were placed into 10 percent neutral buffered formalin and fixed for at least one day, at which time tissues were dehydrated,

cleared, embedded in parafin, hardened, then sectioned at a 5 μm thickness. Sections were stained in hematoxylin and eosin. For SEM evaluation, sections were rinsed briefly in culture medium then placed into room temperature fixative consisting of 2.3 percent glutaraldehyde in a buffer of 0.05 M sodium cacodylate (Electron Microscopic Services, Fort Washington, PA) at pH 7.4 and an osmolarity of 360 ± 10 mOsm (Bastacky et al., 1983). Tissues were held in fixative at 4°C until SEM preparation was initiated by two 15 minute rinses in fresh buffer (0.05 M sodium cacodylate with added sucrose, pH 7.4, 360 mOsm), dehydration through a graded series of ethanol/water rinses (10 min/each in 25 , 50 , 75 , 90 , 95 , 95 , 100 , 100 , and 100 ethanol), transfer to a critical point dryer (Polaron, Wateford, England) in ethanol with substitution and drying through CO_2 (Anderson et al., 1951), and mounting onto carbon stubs with either an evaporative carbon coating (Denton Vacuum DV-502, Cherry Hills, NJ) or platinum sputter coating (Polaron, E5100, Waterford, England).

Morphological evaluation of the explants was begun using a low magnification SEM micrograph for orientation and sample area selection (Figure III.2). A 10 by 10 grid was overlaid onto the micrograph then four gridpoints selected using a random number table for detailed examination. Selected areas were rejected if the gridpoint was off the luminal surface or if the selected point was immediately adjacent to a previously selected point. Selected areas were imaged at 2000 times magnification (following magnification calibration and focusing using

only the stage z-control) after bringing the area roughly perpendicular to the electron beam. A conventional secondary electron (SE) image of the area was used to assess morphology. For particle-exposed explants, a backscattered electron image (BSE) provided increased contrast between particles and tissue and aided in identifying particles. The beam was then placed onto each apparent particle and the presence of Ni and S X-ray peaks confirmed Ni_3S_2 particle identity. Alternately, particles were located by making X-ray maps for the Ni K_α X-ray peak (Figure III.3). SE images of selected areas were analyzed for the presence of certain features and particulate interactions with epithelium and are described in the results.

III.3 RESULTS

III.3.A Descriptive Morphology

Control explants appeared similar in surface architecture throughout the experimental timecourse. Figure III.2 shows a typical explant at low magnification, and figure III.4 shows portions of selected areas such as those used for morphological analysis. The luminal surface was comprised of ciliated and nonciliated cells occurring with variable incidences. Frequently, nonciliated cells greatly outnumbered ciliated cells, and linear clusters of cilia were seen. This was particularly true near peripheral margins of the explants where epithelium spread to colonize explant edges. Cilia usually appeared as numerous, free-standing cylindrical projections into the lumen but were occasionally clumped. Nonciliated cells were present in two general types. The first, as seen in figure III.4A,

was characterized by indistinct cell borders and rounded luminal surfaces, with occasional short microvilli present. The other type, shown in figure III.4B, consisted of polygonally-shaped cells of irregular size, with microvilli clustered at cell edges forming distinct borders. These cells frequently possessed short, stubby microvilli over the entire surface and were flatter than the first type, as determined from stereopair SEM micrographs. Openings in the luminal surface were occasionally seen and are probably the openings of submucosal secretory glands (see figure III.5). The epithelium near these ductular openings was slightly depressed yet continuous, indicating that the opening was not due to mechanical damage or cell sloughing. Sloughing of cells was observed rarely in control explants, and when seen was focal in nature.

In contrast to the control explants, Ni_3S_2 exposed explants displayed a dramatic pattern of cell sloughing and regeneration of epithelium, even though low doses (20 µg/ml) were used to avoid particle loading effects. Figure III.3 illustrates the SE image at top, with the BSE image then x-ray map seen below. Particles in the SE image are more evident by BSE, and confirmed as Ni-containing test particles by the x-ray map. Note that one particle (P) was internal to a sloughing cell, whereas the other three particles were external. Most particles appeared adherent to the lunimal surface, yet external to the cells, with internalized particles observed less frequently. The next series of micrographs (Figures III.6-11) depict stages in epithelial sloughing and regeneration. In Figure III.6, an explant

fixed immediately after exposure, the normal differentiated epithelium was broken up, and both ciliated and nonciliated cells were sloughed from the surface. In Figure III.7, one hour post-exposure, few columnar cells remained and those present were rounded. An underlying network of basal cells was present at this stage. In Figure III.8, four hours post-exposure, even fewer residual sloughed cells remained. More basal cells were present and the lumenal surface was characterized by more complete cell coverage. This process appeared more advanced (Figure III.9, also four hours post-exposure) when cellular coverage was complete and cell borders were beginning to appear. Note that neither ciliated or typical nonciliated cells appear; cell surfaces were characterized by a more ragged appearance. Also, many particles still rested upon the epithelium. Figure III.10 shows two areas from the same explant at seven days post-exposure. In Figure III.10A, cells were of irregular size and shape and were covered by numerous microvilli. A few areas (arrows) were free of surface projections and were slightly lower than surrounding cells; these were probably spaces from which flattened squamous cells had recently sloughed. Several cells were slightly rounded with many densely packed microvilli, and more closely reflected the typical morphology of nonciliated cells as seen in control explants. An even more advanced stage of recovery was observed in Figure III.10B, which appeared very similar to unexposed epithelium. Note that several cells projected short cilia (arrows) into the lumen; these may be cells regenerating cilia. Frequently

areas of normal epithelium are observed abutting squamous-type epithelium, with a narrow transition area between the two types, as shown in Figure III.11.

III.3.B Quantitative Classification

In order to more rigorously describe explant morphology, randomly selected areas of luminal surfaces were classified as seen in Table III.2. Four areas from each explant were examined and the incidence of each morphological type recorded. Classifications used are described below. Score 1 (normal epithelium) consisted of both ciliated and nonciliated cells. Cilia were present either free-standing or clumped, presumably with residual mucus present. Nonciliated cells were generally rounded with variable numbers of microvilli and indistinct cell borders. Essentially normal epithelium with less than 50 percent squamous-like epithelium present constituted Score 2. If greater than 50 percent of an area was squamous, but some normal ciliated areas were present, the area was classified as Score 3. In contrast to the other types, Score 4 epithelium was at least 50 percent squamous and contained only nonciliated cells. Cells were generally flattened and cell profiles were polygonal, with distinct cell bounaries consisting of two parallel rows of densely-packed microvilli.

Whereas the previous scores were used to describe apparently stable or end-type epithelia, the following classifications include surfaces undergoing transitions by either losing or gaining cells. Areas characterized by focal desquamation were at least 50 percent

intact, but had focal areas where the epithelium was broken up. Holes between cells were evident and often sloughing cells were observed on the surface. Cilia may or may not be present. When damage was not yet complete, cilia were usually evident and were occasionally observed on sloughing cells. As sloughing progressed, surfaces were typified by complete desquamation in which at least 50 percent of the epithelium was sloughed. Remnants of columnar cells were usually present and were rounded up from the superficial layer of basal cells. Cilia were not observed at this stage. Basal cells were observed to be resting upon the basement membrane, although not completely covering it, were usually elongated, and were occasionally observed to interdigitate among neighbor cells. The classification termed basal cell replacement was used to describe the next stage observed. After complete desquamation, apparent basal cells proliferated to first cover the lumenal surface, then later to form a flattened surface with or without developing cell boundaries. This class at later stages appeared to develop into Score 4 epithelium; the distinction between the two types was made on the basis of the presence (squamous-type) or absence (basal cell replacement) of microvilli covering the flattened superficial cells and lining cell borders.

Examination of Table III.2 shows that the surface morphology of explant epithelium was severely altered by exposure to 20 μg/ml Ni_3S_2. Control explants appeared similar to explant epithelia and *in vivo* tracheal epithelium as described in the literature. When

Scores 1 and 2 were grouped, representing essentially "normal" epithelium, 78 percent of all control explant areas examined fell into this grouping. Immediately after exposure up to 4 hours post-exposure no areas displayed these features. By 20 hours, a limited amount of normal epithelium is present once again, and by 3 to 7 days, fields of view exhibited essentially normal characteristics, with 75 percent of all areas falling into these two classes compared with 78 percent of controls. Equally striking is the alteration in incidence of fields of view containing ciliated cells. All of the control areas had at least one ciliated cell present; the incidence of ciliated cells fell to 0 percent shortly after particle exposure. Regeneration was evident most prominent after 3 and 7 days (87 percent of areas contained ciliated cells) although was first evident after 20 hours. Thus, it appeared clear that normal ciliated epithelium could be regenerated following a single one hour exposure to the low dose of Ni_3S2 used in these experiments.

The early events of epithelial sloughing and regeneration can also be followed by examining Table III.2. Although it was not possible to conclusively describe dynamic events using the "static world" of electron microscopy, it appeared that both desquamation of the normal columnar epithelium and basal cell replacement occured rapidly following the administration of Ni_3S_2 particles. Whereas 4 percent of control explants were desquamating (either focally or globally), 87 percent of all areas were sloughing immediately after particle exposure; this declined to 69 percent after 0.25 to 1 hour,

12 percent after 4 to 20 hours, and essentially no sloughing after 3 to 7 days. Concomitantly, basal cell replacement, not evident in control explants, became common within a few hours, reaching 31 percent and 38 percent of all areas examined after 0.25 to 1 hour and 4 to 20 hours, respectively. Even immediately post-exposure, 12 percent of all areas had increased numbers of basal cells; however, this may represent focal areas of increased basal cell numbers rather than a rapid response to administered Ni_3S_2.

Particles were observed predominantly on the exterior of the mucosal surface. Occasional internal particles were observed in both sloughing cells and residual basal cells. The SEM techniques used in this study were sufficient to image particles only very near the lumenal surface. Particles greater than a few microns into the mucosa (for example, deep within basal cells) or translocated into the submucosa were not imaged in this study. All particles observed in each field of view were confirmed as Ni_3S_2 using x-ray analytic techniques. High magnification imaging, with or without stereopairs, of particles permitted the distinction between internal and external particles. Clearance of particles from at or near the luminal surface overtime was documented by counting particles present in fields of view (see Figure III.12). The number of particles per field of view and percentage of internal particles is presented in Table III.3. Particle loadings were similar up to 1 hour post exposure, with an average of approximately 12 particles observed per field of view. This decreased to 6.3 particles per field of view after 4 and 20 hours

in culture; this decrease in particle loading was significant at the $p \leq 0.05$ level using a one-tailed Student's t-test (Remington and Schork, 1970). A similarly significant decrease was observed at 3 and 7 days, at which times no particles were observed. This absence of particles may be due either to clearance from the surface or translocation of particles into the mucosa and submucosa. Particles were internalized by both columnar cells and basal cells. Columnar cells containing particles were generally sloughing from the mucosal surface, and were observed only at early timepoints post-exposure. Of the 7 and 13 percent of internal particles at the 0, and 0.25 and 1 hour timepoints, respectively, most internal particles were in sloughing cells. Later, after 4 and 20 hours post-exposure, only 2 percent of observed particles were internal. These particles appeared to be exclusively within proliferating basal cells.

III.4 DISCUSSION

Scanning electron microscopic studies of cultured tracheal explants clearly demonstrated that 20 µg/ml of particulate Ni_3S_2 had a potent effect on the respiratory epithelium. Control explants appeared normal throughout all timepoints with varying numbers of ciliated and nonciliated cells present at the luminal surface. This type of epithelium has been reported using SEM by many researchers (Becci et al., 1978; Schiff et al., 1979; and Gabridge et al., 1977). Nonciliated cells appear either rounded into the lumen with generally few microvilli, or as flattened, polygonal cells with distinct

microvilli-lined borders, more typical of a squamous type epithelium (Woodworth et al., 1983; Schiff et al., 1981, 1981b). Ciliated cells, a developmental end-stage cell (McDowell et al., 1980), are observed with varying incidences in various fields of view here and dependent on hamster tracheal anatomic location in the literature (Schiff et al., 1979b; Gabridge et al., 1977). Since cilia are an important factor in particle clearance, different incidences of ciliated cells dependent on location may influence particle clearance studies from explant surfaces as well as studies quantifying cell types in the epithelium, and should therefore be controlled by using large numbers of randomly selected rings or explants consistently taken from the same anatomic location (Gabridge et al., 1977). Several groups have described ciliated cells as being especially sensitive to exposure (Mossman et al., 1979; Kennedy and Allen, 1979; Schiff et al., 1981b). We observed a complete sloughing of ciliated and nonciliated cells but were not able to determine if ciliated cells are more susceptible to damage. Studies conducted by Sorokin and Brain (1975) may be of bearing in this regard. They reported that ciliated cells are most likely involved in phagocytizing and transporting inhaled Fe_2O_3 particles towards the basement membrane. If this were the case, one might hypothesize that increased susceptibility is related to ciliary particle trapping, thus increasing the likelihood of particle/cell contact with resulting deleterious effects.

The severe sloughing of columnar epithelium and subsequent basal cell hyperplasia observed here is consistent with numerous studies in

the literature examining epithelial response to administered particles (Mossman et al., 1977, 1978, 1980, and 1981; and Schiff et al., 1979, 1981, and 1981b). Of interest here is the apparent ability of proliferating basal cells to rapidly differentiate resulting in a seemingly normal epithelium containing ciliated cells. In some fields of view exhibiting regeneration shortened cilia are present; there may be characteristic of a stage of ciliary differentiation (Schiff et al., 1979b). Although regeneration of normal epithelium has been observed in some cases (Schiff et al., 1979; and Gordon and Lane, 1976), another common response is the development of squamous metaplasia (Woodworth et al., 1983). The factors involved in determining whether a normal or squamous-type luminal surface results are not clear but may be related to amount of dose or time of exposure.

Squamous metaplasia can be modelled by culturing explants in a vitamin A deficient medium (Clamon et al., 1974; Woodworth et al., 1983). The luminal surface which results appears similar to the post-exposure morphology described here and in the literature (unpublished observations). Interestingly, the response of squamous epithelium to administered particles is much less marked compared with normal, differentiated epithelium. Woodworth et al. (1983) observed no necrosis of squamous cells after asbestos exposure to culture medium-induced squamous metaplastic explant epithelium. Similar observations were made in our laboratory after a 20 µg/ml Ni_3S_2 dose with 1 hour exposure to vitamin A deficient explant cultures displaying squamous epithelium.

A general clearance of particles from the luminal surface was observed here over the course of several days, with no particles evident at 3 and 7 days post-exposure. Although clearing of particles to the explant margins has been observed (Woodworth et al., 1983), with subsequent particle buildup, this was not observed here. Other clearance routes such as phagocytosis by and/or passage between basal cells and transport to submucosal cells (Woodworth et al., 1983; Mossman et al., 1977) may be operating but were not examined here. It is not clear to what extent epithelial sloughing is a result of general particle loading versus a response to the physical and/or chemical nature of administered particles. The complete sloughing of the epithelium at a low dose, 20 μg/ml Ni_3S_2, suggests toxic response may play a role, in light of the heavier loadings of carbon (Woodworth et al., 1978) and carbon/H_2SO_4 (Schiff et al., 1979) used to obtain similar responses. It is interesting to speculate on the mechanisms leading to epithelial sloughing since few Ni_3S_2 particles are present at the luminal surface (for example, $\bar{x}$ = 11.8 particles per field of view at 0 hr.). Either many particles are quickly transported into the mucosa, or the ratio of particles to cells is much less than 1.0; yet the entire columnar epithelium is sloughed. Additional work addressing the mechanisms of this marked response is indicated.

III.5 CONCLUSIONS

This paper has examined the morphological alterations caused by Ni_3S_2 to the luminal surface of hamster tracheal explants

maintained in tissue culture for up to 7 days after exposure. Compaired with controls, a pattern of early sloughing of columnar epithelium was evident in the Ni_3S_2-exposed samples. Initial sloughing was followed by basal cell replacement which then led to the regeneration of approximately normal epithelium. Although SEM examination revealed particles only very near the respiratory lumen, it was possible to document Ni_3S_2 clearance and internalization within cells over time. Particle clearance mechanisms appeared sufficient to clear particles from the mucosal surface after 3 and 7 days post-exposure. Epithelial sloughing and regneration, or the induction of squamous metaplasia, are responses to external agents widely observed in the literature, and it is not clear to what extent such alterations are due to non-specific particle loading effects versus effects dependent on the physical, chemical, or toxicologic parameters of the agents involved.

Table III.1 Experimental Design Timepoints for Fixation of Tracheal Explant Sections Exposed to Ni_3S_2

Explants Exposed For 1 Hour To:	Timepoints After Exposure[a] 0 min.	15 min.	1 hr.	4 hr.	20 hr.	3 days	7 days
Control (fresh medium)	4	4	4	4	4	4	4
Ni_3S_2 - 20 ug/ml	4	4	4	4	4	4	4

[a] Number indicates number of explant sections per group. Within each group two explants were designated for SEM and two sections for light microscopic histopathology.

Table III.2. Incidence (%) of Epithelial Types[a] in Selected Tracheal Explant Fields of View.

Treatment[b]	Score 1	Score 2	Score 3	Score 4	Focal Desquamation	Complete Desquamation	Basal Cell Replacement
Control (n=28)[c]	39	39	18	0	4	0	0
Ni_3S_2 0 hr (n=8)	0	0	0	0	25	62	12
Ni_3S_2 0.25 and 1 hr (n=16)	0	0	0	0	19	50	31
Ni_3S_2 4 and 20 hrs (n=16)	38	12	0	0	0	12	38
Ni_3S_2 3 and 7 days (n=16)	50	25	12	12	0	0	0

a See text for description of morphological classifications

b Ni_3S_2 dose used was 20 µg/ml. Times given are post-exposure timepoints.

c n refers to number of fields of view per group.

Table III.3. Ni_3S_2 Particle[a] Distribution as a Function of Time in Tracheal Explant Epithelium.

Timepoints (postexposure)	Particles per field of view n ± S.E.	Particles Internal to Epithelial Cells X ± S.E. (%)
0 hr (n=8)[b]	11.8[d] ± 2.5	7.1 ± 3.0
0.25 and 1 hr (n=16)	11.7[d] ± 1.8	13.1 ± 3.1
4 and 20 hrs (n=16)	6.3 ± 1.9	2.1 ± 1.0
3 and 7 days (n=16)	0	—

a Particle dose used was 20 µg/ml

b n refers to number of fields of view per group

c Particles identified as Ni_3S_2 using BSE and x-ray imaging modes

d Values for number of particles with same superscript letter are not significantly different ($p \leq 0.05$, one-tailed student's t-test).

Figure III.1 TRACHEAL EXPLANT ORGAN CULTURES

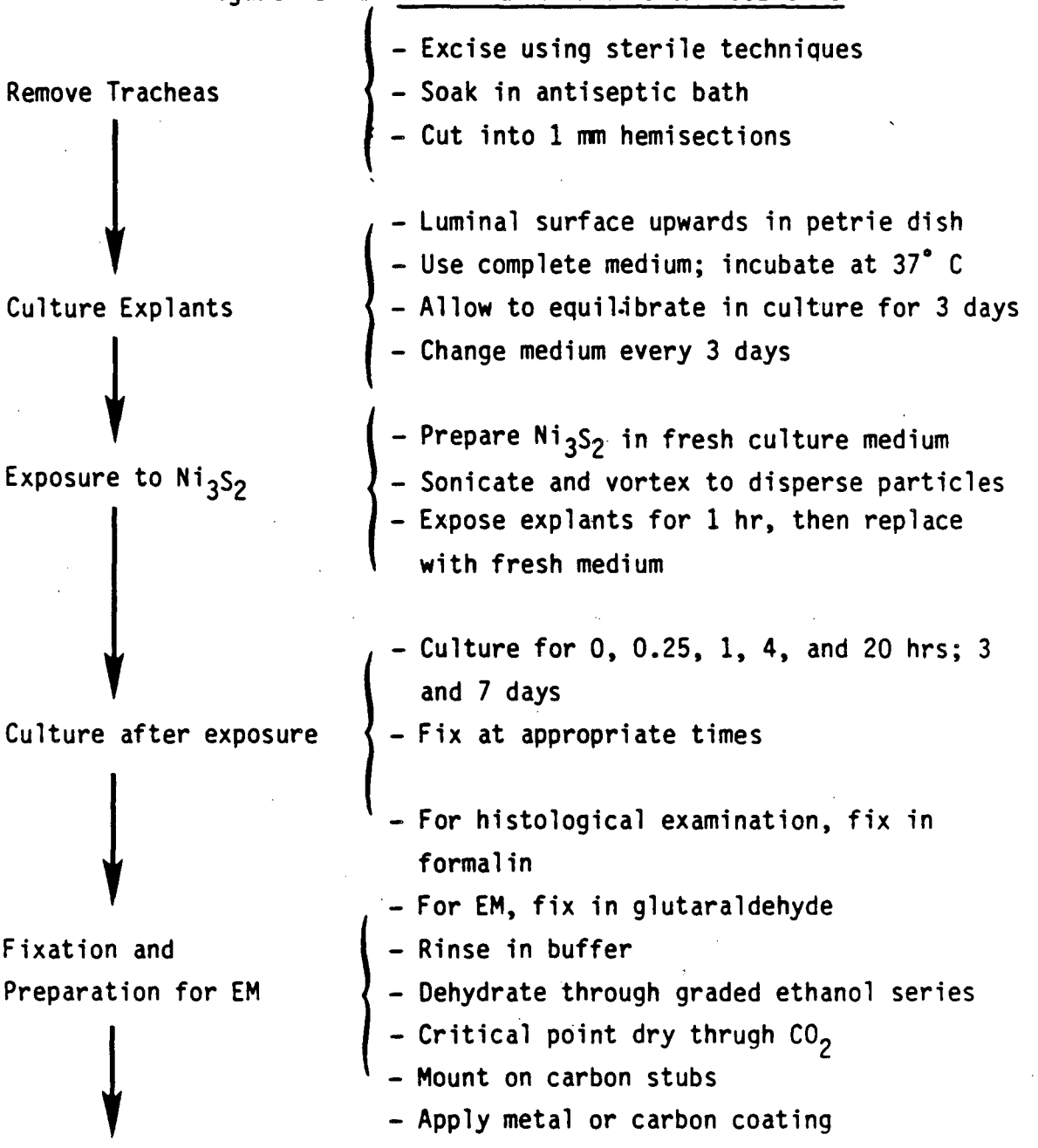

Figure III.1 (continued)

Scanning EM Observation

- Low magnification view for orientation
- Grid overlay plus random number table for sampling area selection
- Image 4 selected areas at 2000X
- For particle-exposed samples, correlate with back-scattered electron image
- Use x-ray microanalysis to confirm particle identity (optional)
- Classify morphological features observed

Transmisson EM Observation

- Embed SEM-examined explant in known orientation
- Thick selection to reach area of interest
- Thin section for TEM
- Stain with uranyl acetate and lead citrate
- Examine multiple sections from each sample

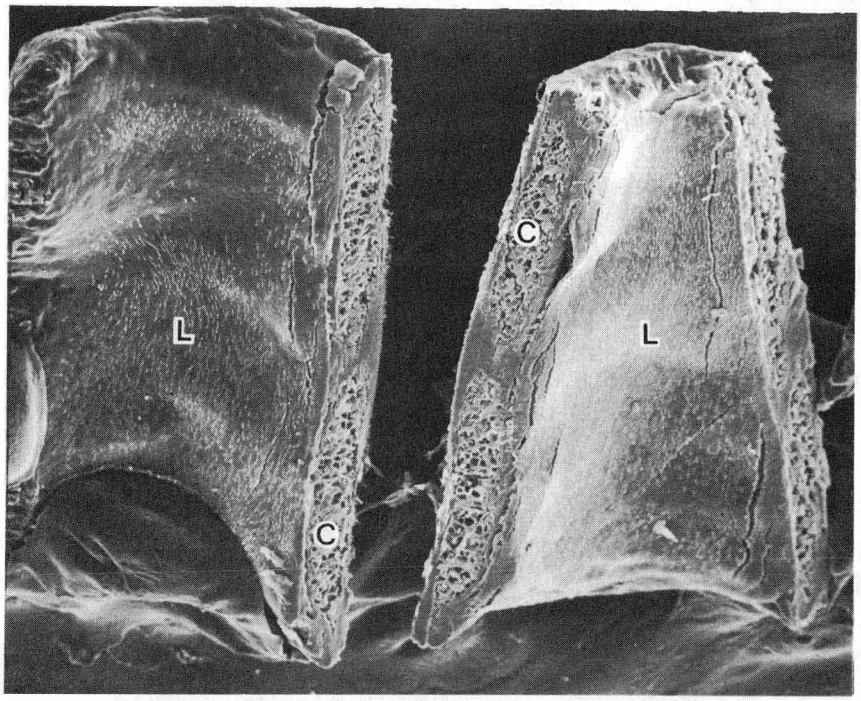

Figure III.2. Scanning electron micrograph (SEM) of explant sections displaying airway surfaces (L) for morphological analyses. At this low magnification ciliated areas appear as light patches. Sections through rings of cartilage (C) are evident where explants have been cut. Bar = 0.5 mm, original magnification = 80 X. XBB 8311-10269A

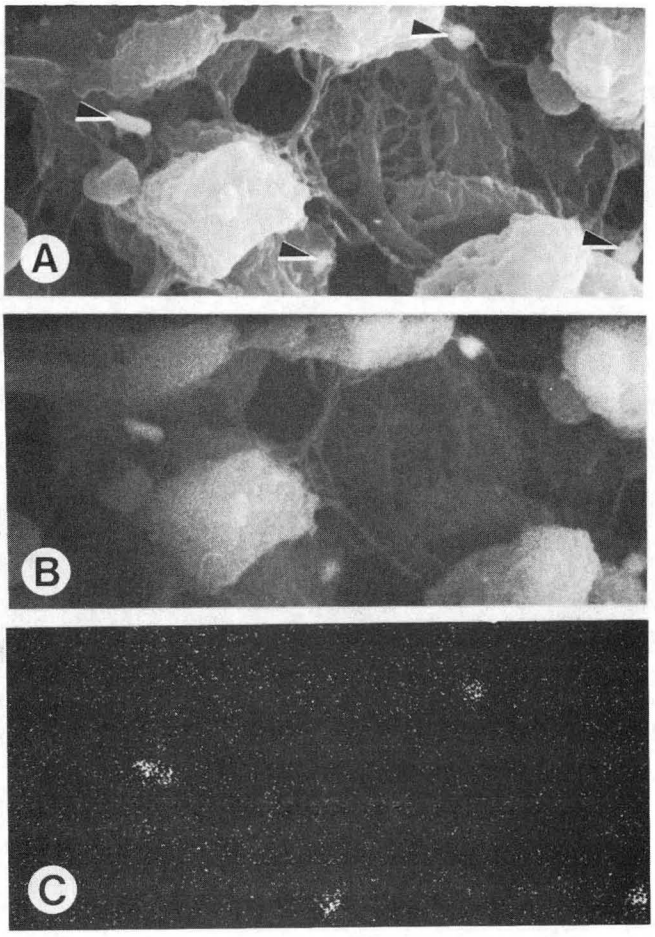

Figure III.3. Various SEM imaging modes used in examining cell/particle interactions. A. Secondary electron image used to assess morphology. Arrows point to four Ni_3S_2 particles. B. Backscattered electron mode gives increased contrast which is useful in locating particles. C. X-ray map for nickel (energy range 7.42 to 7.58 KeV) proving that four particles are present. Bar = 5 μm, original magnification = 4000 X. XBB 8311-10270A

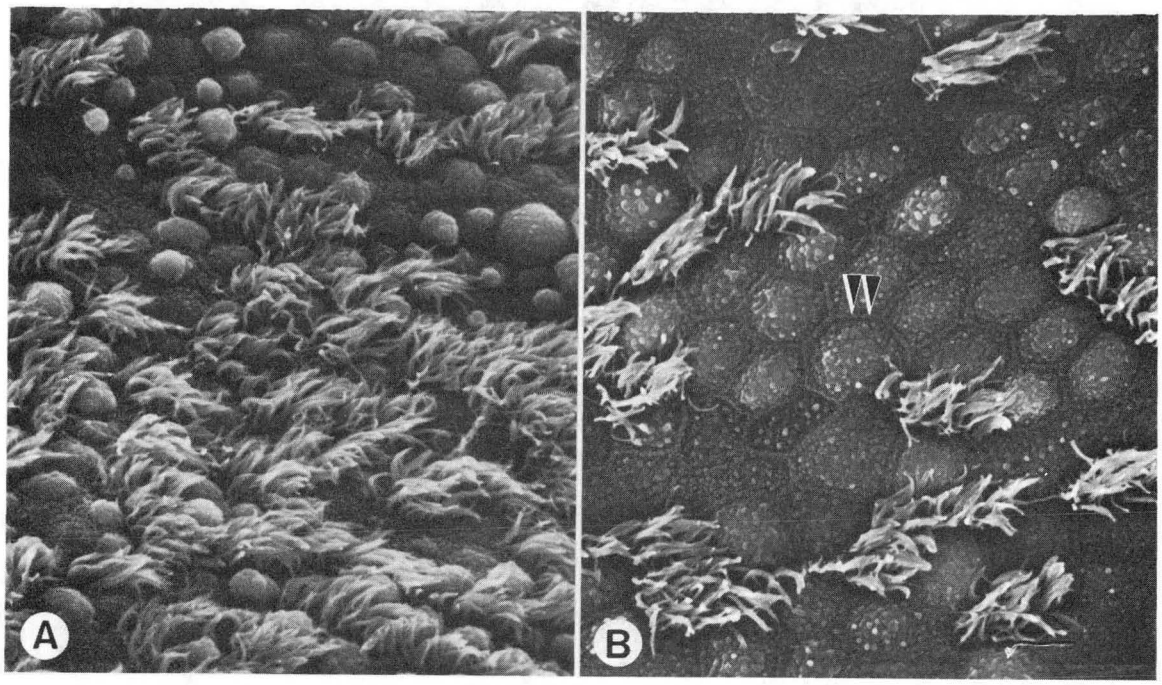

Figure III.4. Lumenal surface of control explants displaying ciliated and nonciliated cells. A. Many of the nonciliated cells are rounded into the lumen. B. Occasionally ciliated cells are sparse and nonciliated cells have polygonal shapes with well-defined cell boundaries (arrowhead). Bar = 10 μm, original magnification = 2000 X. XBB 8311-10272A

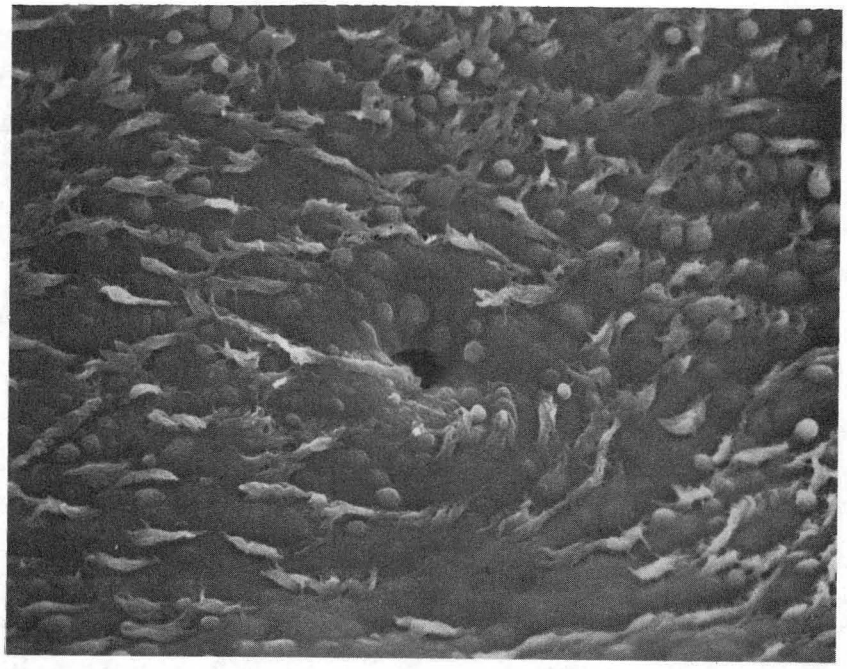

Figure III.5. Explant epithelium exhibiting a submucosal gland opening into the lumen. Note that the cell coverage is continuous into the opening. Bar = 10 μm, original magnification = 1000 X. XBB 845-3405A

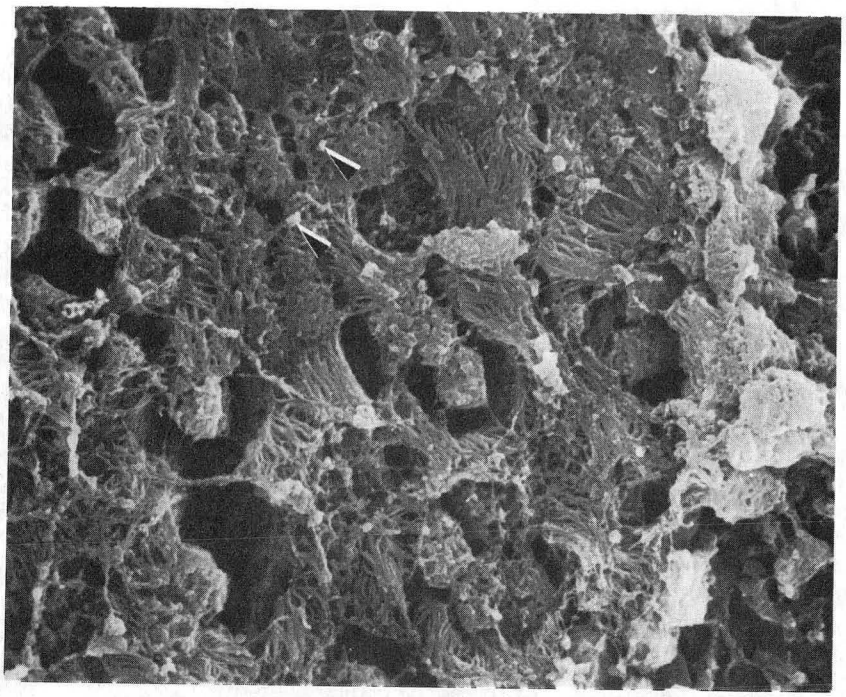

Figure III.6. Tracheal explant immediately after one hour exposure to Ni_3S_2. Cell sloughing is occurring and several particles are present (arrows). Bar = 10 μm, original magnification = 2000 X. XBB 8311-10273A

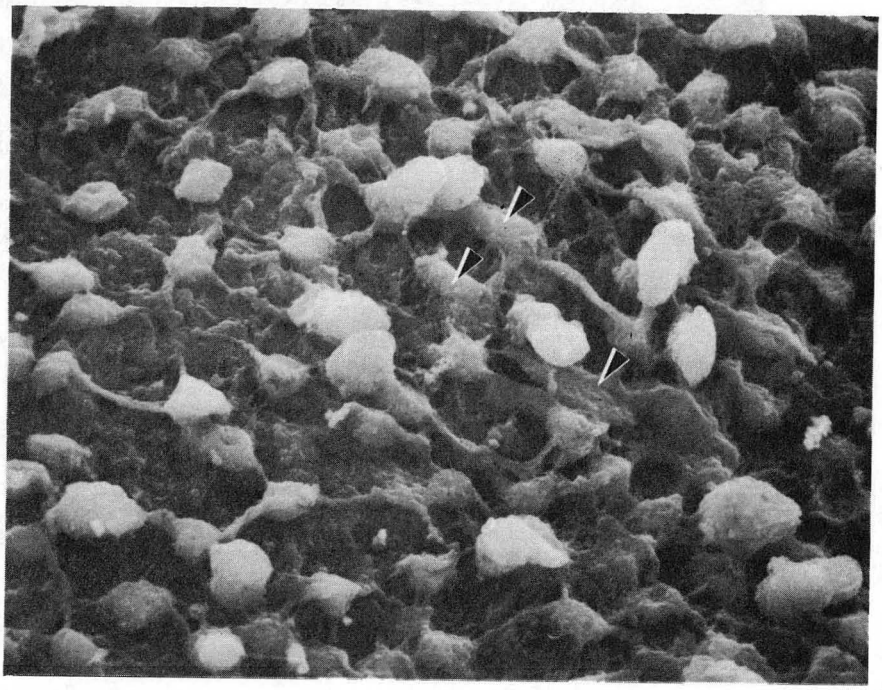

Figure III.7. Explant one hour after cessation of Ni_3S_2 exposure. Most of the differentiated columnar cells are gone and underlying basal cells are visible (arrows). Bar = 10 μm, original magnification = 2000 X. XBB 8311-10274A

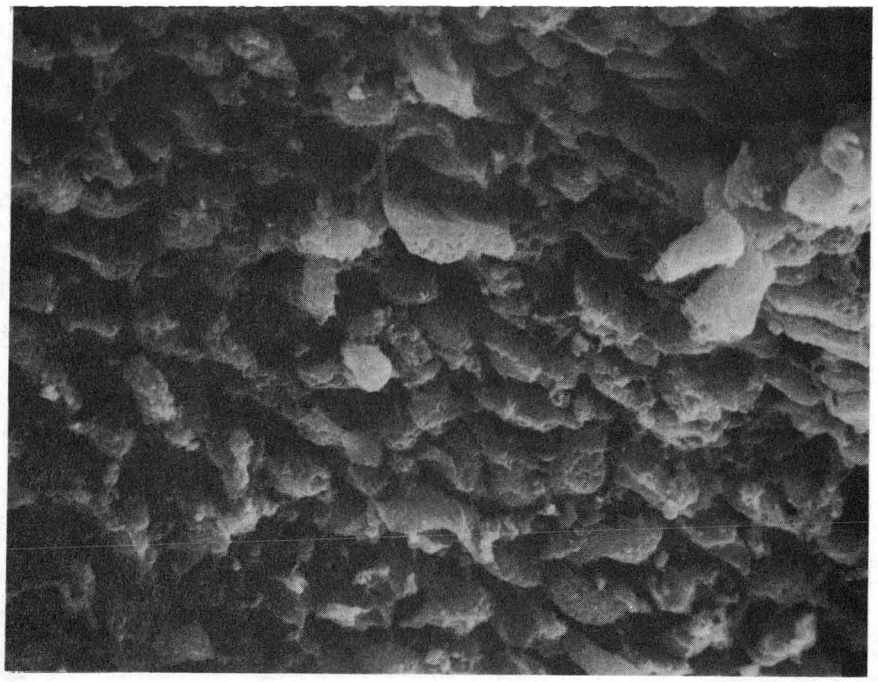

Figure III.8. Explant surface four hours post-exposure. Basal cell coverage is more complete than in Figure 7. Bar = 10 μm, original magnification = 2000 X. XBB 845-3404A

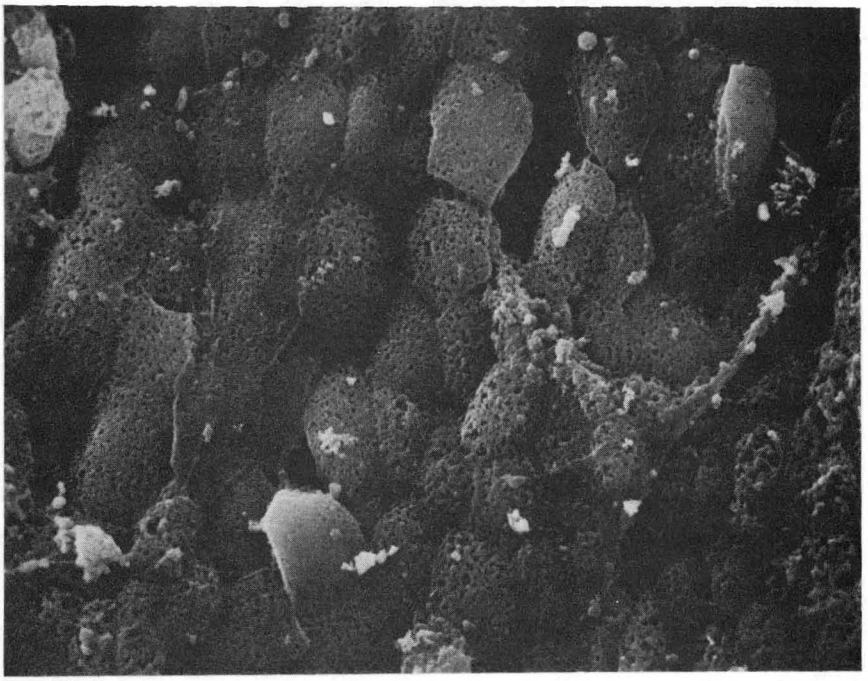

Figure III.9. Four hours after exposure; many Ni_3S_2 particles are still present. Cell coverage is more complete and cell borders are beginning to appear. No ciliated cells are present, and the recolonizing basal cells do not appear typical of either normal or squamous epithelium. Bar = 10 μm, original magnification = 2000 X. XBB 8311-10275A

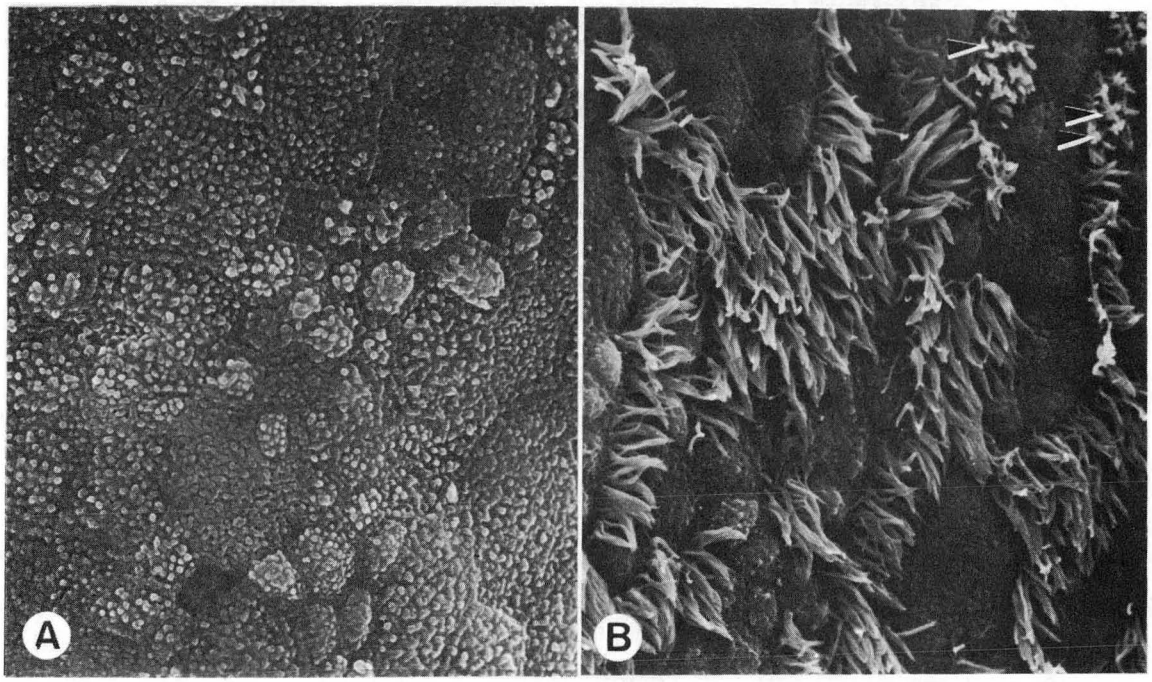

Figure III.10. Two areas from the same explant seven days after particle exposure. At this time no particles are evident at the lumenal surface. A. Cells are of irregular size and shape, with no cilia present. B. Both ciliated and nonciliated cells are present giving the surface a relatively normal appearance. Several patches of short cilia are evident (arrows). Bar = 10 μm, original magnification = 2000 X. XBB 8311-10271A

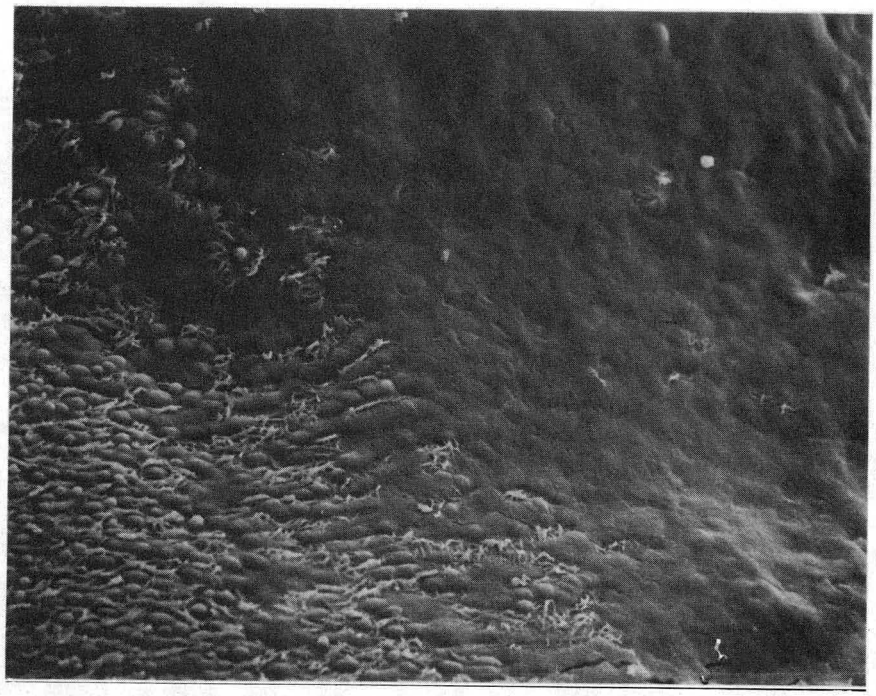

Figure III.11. Lower magnification SEM micrograph showing that the boundary between normal epithelium, with ciliated cells and rounded nonciliated cells, and squamous type epithelium, with few cilia and polygonal cell outlines, can be quite abrupt, with a narrow zone of transition between epithelial types. Bar = 100 μm, original magnification = 500 X. XBB 845-3401A

Figure III.12. Field of view from one hour post-exposure explant used in quantifying Ni_3S_2 particles, circled. Particles were identified using both backscattered electron imaging and x-ray microanalytic techniques. Bar = 10 μm, original magnification = 2000 X. XBB 845-3403A

CHAPTER IV

IN VITRO INTERACTIONS BETWEEN ALVEOLAR MACROPHAGES AND RESPIRABLE PARTICLES

IV.I Introduction

Particles deposited in the distal airspaces are rapidly encountered by alveolar macrophages (AM), and such interactions may be involved in expressions of pulmonary disease depending on the nature of the particular challenge (Brody and Davis, 1982). In this paper we undertake to describe morphological aspects of AM population changes due to administered particles as revealed by electron microscopic techniques. Since AM are highly pleomorphic, and since objective descriptions of cell morphology can be difficult, we have employed classificaton systems to examine the variety of AM shape and feature characteristics. The use of morphologic classes permits the rigorous quantitative description of not only "normal" features and shapes, but also varying degrees of cell surface alterations apparently indicative of cell damage. We have described (Finch et al., 1980) a quantitative classification scheme for the in vitro characterization by scanning electron microscopy (SEM) of human AM lavaged from cigarette smokers and nonsmokers. The quantitation of surface features such as ruffles, ridges, cobblestones, lamellipodia, filopodia, microvilli, blebs, and the shape classes rounded, spread, and intermediate, was acheived through the use of random sample selection. Here we expand this classification system to include surface characteristics apparently indicative of AM degenerative changes.

Many research groups have employed the SEM to explore alterations to AM surfaces caused by exposures to toxic substances. Waters et al. (1975) exposed cultured rabbit AM to several soluble metals (including

Ni^{2+}) and observed alterations in cell surface morphology culminating in complete cell lysis. The authors hypothesized a sequence of morphologically observable events leading to cell death; withdrawal of spread pseudopodia, appearance of surface blebs, membrane smoothing, and final cell breakup. However, the stage at which this progressive damage correlated with cell death was not established. Loss of external membrane integrity, leading to a "moth-eaten" type of cell appearance, has been reported by many research groups in AM exposure to various agents. Hill et al. (1982) found that quartz particles, but not fly ash, caused alterations in canine AM surface morphology, cell death (determined by trypan blue dye exclusion), and release of cytoplasmic enzymes. Quartz-exposed AM exhibited fewer filopodia and were more rounded. The presence of membrane mottling was correlated with internalized quartz particles using SEM backscattered electron imaging. Marked degenerative changes were also observed in rat AM (Miller et al., 1978; Miller, 1979) and peritoneal macrophages (Barhad, 1983) exposed to quartz particles; cells developed bleb-like structures and the loss of normal surface topography. Quartz particles were more avidly phagocytized than crocidolite asbestos, and AM degenerative effects were judged more severe. Similar morphological alterations were observed in bovine AM after chrysotile asbestos exposure by Valentine et al. (1983). Only a small percentage of AM exhibited membrane degenerative changes; however, all damaged cells were associated with asbestos fibers. Exposure to $CdCl_2$ caused morphological alterations to rabbit AM; cells became more rounded, with

more blebs and fewer ruffles, and large defects of the plasma membrane were observed using SEM (Bell et al., 1979). Similarly, AM lavaged from rabbit lungs after inhalation of $CdCl_2$ aerosol displayed increased surface blebbing (Johansson et al., 1983). Lead exposed AM also displayed altered surface features including the loss of surface ruffles, plasma membrane smoothing, and total cell lysis (DeVries et al., 1983). Particles were observed using backscattered electron and x-ray imaging techniques, and it was concluded that particle phagocytosis was required to produce alterations. Finch et al. (1982) and Fisher et al. (1982) have described the morphology of bovine AM exposed to nickel subsulfide (Ni_3S_2) particles in vitro. Cells with particles underwent loss of surface features and membrane damage leading to total cell lysis after a 20 hour exposure. X-ray maps and microanalysis were used to identify Ni_3S_2 particles. At one to three hours culture time, however, occasional undamaged AM with particles were observed, suggesting that degenerative effects were not an immediate effect of AM/Ni_3S_2 particle contact.

Crystalline nickel subsulfide is a potent inorganic carcinogen (Sunderman, 1981) which is apparently more actively phagoytized by cultured cells than amorphous nickel sulfides (Costa et al., 1981; Kuehn et al., 1982). The phagocytosis of crystalline NiS in cultured Chinese Hamster ovary cells has been described by Evans et al. (1982) using time-lapse video microscopy; particles were internalized at sites of membrane ruffling then transported to perinuclear vacuoles. It has

been hypothesized that negative surface charges at crystalline particle surfaces may be directly related to a greater likelihood of particle phagocytosis (Abbracchio et al., 1982), thus leading to increased lysosome-mediated Ni dissolution and expression of toxic or cell transforming effects. The negatively-charged surface of other particle types (amphibole asbestos, quartz) has also been related to the likelihood of phagocytosis (Van Oss, 1978). However, AM phagocytized and respond to not only crystalline particles but a wide range of particle types (Brody and Davis, 1982), and the cytotoxic potential may also involve factors independent of increased phagocytic uptake.

It is generally acknowledged that in response to various stimuli AM can release cytoplasmic constituents into the extracellular environment. Furthermore, this release may play a role in initial pulmonary responses, such as inflammation, to administered particulate materials (Brody and Davis, 1982). Kang et al. (1979) observed the release of lysosomal hydrogenases from cultured rabbit AM following exposure to beryllium and asbestos. Such release was not associated with increased enzyme synthesis and the researchers concluded that degrative alterations to the plasma membrane were responsible. Similarly, Barhad et al. (1983) hypothesized that quartz particles had cytotoxic effects at the level of the molecular components of the plasma membrane. In neutrophils, Henson (1971) observed that the release of cytoplasmic granules was correlated with the formation of spherical blebs at the cell surface; such cells often remained viable (as determined by trypan dye exclusion) even though a considerable

amount of cytoplasm was extracted. As discussed above, several groups employing electron microscopic techniques have observed blebs in exposed, cultured AM cells undergoing degeneration and lysis (Waters et al., 1975; Bell et al., 1979; and Miller et al., 1978). In our studies, we observe and characterize surface blebs as the initial morphologically identifiable change evident at the cell surface leading to complete cell lysis and death. Furthermore, we expand on previous morphological characterizations of exposed AM cultures that (1) cells examined by SEM were previously identified as live or dead using light microscopy (LM), (2) objective feature classifications were used to describe AM populations, and (3) selected cultures were examined by conventional and high voltage transmission electron microscopy (CTEM and HVEM, respectively) following LM and SEM analysis. In conjunction with SEM and x-ray analyses, information relating cell viability, morphology, and particle content were accumulated. Several studies using correlative microscopy have been descrbied. Thorin and Holma (1983) examined AM attached to oriented plastic culture dishes and viewed by both vital dye-staining LM and SEM/x-ray analysis. Individual cells were successfully followed through LM and SEM, and the differences between viable and nonviable AM were described. Since cell populations were adherent to thick plastic culture dishes, no attempts at TEM analysis were possible. Kumon et al. (1983) employed similar techniques in examining human exfoliated urothelial cells. Cellular surface structures were correlated with the Giemsa-stained LM appearance following LM photography and conventional SEM preparation.

Many investigators have employed whole cell mount techniques which correlate SEM with TEM of intact, critical point dried cells grown on or plated onto thin substrates. These techniques permit investigators to visualize both the interior and exterior of intact cells at high resolution with a minimum of cellular disruption. Adler et al. (1979) examined formvar-adherent particle-exposed human AM using SEM, back-scattered SEM, and whole mount TEM, in order to visualize internalized particles. The authors determined that flattened AM were more efficient phagocytes when compared with rounded cells. Correlative SEM/stereoscopic TEM examinations of blood platelets were described by Lewis et al (1980). Cytochalasin B treated, formvar-attached cells exhibited numerous bleb-like structures, which by TEM were characterized as organelle-free. Pudney and Singer (1979) employed similar techniques to visualize the cytoskeleton of detergent-extracted myoblasts; the precise correlation of specific structures by SEM and TEM was demonstrated. Finally, Wolosewick and Porter (1977) characterized human diploid cells using SEM and HVEM techniques. Cell ultrastructure was observed to be heterogenous between individual cells.

IV.2 MATERIALS AND METHODS

IV.2.A Cell Collection. Pulmonary alveolar macrophages (AM) were obtained from excised bovine lung lobes using bronchopulmonary lavage techniques (Fisher et al., 1982, 1978; Myrvik et al., 1961). A 15 ga. sterile blunt needle was sutured, into the lobar bronchus and the lobe washed with 50 ml aliquots of ice-cold Ca^{++}- and Mg^{++}-free phosphate

buffered saline (PBS, Grand Island Biological Co. (GIBCO), Grand Island, NY) to a final lavage effluent of 500 ml. The lavage effluent was held in 250 ml centrifuge tubes over ice during lavage, then centrifuged at 1100 rpm (300 g) for 30 minutes. The supernatant was decanted and the cell pellet resuspended in cold PBS. Viability of the cell population was determined by the ability of live cells to exclude dye (0.4 percent trypan blue dye, GIBCO) from the nucleus. The total number of cells lavaged was determined by a hemacytometer count. A cell smear was stained with Wright's stain (Sigma Chemicals, St. Louis, MO) for a differential count; typically AM constitute at least 95 percent of the lavaged cell population in healthy bovine lungs. Any lavage effluents containing less than 95 percent AM were excluded from these studies.

After cell counting, 4×10^5 viable AM were seeded into sterilized Leighton tubes containing 35 x 10.5 mm glass coverslips covered with 1 ml complete medium consisting of 79 percent minimal essential medium (GIBCO) with 1 percent penicillin-streptomycin (GIBCO), 1 percent l-glutamine (GIBCO), and 20 percent heat-inactivated fetal bovine serum (Flow Laboratories, McLean, VA). For some experiments, coverslips with formvar-coated finder grids were used for monolayer cultures. Formvar films were prepared by dissolving 0.5 percent formvar resin (Ted Pella Inc., Tustin, CA) in 1,2-dichloroethane (JT Baker, Phillipsburg, NJ), floating a thin film onto clean water, applying a 135 mesh copper finder grid (Ernest Fullam Inc., Schenectady, NY), then picking up the grid and film with a

cleaned coverslip. Coverslips thus prepared were rinsed with ethanol and dried in a UV hood to sterilize before being inserted into sterile Leighton tubes. Previous studies indicated that AM are not morphologically distinct when cultured on formvar substrates when compared with glass substrates.

After seeding cells, cultures were allowed to attach to substrate for 1 hour at 37°C, then the culture medium was decanted and tubes were washed 2 times with 1 ml of Hank's buffered salt solution (HBSS, GIBCO) prewarmed to 37°C, and finally refilled with 1 ml fresh complete medium. At this point AM populations were ready for exposure to test particles.

In some experiments, AM were lavaged from male stain A/J mice (Jackson Laboratory, Bar Harbour, Maine, age 8-10 wks, wt. ca. 25g) at various timepoints following in vivo exposure to Ni_3S_2. Mice were exposed using an intratracheal intubation technique (Ho and Furst, 1973) in which particles were suspended in PBS then introduced just proximal to the carina (for a complete description see Fisher et al., 1982). After various periods AM were lavaged, assayed, and allowed to settle onto glass coverslips for one hour (as described above) before chemical fixation for SEM.

IV.2.B In Vitro Particle Exposure. After the initial 1 hour attachment period, AM were exposed to test particles. Particles used were Ni_3S_2 (INCO Co., Canada; VMD = 1.83 μm, σ_g = 2.3; prepared as described in Fisher et al., 1982), TiO_2 (Alfa Products, Danvers, MA; VMD = 1.57 μm, σ_g = 2.3 after grinding, settling, and sizing by

C. Democko, Batelle Laboratory), and glass beads (1-4 μm, Particle Information Services, Grants Pass, OR). Particle exposures employed are listed in Table IV.1. For dose preparation, milligram quantities of test particles were weighed on either a Perkin-Elmer autobalance (Perkin-Elmer Corp., Model AD-2Z, Norwalk, Conn.) or on a Sartorius balance (Westbury, NY) in a negative pressure glove box for Ni_3S_2 weighings. Particles were weighed into sterile dose vials and diluted to the proper concentrations using sterile PBS, then sonicated for 10 minutes and vortexed immediately before dose withdrawal. All particle suspensions were made within 2 hours of use to decrease particle solubilization into the PBS. Particle exposures were carried out for varying periods (see Table 1) before AM cultures were ready for either chemical fixation or viability assay.

IV.2.C Viability Assay Techniques. Several AM cultures were designated for assessment of individual cell viability to permit correlation with SEM morphology and particle burden. At appropriate timepoints, coverslips were removed from the Leighton tube and a small portion of glass was broken off, rinsed in PBS, and plunged into room temperature fixative (described below). The remainder of the coverslip, containing the formvar-coated finder grid, was inverted into a few drops of trypan blue dye in a concave micro culture slide (Arthur Thomas Co., Philadelphia, PA) and viewed with a Nikon light microscope. The grid was scanned for areas with intact formvar, good cell coverage, and as many dead cells as possible. Since live cells predominated, it was desirable to maximize the number of dead cells included in the

analysis. Appropriate areas were photographed at approximately 130 times magnification using Polaroid Type 108 color film, and dead cells were identified on the micrographs by a pinprick for subsequent localization after SEM processing. Cell cultures were left inverted in the trypan for not more than 10 minutes before being rinsed with room temperature PBS then plunged into room temperature fixative. Cells successfully survived this treatment since the number of dead cells was constant during the 10 minute period (indicating no additional cell death occurred due to this treatment).

IV.2.D SEM Preparation. Cell monolayer preparation techniques used were similar to those developed for cultured human AM (Finch et al., 1980). Initial cell fixation was carried out for at least 2 hours at room temperature with 2.3 percent glutaraldehyde in 0.05M sodium cacodylate (CAC) buffer (Electron Microscopic Services, Fort Washington, PA) pH 7.4, 360 mOsm osmolarity (Bastacky et al., 1983). Cell cultures were stored in fixative at 4°C until preparation was initiated by two 5 minute rinses in CAC buffer (with sucrose added to produce a 360 mOsm solution). Glass-adherent samples were then dehydrated through a graded series of ethanol rinses, 10 minutes per rinse, in 25 percent, 50 percent, 75 percent, 90 percent, 95 percent (2X) and 100 percent (3X) ethanol in doubly distilled, deionized water. Samples were transferred to a Polaron critical point dryer (Polaron, Wateford, England) in 100 percent ethanol, where substitution with CO_2, flushing, and drying were carried out using methods described by Anderson (1951). Coverslips were then removed, broken,

mounted onto acetone-washed aluminum samples stubs, and coated with ca. 10 nm of platinum using a cool diode sputter coater (Polaron E5100, Wateford, England). Samples were then ready for examination by SEM.

Similar preparative procedures were used for formvar-attached cell populations. After initial CAC rinses, the same graded series of ethanol rinses were employed, but for only 3 to 5 minutes per rinse to reduce possible formvar solubilization into the ethanol. Following critical point drying, the formvar-coated grids were carefully removed from the coverslip substrates and placed on the rotating, tilting stage of a vacuum evaporator (Denton DV-502, Cherry Hill, NJ) and carbon coated by evaporation. Also, some grids were prepared for whole cell mount transmission electron microscopy (TEM) as described below.

IV.2.E SEM Analysis. Following preparation, AM populations were ready for SEM examination. Conventional secondary electron images were made at a 20 keV accelerating voltage using an AMRay 1000A SEM (AMRay Inc., New Bedford, MA) using Polaroid Type 55 P/N film and equipped with an energy dispersive x-ray microanalytic system (NEC detector, KEVEX 5100C spectrometer, and Digital Equipment Corp. PDP 11V03 computer). Individual AM cells were examined and the presence of test particles confirmed by x-ray mapping and/or by microanalysis with the beam as follows. The electron beam was placed in reduced raster mode on each cell for 15-30 seconds to see if characteristic x-ray peaks were generated (Ni for Ni_3S_2, Ti for TiO_2, and Si for GB). It was almost always possible to image particles using SEM

and backscattered electron SEM in conjunction with the LM viability map. In some cases x-ray mapping was performed (energies mapped were 7.42–7.58 keV for the Ni Kα peak, 4.46–4.60 keV for the Ti Kα peak, and 1.68–1.82 KeV for the Si Kα peak; with no background noise subtraction).

For glass adherent AM populations, a quantitative analytic technique was employed to correlate particle burden with morphologic damage. For each individual cell examined, the particle burden was first established by x-ray microanalysis. Attempt was made to determine if particles were present internal, external, or both internally and externally to the cell. The extent to which the cell membrane was intact or damaged was then assessed. Intact cells had generally smooth membranes, with a variety of surface features present including ruffles, filopodia, lamellipodia, microvilli, and blebs as described in murine and human AM populations (Finch et al., 1983). No membrane tears, bleb clusters, or cell degranulation appeared in AM classified as intact. In contrast, cells characterized by mild damage exhibited slight degranulation or membrane tearing. Degranulation occurred focally or multifocally and often gave the appearance of spherical blebs resting on or emanating from cell surfaces. Jagged membrane tears were occasionally observed near such areas and appeared to be distinct from tears often observed in peripheral areas and thought to be an artifact due to cell shrinkage during critical point drying. The remainder of these mildly damaged cells, greater than 50 percent of the cell surface, appeared normal. Severely damaged

cells, on the other hand, had little if any intact surface. Extensive degranulation with accompanying membrane disruption was observed. Many cells had a "moth-eaten" appearance as described by other researchers (Hill et al., 1982; Valentine et al., 1982). Occasionally cellular organelles and nuclei were found to bulge up from degranulated areas. Data relating particle content were correlated with individual AM morphological classification in a tabular format to assess the degree to which particle association was related to the disruption of normal cell architecture.

A morphological classificaton system (Finch et al., 1980) was used to describe AM populations lavaged from Ni_3S_2-intubated mice, settled onto glass coverslips, and prepared for SEM as described above. For detailed morphological analysis fifty cells per sample were randomly selected and viewed at 0° tilt to quantify the percent incidence of various features, including surface ruffles, filopodia, blebs, microvilli, and featureless cells. Degrees of cell spreading along the coverslip were determined by using three shape profile classes, spread, rounded, and intermediate.

Cell populations examined using the viability assay technique were observed by SEM while adherent to the same formvar-coated finder grids photographed by light microscopy. Cells identified as dead were marked by pinpricks on the light micrographs and were easily located by SEM. Each cell included in the light micrograph was then analyzed for particle content. Particles observed were verified as test

particles by elemental composition, and were identified as being internal or external to AM through the use of high tilt and stereopair imaging.

Samples prepared for HVEM (see below) were first prescreened by SEM and conventional TEM with the intent of locating AM in several different stages of particle association. These stages of particle ingestion are described by Stossel (1975) and include cell-particle adhesion, formation of pseudopodia to engulf particles, internalization of particles into phagosomes, and sequestering of phagosomes within the cytoplasm.

IV.2.F Whole Cell Mount TEM. Selected AM cultures mapped for viability were prepared for the TEM by altering the fixation protocol described above (modification to Wolosewick and Porter, 1979) Following fixation in glutaraldehyde and two CAC buffer rinses, coverslips were postfixed in 1 percent OsO_4 (Electron Microscopic Services, Fort Washington, PA) in 0.05 M CAC for 3 minutes. After staining, cultures were again rinsed twice in fresh buffer then dehydrated, critical point dried, and carbon coated by evaporation on both sides. Samples exposed to particles, or unexposed grids were prescreened by SEM to identify either live or dead cells in various stages of phagocytosis. Grids were imaged at 1.2 to 1.5 MeV on a Kratos EM1500 (Kratos, AEI, England) or at 80 to 100 KeV on a Zeiss EM 10A (Zeiss, NY), both in standard bright field imaging mode using a double tilt stage and Kodak SO136 film. Stereopair TEM micrographs were routinely employed and were necessary to interpret three

dimensional cellular organization. Unstained grids and grids postfixed by exposure to OsO_4 vapor were also examined in preliminary studies, but appeared inferior to grids prepared as above.

IV.3 RESULTS

The interactions between bovine AM cells and respirable particles (Ni_3S_2, TiO_2, and GB) were observed using correlative microscopic techniques. Cell populations were successfully examined first by trypan blue dye-staining LM (Figure IV.1A) to determine viability, by SEM following glutaraldehyde fixation, osmication, and critical point drying (Figure IV.1D,F,G), then using either CTEM or HVEM to view internal ultrastructure (Figure IV.1E). It was therefore possible to examine not only the SEM-revealed external interactions between particles and AM known to be live or dead at the time of fixation, but also to observe the internal sequestration of phagocytized particles. The phagocytic process, as described by Stossel (1975, 1976) and Evans et al. (1982), appeard similar for the three particle types, with recognizable adhesion, pseudopod formation, engulfment, internalization to phagolysosomes, and transport to perinuclear areas. The differential effects of the administered particles were clearly evident at the SEM level of examination. Although AM were observed to attach to and phagocytize all particles, Ni_3S_2 was generally associated with cellular architecture and death, GB induced no obvious deleterious effects, and TiO_2 exhibited intermediate effects. The techniques used to identify particles are illustrated in Figure IV.2.

IV.3.A Qualitative Observations of Surface Alterations The following sequence of morphological events leading to AM disruption were observed. These events were most evident in in vitro exposed, Ni_3S_2-associated cells, although were present to a lesser extent in TiO_2 and GB-exposed as well as control preparations. In vitro AM/particle exposure experiments are summarized in Table IV.1. The least severe alteration to intact AM surface morphology was the appearance of focal bleb clusters, consisting of small (<0.5 μm) spherical blebs, either emanating from or attached to the plasma membrane (see Figure IV.3B and D). Such clusters were often associated with jagged membrane tears or holes, and were found on both flattened and rounded AM. Bleb formation appeared to progress in some cells to include either multifocal or large, widespread patches of blebs. At this stage, cells were generally more rounded, and spherical blebs were evident as debris on the coverslip immediately adjacent to the afflicted cell. However, the nuclear membrane was usually intact at this stage, and such cells were thus identified as live. The next morphological stage represented the difference between mild and severe damage in the quantitative classification system and was more often associated with cell death. Cells lost typical surface features, such as ruffles and pseudopodia, as degranulation proceeded, and the plasma membrane exhibited marked degenerative changes. Numerous pits, holes, and/or tears gave the cells a "moth-eaten" appearance; often, rounded bulges (larger than surface blebs) were evident in the cytoplasm, giving the appearance of a cell packed with spheres. This progressed

to complete cellular disruption, with the nucleus either exposed or washed away, and a number of microfilaments and sites of attachment to the substrate revealed as the bulk of the cell was removed (Figure IV.3G and H). At this stage, AM were either dead or enucleated. Further examples of AM degradative alterations are shown in Figure IV.4.

IV.3.B Quantitative Analyses

The association between AM alteration and particle content is presented in Tables IV.2 and IV.3. Within each experiment, culture times and doses were pooled. In all three Ni_3S_2 exposures, particle content was correlated with AM alteration ($p < 0.001$), verifying the observations made above. Although GB were not correlated with cell damage, the association with TiO_2 was significant at the $0.01 < p < 0.05$ level. Thus, although not as pronounced as Ni_3S_2 effects, TiO_2 particle association did result in altered AM surface morphology.

As evident from Table IV.3, control AM cultures contained cells (24 ± 3.8%) with altered morphology, primarily bleb clusters. Similar percentages of degrading AM not associated with particles were observed in Ni_3S_2 (25 ± 2.9%), GB (22 ± 1.4%), and TiO_2 (26%) cultures, leading us to conclude that particle solubilization into the culture medium, if it exists, does not play a role in the alteration of AM not directly in contact with particles.

Table IV.4 presents data relating particle burden and cell viability on an individual cell basis. Cultures were pooled (1 and 3

hour periods in experiment II, 2 and 20 hour periods in experiment IV) since no differences between the periods were obvious, and since it was desirable to include more dead cells in the analysis. When the association beween Ni_3S_2 (2 experiments), TiO_2, or GB and AM viability was examined, only Ni_3S_2 (in one experiment, $p < 0.01$) content was correlated with cell death. There was a suggestion ($0.05 < p < 0.10$) of TiO_2 association with cell death. However, when particle internalization (as determined by SEM analysis) was correlated with cell death, a significant association between Ni_3S_2 (both experiments $p < 0.001$) and TiO_2 ($p < 0.05$) was observed. Few dead cells were observed in GB-exposed cultures, and GB uptake did not appear to be cytotoxic. In Table IV.5 the percentage of non-viable AM in experiment IV is presented. Ni_3S_2 cultures contained significantly more ($p < 0.05$) dead cells when compared with GB-exposed or control cultures; the number of dead AM in TiO_2 cultures was greater than although not significantly different from either GB or control cultures. It therefore appears that the individual cell burden correlated with particle internalization, in which phagocytized TiO_2 was associated with cell death, is a more sensitive indicator of cultured AM response to administered particles.

Male strain A/J mice were intratracheally intubated in three different experiments with either one or multiple Ni_3S_2 doses, then pulmonary lavage was performed from 2 to 5 weeks after the last exposure to recover free lung cells. After attachment to glass coverslips and preparation for SEM, a quantitative morphological

classification system (Finch et al., 1980) was employed to characterize cell populations. In over 800 cells analyzed only one was observed to contain Ni_3S_2. The results of the morphological analyses are presented in Table IV.6. Within each experiments (V, VI and VII) the relative Ni_3S_2 dose is ratioed to the lowest dose (defined as =1.0). The incidence of blebs was observed to increase with increasing Ni_3S_2 dose, reaching a level in the highest doses of approximately two times the control incidence. Conversely, the percent incidence of both ruffles and rounded cells appeared to decrease with increased Ni_3S_2 dose. The incidence of other features (filopodia, microvilli, craters, cobblestones, featureless or multiply featured cells, or spread AM) appeared independent of Ni_3S_2 dose level. The significance of these observations is assessed in Table IV.7, in which a linear regression between Ni_3S_2 dose and various features is plotted. The values of the fitted line slope and the correlation coefficient r^2 give a measure of goodness of fit for the calculated linear correlation (Remington and Schork, 1970). A two-tailed Student's t-test was used to test the hypothesis that the fitted line's slope = 0. In experiments V and VI the slope of the line relating Ni_3S_2 dose with bleb incidence was significantly different ($p < 0.05$) from zero, indicating a relationship existed between the two parameters. Similarly, a relationship existed between ruffles and rounded cells in all three experiments.

IV.3.C Whole Cell Mount TEM

Osmium stained, critical point dried AM revealed a rich diversity of internal detail when observed by CTEM and HVEM (Figures IV.5-7). The 1.2 - 1.5 MeV HVEM beam successfully penetrated cell nuclei and the thick perinuclear cytoplasm, which was frequently packed with electron lucent spherical vacuoles. In contrast, the 80 - 100 KeV CTEM could not completely image thick, central areas, but was useful for more spread areas of AM cytoplasm. Stereoscopic imaging proved essential to understand the complex arrangement of AM features. Pseudopodia at the cell margin were evident, as were the lightly carbon coated surface ruffles and blebs. These structures projected above the cell surface and were evident as areas of increased electron density. A three dimensional network of interconnecting filaments of varying diameter was observed to fill the cytoplasm; interspersed within this network were vacuoles, electron-dense osmophilic granules (lysosomes?), elongated mitochondria, endoplasmic reticulum, and numerous ribosomes associated with microfilaments. As mentioned above, vacuoles (usually 0.8 - 1.0 μm, but ranging up to 3 μm) were most common in the thick perinuclear cytoplasm, but were also found in roughly linear orientations aligned between the nucleus and pseudopodial extentions along the formvar substrate. Osmophilic granules were of two basic types, dense clusters of ca. 0.2 μm granules free in the cytoplasm, and slightly larger (0.2 - 0.5 μm) single granules located in the center of vacuoles. The finest microfilaments (5-10 nm) formed a cytoplasmic-filling meshwork of

strands identical in appearance to the microtrabecular lattice described by many researchers (for example see Wolosewick and Porter, 1979).

When present, particles could be seen as electron dense spheres (GB) or irregular (Ni_3S_2 or TiO_2) bodies associated with AM. Cells with particles were examined at various stages of phagocytosis as determined by SEM (Figure IV.7). External particles were clearly seen above or to the side of the main body of a cell. Occasional bleb clusters associated with sites of particle uptake were observed either at the AM surface or on the formvar. Such blebs had no apparent internal structure, contained no organelles, and when associated with the AM surface, there were no unique morphological features evident immediately internal to the clusters. Internalized particles were most commonly located within vacuoles, and less frequently appeared to be free within the cytoplasm. Occasionally vacuoles were evident directly beneath the site of phagocytosis. Particles were often within vacuoles in the dense perinuclear area, and since most phagocytic events were in marginal areas, perinuclear particles were probably internalized long enough for vacuole inclusion and phagolysosome transport as described by Evans et al. (1982). Spherical glass beads, which were generally larger than Ni_3S_2 and TiO_2, were difficult to distinguish as being internal or external to AM vacoules. There were no apparent differences in the way in which AM sequestered TiO_2 versus Ni_3S_2 particles.

Severely damaged cells were also observed by TEM (Figure IV.6), and were clearly different from intact cells in that the cytoplasm-filling meshwork of filaments was either partially or completely unrecognizable. Often, cells were enucleated and consisted only of amorphous, spherical, large cytoplasmic (several μm) granules, corresponding to the degranulated appearance observed by SEM. Internal particles could usually be identified in such cells.

IV.3.D Methodological Considerations

It was found that approximately 23 percent of all fully hydrated AM identified by LM had detached from the formvar substrate. This could be due to an artifact of processing independent of cell status, an artifact in which live or dead cells were preferentially detached, or an artifact associated with particle content. Chi square contingency tests were performed to determine which parameters may be associated with AM detachment (see Table 8). Although in experiment IV there was an indication of association between viability and detachment ($0.05 < p < 0.10$) for all cells, there were no significant associations observed at the $p < 0.05$ level. Thus, although there may exist a tendency for dead cells to preferentially detach, in general detachment may be a result of mechanical stresses involved in SEM preparation.

Examination of large numbers of AM populations cultured on both glass and formvar substrates has shown no apparent morphological differences dependent on substrate. In our laboratory, we observed no differences between glass vs. formvar in the incidence of various

human AM features (B. Clark, unpublished observations). In the present study, we employed the morphological classification system desribed above to examine control AM (from experiment IV, 2 hour culture) cultured on glass, on formvar, or on formvar with trypan exposure. The results of duplicate analyses are presented in Table 9. It is clear that there are no major differences between substrate and/or trypan blue dye exposure on either the tendency of AM to spread, as evidenced by the incidence of round, spread, or intermediate cells, or the expression of surface features such as ruffles, filopodia, or blebs.

IV.4 DISCUSSION

The alveolar macrophage is an important component of the pulmonary response to administered particles (Brody and Davis, 1982) and it is therefore of interest to characterize alterations in AM morphology related to exposures. As discussed in the introduction, many research groups have employed SEM in such studies (Waters et al., 1975; Hill et al., 1982; Miller et al., 1978; Bell et al., 1979; DeVries et al., 1981; and Fisher et al., 1982). Decriptions of AM disruption after exposure to toxic agents often include cell rounding, bleb formation, membrane smoothing and/or breakup, and complete cell lysis. Our studies generally confirm these observations. Furthermore, we expand on subjective evaluations by employing quantitative morphological classifications which are statistically associated with cell viability, particle content, and internal ultrastructure on an individual cell basis. Alveolar macrophages were exposed in vitro to Ni_3S_2,

TiO_2, and GB. In all cases, both external and internal particles were observed using SEM and whole cell mount TEM. There was a significant association between Ni_3S_2 content and the AM damage markers consisting of focal blebs clusters, membrane mottling, and degranulation, whereas the less bioreactive GB exerted no such effects. Similarly, Ni_3S_2 and TiO_2 internalization was significantly associated with cell death, with GB apparently nontoxic. It is interesting to consider the case of TiO_2 cultures, which did not contain significantly more dead AM compared with controls. When TiO_2 content was correlated with cell death, there was an indication ($0.05 < p < 0.10$) of association. However, TiO_2 internalization as evaluated by SEM and TEM was clearly related to cell death ($p < 0.05$). Although TiO_2 is widely considered to be a nontoxic nuisance dust (World Health Org., 1982), we find that TiO_2 has some bioactivity. The reason for this is unclear, but may relate to the jagged TiO_2 particle morphology resulting from grinding to obtain specifically sized particles. Correlative microscopic techniques, although time-consuming, proved essential in describing morphological alterations dependent on particle exposure on an individual cell basis.

Such techniques also permitted the assessment of morphologic correlates with AM death as determined by trypan blue dye exclusion from the nucleus. Cells exhibiting bleb clusters generally remained viable, even when blebs were widespread and/or sloughed onto the substrate. Often, some membrane degradation was evident in viable AM.

It is widely recognized that AM can release lysosomal enzymes and other substances (Brody and Davis, 1982; Kang et al., 1979); furthermore, Brody and Davis (1982) point out that such release may occur either during cell lysis, or selectively, without cell injury. Brody and Davis (1982) have shown that resting, unexposed AM are capable of enzyme release, and that a variety of particle types elicit variable degrees of enzyme release. The researchers concluded that certain particle types are inert and cause no pathological consequences. We hypothesize that glutaraldehyde-stabilized surface blebs and bleb clusters may represent the leakage of cytoplasmic components through external membrane defects in AM. If bleb formation were simply a nonspecific result of particle phagocytosis, we would expect similar expression of this feature (mild damage in our system) independent of particle type. However, this is not the case; Ni_3S_2, the most toxic particle we have examined, was most strongly associated with damage parameters. Since particles appear to be phagocytized in similar manners, and since bleb clusters are often seen in areas distant from particle internalization, it may be the case that Ni_3S_2 causes membrane damage resulting in cytoplasmic leakage, as proposed by Kang et al. (1979) with beryllium and asbestos. Such a mechanism is consistent with our observed absence of specific internal features, as revealed by whole mount TEM, correlated with bleb clusters. Such damage, if it exists, may lead to observable degradation of the plasma membrane as described here and by other

researchers (Waters et al., 1975; Hill et al., 1982; Miller et al., 1978; Bell et al., 1979; and Fisher et al., 1982). This stage of AM degradation, classified as severe damage in our studies, was generally although not always associated with cell death. It is not clear to what extent bleb cluster formation and minor membrane damage may be reversible, or alternately, to what extent nuclear membrane integrity (as measured by trypan dye exclusion) is an appropriate characterization of AM which may or may not be able to regain normal structure and function following morphological alterations.

Two to five weeks after in vivo Ni_3S_2 intubation, murine AM were lavaged then viewed by SEM after glass coverslip attachment. Only one AM contained particles, indicating that clearance from luminal spaces had largely occurred, that Ni_3S_2-containing AM were present but not recovered by lavage, or that such AM failed to remain adherent to the coverslips. Cell populations that were viewed, however, did exhibit certain surface morphological alterations dependent on Ni_3S_2 dose, even though no detectable Ni was observed. The incidence of blebs was directly related to relative Ni_3S_2 dose in all three experiments, in agreement with our in vitro findings and in vivo exposures carried out by other researchers (Miller et al., 1977). Also, a strong correlation existed between the incidence of ruffles and rounded cells, indirectly supporting the hypothesis that ruffles may seve as membrane storage reservoirs as cells round up (Erickson and Trinkaus, 1976).

Many investigators have employed whole cell mount techniques which correlate SEM and TEM of intact, critical point dried cells grown on or plated onto formvar substrates (Wolosewick and Porter, 1976, 1979; Porter and Stearns, 1981; Buckley and Porter, 1975). Such techniques permit the visualization of intact cells at high resolution, and are used here to examine the interaction between AM and various particle types. The internal morphology of AM appears similar to a number of cell types including embryonic fibroblasts (Buckley and Porter, 1975; Wolosewick and Porter, 1979), human diploid cells (Wolosewick and Porter, 1977), rat kidney cells, neuroblastoma cells, and myoblasts (Porter and Stearns, 1981). Intracytoplasmic vacuoles, occasionally containing particles, appear clustered near the nucleus, supporting the findings of Evans et al. (1982) who describe NiS particle sequestration to perinuclear regions. Stereo imaging techniques, coupled with SEM observations, allowed the distinction between internal and external particles in this study. It was difficult to compare AM interactions between GB and the irregular particles of Ni_3S_2 and TiO_2, since vacuoles were generally spherical, and the spherical GB interfered with vacuole imaging. Internal Ni_3S_2 and TiO_2 particles were generally inside vacuoles, although occasionally vacuoles were not associated with these particles. Cells appeared to handle TiO_2 and Ni_3S_2 in a similar fashion. Electron-dense granules, probably representing lysosomes (Buckley and Porter, 1975), were observed and were occasionally at the center of the vacuoles, perhaps constituting phagolysosomes. The entire cytoplasm of intact

AM was filled with a meshwork of variously-sized microfibers as described by Wolosewick and Porter (1979) as well as others. This structure was not apparent in severely degranulating AM.

In spite of observing a large number of cell/particle interactions, surprisingly few AM were "caught in the act" of phagocytosis. This finding suggest that phagocytosis proceeds rapidly once begun, as observed by Evans et al. (1982) and Stossel (1976), since a rapid internalization process implies fewer cells would be phagocytizing at any particular time.

It has been suggested that many factors, including crystalline form, solubility, and intrinsic toxicity of particles, as well as serum factors, are important in cell phagocytosis and expression of deleterious effects (Waters et al., 1975; Miller et al., 1979; and Brody and Davis, 1982). Abbracchio et al. (1982) and Evans et al. (1982) hypothesize that the influence of crystalline form on phagocytosis is of critical importance in the expression of toxicity of NiS to cultured cells. We report that both TiO_2 and Ni_3S_2 are phagocytized by AM, although we do not examine phagocytic rates, and find that differential effects are expressed. Waters et al. (1975) theorize that the mode of AM death is important in determining biological responses; if AM lyse rapidly, the pulmonary residence time of toxic particles may increase. The use of correlative microscopic techniques, as reported here, are useful in describing the effects of particulate material at the individual cell level. Such techniques in

combination with x-ray microanalysis may be of particular value when examining complex particulate mixtures, since Hayes et al. (1980) point out that segregation of elements into specific particles results in higher exposure levels to individual cells compared with a uniform elemental distribution.

Table IV.1. Experimental Summary of In Vitro Particle-Exposed Bovine AM Morphology

Expt. No.	Agent	Doses[a]	Culture time	Samples
I	Control			
	Ni_3S_2	4, 40, 400 µg/ml	20 hr	Glass adhr.
II	Control			
	Ni_3S_2	1, 5 µg/ml	1, 3 hr	Glass adhr. Formvar adhr[b,e]
III	Control			
	GB	5 µg/ml	2, 4, 20 hr	Glass adhr.
	Ni_3S_2	1, 5 µg/ml		Formvar adhr[c]
IV	Control			
	GB	5, 8.4 µg/ml[d]		Glass adhr.
	TiO_2	5, 2.3 µg/ml[d]	2, 20 hr	Formvar adhr[b,c,e]
	Ni_3S_2	5 µg/ml		

a EC_{50} = 4.5 µg/ml for phagocytic depression caused by Ni_3S_2.

b Included in LM viability studies.

c Included in CTEM and HVEM studies.

d GB and TiO_2 administered at same mass loading (5 µg/ml) and same particle: cell loading (8.4 or 2.3 µg/ml) as Ni_3S_2 in experiment IV.

e Included in detachment dependence on viability studies.

Table IV.2. Association Between Particle Content (Ni_3S_2, TiO_2, and GB) and Morphological Degradation.[a]

		In Vitro Study, Experiments II and IV AM Alteration:				
Particle Type[b]	Particle Content[c]	Intact	Mild	Severe	χ^2	Association Significance
I-Ni_3S_2	+	9	49	220	133.8	$p < 0.001$
	-	16	5	1		
III-GB	+	52	24	4	4.063	N.S. ($p > 0.10$)
	-	54	11	3		
III-Ni_3S_2	+	51	78	64	79.9	$p < 0.001$
	-	114	34	9		
IV-GB	+	32	12	2	2.295	N.S.
	-	86	28	1		
IV-TiO_2	+	32	21	3	6.265	$.01 < p < .05$
	-	142	44	5		
IV-Ni_3S_2	+	33	30	10	20.99	$p < 0.001$
	-	74	19	2		

a Association between particle content (presence or absence) and AM damage determined from contingency tests of the hypothesis: no association between row and column variables.

b Roman numeral indicates experiment number. Data represents pooled doses and culture times within experimental agent.

c Plus and minus sign indicate presence (+) or absence (-) of particle type.

Table IV.3. Percentage of AM Exhibiting Altered Morphology After Particle Exposure.[a]

Particle Type[b]	Particle Content[c]	Damaged Cells (%)
I-Control	-	22
I-Ni_3S_2	+	97
	-	27
III-Control	-	28
III-GB	+	35
	-	21
III-Ni_3S_2	+	74
	-	27
IV-Control		21
IV-GB	+	30
	-	25
IV-TiO_2	+	43
	-	26
III-Ni_3S_2	+	55
	-	22

a Includes mild and severe damage classes.

b Roman numeral indicates eperiment number. Data represents pooled doses and culture times within experimental agent.

c Plus and minus sign indicate presence (+) or absence (-) of particle type.

Table IV.4. Association Between Particle Content (Ni_3S_2, TiO_2, and GB) and Cell Viability.[a] In Vitro Study, Experiments II and IV.

Particle[b] Type	Cell Viability	No Particles	≥1 Particle	χ^2	Association Significance
II-Ni_3S_2	Live	34	15	2.423	N.S. ($p > 0.10$)
	Dead	6	7		
IV-GB	Live	276	32	0.247	N.S.
	Dead	5	1		
IV-TiO_2	Live	180	51	3.403	$0.05 < p < 0.10$
	Dead	4	4		
IV-Ni_3S_2	Live	129	128	8.575	$.001 < p < .01$
	Dead	2	14		

Association Between Particle Internalization and Cell Viablity.[d]

Particle Type	Cell Viability	No Internal Particles	≥1 Internal Particle	χ^2	Association Significance
II-Ni_3S_2	Live	46	3	13.27	$p < 0.001$
	Dead	7	6		
IV-GB	Live	294	14	1.901[c]	N.S.[c]
	Dead	5	1		
IV-TiO_2	Live	202	29	4.149	$0.01 < p < .05$
	Dead	5	3		
IV-Ni_3S_2	Live	226	31	44.96	$p < 0.001$
	Dead	4	12		

a Cell viability determined by trypan blue dye exclusion. Association determined using contingency test of the hypothesis: no association between row and column variables.

b Roman numeral indicates experiment number. Data respresents pooled culture times within experimental agent. 3 or 4 grids per group.

c Chi-square statistics do not strictly apply since there exists an expected frequency ≤1.

d Data from above broken down to reflect particle internalization. No internal particle class includes cells without particles and cells with external particles only.

Table IV.5. Alveolar Macrophage Viability Following Particle Exposure, Experiment IV.

Exposure	N[a]	Non-Viable Cells (%) $\bar{X}$	S
Control	3	1.5	1.3[b]
GB	3	1.4	1.6[c]
TiO_2	3	4.1	3.0
Ni_3S_2	4	6.1	3.3[b,c]

a N = number of grids analyzed per compound tested.

b,c Groups with the same superscript are significantly different ($p < 0.05$) using a one-tailed student's t-test.

Table IV.6. Percent Incidence of AM Features as a Function of Administered Ni_3S_2, Intubation Study[a]

	Relative Ni_3S_2	Percent Incidence of Features (%)		
Expt. No.[b]	Dose[c]	Blebs[c]	Rounded	Ruffles
V	0 (saline control)	6	16	48
	0	16	30	74
	1 (0.08 mg/kg)	8	18	60
	5	10	12	42
	25	26	10	44
VI	0 (saline control)	14	46	60
	0	18	34	43
	1 (0.15 mg/kg)	20	22	46
	3	22	4	22
	9	36	4	26
VII	0 (control)	34	38	40
	1 (0.21 mg/kg)	42	26	28
	2.1	30	30	24
	6.2	48	24	20
	6.8	50	34	38

a A/J mouse, PBS used as dosing vehicle, control animals received PBS alone; 50 randomly selected AM per sample.

b Expt. V received 1 dose, sacrifice at 2 weeks; Expt. VI and VII received 5 or 15 doses, sacrificed 5 weeks after last dose.

c Total Ni_3S_2 administered in all doses; relative doses given are within each experiment.

Table IV.7. Association Between Various Features and Ni_3S_2 Dose, Intubation Study, as Determined by Linear Regression.[a]

	Ni_3S_2 Dose Correlation with Incidence of:						Rounded Cells Associated with Ruffles	
	Blebs		Rounded Cells		Ruffles			
Expt. No.	Slope	r^2	Slope	r^2	Slope	r^2	Slope	r^2
V	0.651b	0.764	-0.447	0.375	-0.636	0.259	1.64b	0.925
VI	2.17b	.960	-3.78c	.596	-2.91c	.501	.798b	.905
VII	2.24c	.639	- .534	.083	- .580	.042	1.37b	.812

a Linear regression performed on paired data sets. Raw data from Table 6.

b Slope significantly different ($p < 0.05$) compared with zero, using a one-tailed student's t-test.

c Suggestion of difference ($0.05 < p < 0.10$) when compared with zero.

Table IV.8. In Vitro Particle-Exposed Detachment Study.[a] Dependence on Viability.[b]

Experiment		Live	Dead	χ^2	Association Significance
II-Control	Present	12	19	1.028	N.S. ($p > 0.10$)
	Detached	5	15		
II-Ni_3S_2 Exposed	Present	49	13	0.238	N.S.
	Detached	25	5		
II-All Grids	Present	62	32	0.502	N.S
	Detached	30	20		
IV-Control	Present	350	5	0.202	N.S
	Detached	96	2		
IV-GB	Present	308	6	0.160	N.S.
	Detached	79	1		
IV-TiO_2	Present	213	7	2.404	N.S.
	Detached	77	6		
IV-Ni_3S_2	Present	171	9	1.079	N.S.
	Detached	65	6		
IV-All Cells	Present	1042	27	3.458	$.05 < p < .1$
	Detached	317	15		

a Detachment from substrate between LM and SEM examination.

b Contingency test used to test the hypothesis: Cell viability is not associated with detachment.

c Data from Experiment II consists of pooled 1 and 3 hour cultures; from Experiment IV consists of pooled 2 and 20 hour cultures.

Table IV.9. Alveolar Macrophage Morphology. Independence of Substrate and Trypan Dye Exposure.[a]

AM Sample	Shape Classifications:[b] Round	Spread	Intermediate	Feature Classifications:[c] Ruffles	Filopodia	Blebs
Glass adherent	44 ± 5.7	41 ± 1.4	15 ± 4.2	61 ± 4.2	39 ± 4.2	22 ± 5.7
Formvar adherent	46 ± 5.7	36 ± 2.8	18 ± 2.8	62 ± 5.7	38 ± 5.7	23 ± 4.2
Formvar and Trypan	49 ± 4.2	39 ± 1.4	12 ± 5.7	65 ± 4.2	41 ± 1.4	21 ± 4.2

[a] Morphological classification system used to examine glass adherent, formvar adherent, and formvar adherent plus trypan-exposed AM; experiment IV, control AM population, 2 hour cultures.

[b] Percent incidence of shapes and features ± standard deviation determined from duplicate analyses.

[c] Three most prevalent features listed. Figures do not necessarily equal 100 percent since some AM exhibit multiple features.

IV.6 APPENDIX: STATISTICAL METHODS

1. Test for Association in Contingency Tables (Remington and Schork, 1970). Used for both 2 x 2 and 2 x 3 tables

2 X 2

	1	2	
1	O_{11}	O_{12}	$O_{1.}$
2	O_{21}	O_{22}	$O_{2.}$
	$O_{.1}$	$O_{.2}$	n

2 X 3

	1	2	3	
1	O_{11}	O_{12}	O_{13}	$O_{1.}$
2	O_{21}	O_{22}	O_{23}	$O_{2.}$
	$O_{.1}$	$O_{.2}$	$O_{.2}$	n

Hypothesis: No association between row and column parameters.

Test statistic $$\chi^2 = n \left[\sum_{i=1}^{r} \sum_{j=1}^{c} \frac{O_{ij}^2}{O_{i.}\ O_{j.}} - 1 \right]$$

Degrees of Freedom = (r-1) (c-1) = 1 for 2 x 2 table

= 2 for 2 x 3 table

Critical $\chi^2 = \chi^2_{0.95;1} = 3.841$

$\chi^2_{0.95;2} = 5.991$

2. Linear regression fits the line $y = A + Bx$. Inferences concerning fitted line slope = B

Hypothesis: B = 0

Test statistic $$t_o = \frac{b s_x \sqrt{n-1}}{s_{y\ x}}$$

where $$s_{y\ x} = \sqrt{\frac{n-1}{n-2}(S_y^2 - b^2 s_x^2)}$$ and $$S_x = \sqrt{\frac{\sum_{i=1}^{n}(X_1 - \bar{X})^2}{n-1}}$$

Select one-tailed test. Critical $t_{0.95;n-2}$ at 95 percent confidence level.

3. Student's t-test. Used to test hypothesis concerning two population means μ_1 and μ_2.

H_o: $\mu_1 - \mu_2 = 0$.

Will use test statistic t_c for unknown, unequal variances.

$$t_c = \frac{\bar{X}_1 - \bar{X}_2}{\sqrt{\frac{s_1^2}{n_1} + \frac{s_2^2}{n_2}}}$$

For a one sided test critical $t_{.95;\ 5} = 2.015$

$t_{.95;4} = 2.132$

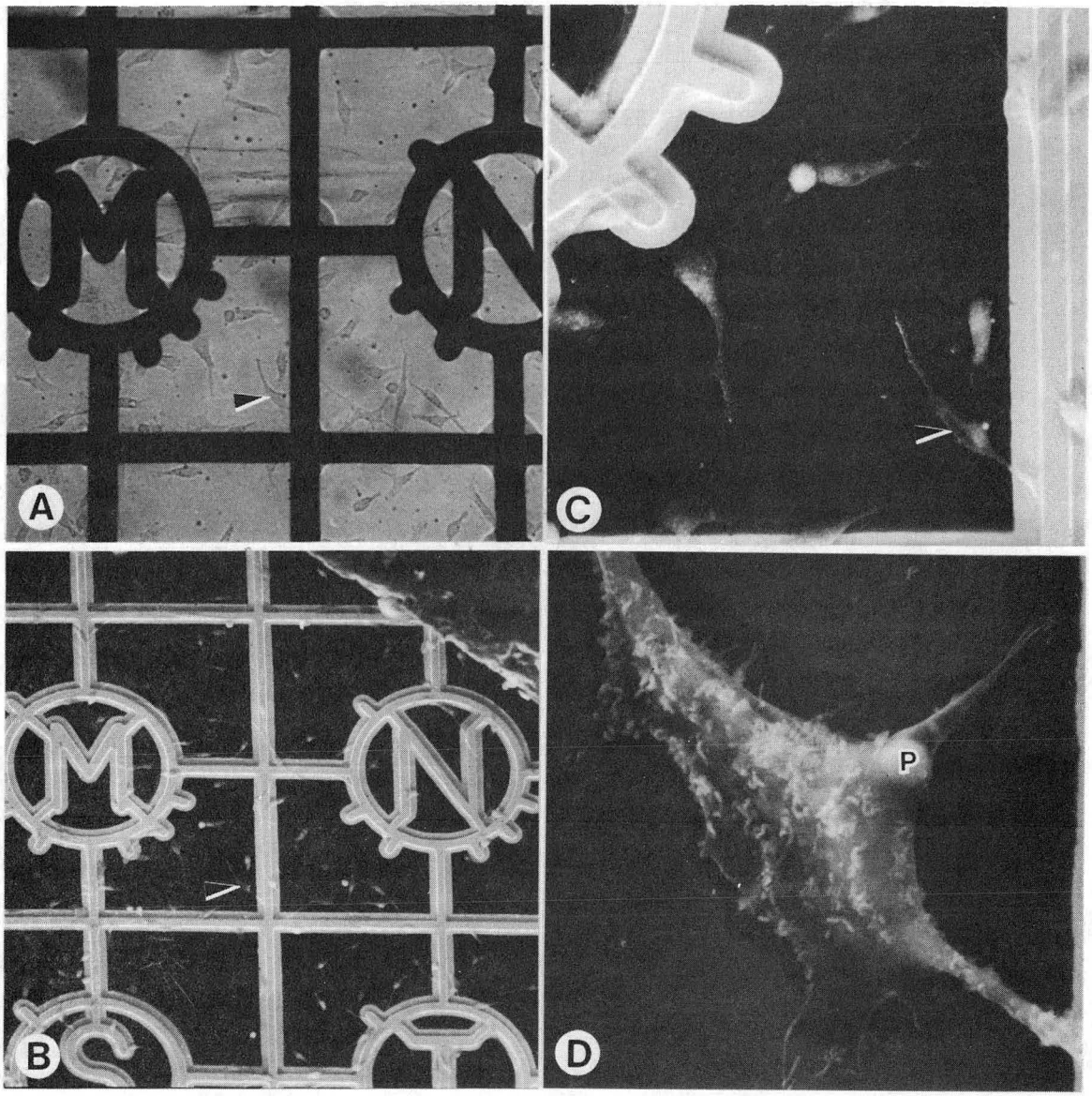

Figure IV.1 Glass bead exposed AM, 20 hours culture, examined using correlative microscopic techniques. A. Formvar-attached AM culture photographed by light microscopy (LM) in saline with trypan blue dye. Arrow identifies cell shown below; magnification = 135X. B. SEM of grid shown in (A); magnification = 120X. C. Higher magnification SEM of grid with several AM, all identified as live at the time of fixation. Cell of interest identified by arrow; magnification = 500X. D. Spread AM with internal particle (P). Numerous ruffles and cytoplasmic extensions are evident. Dark shadow around cell is a artifact due to insufficient charge conduction; carbon coated sample, magnification = 3,000X.

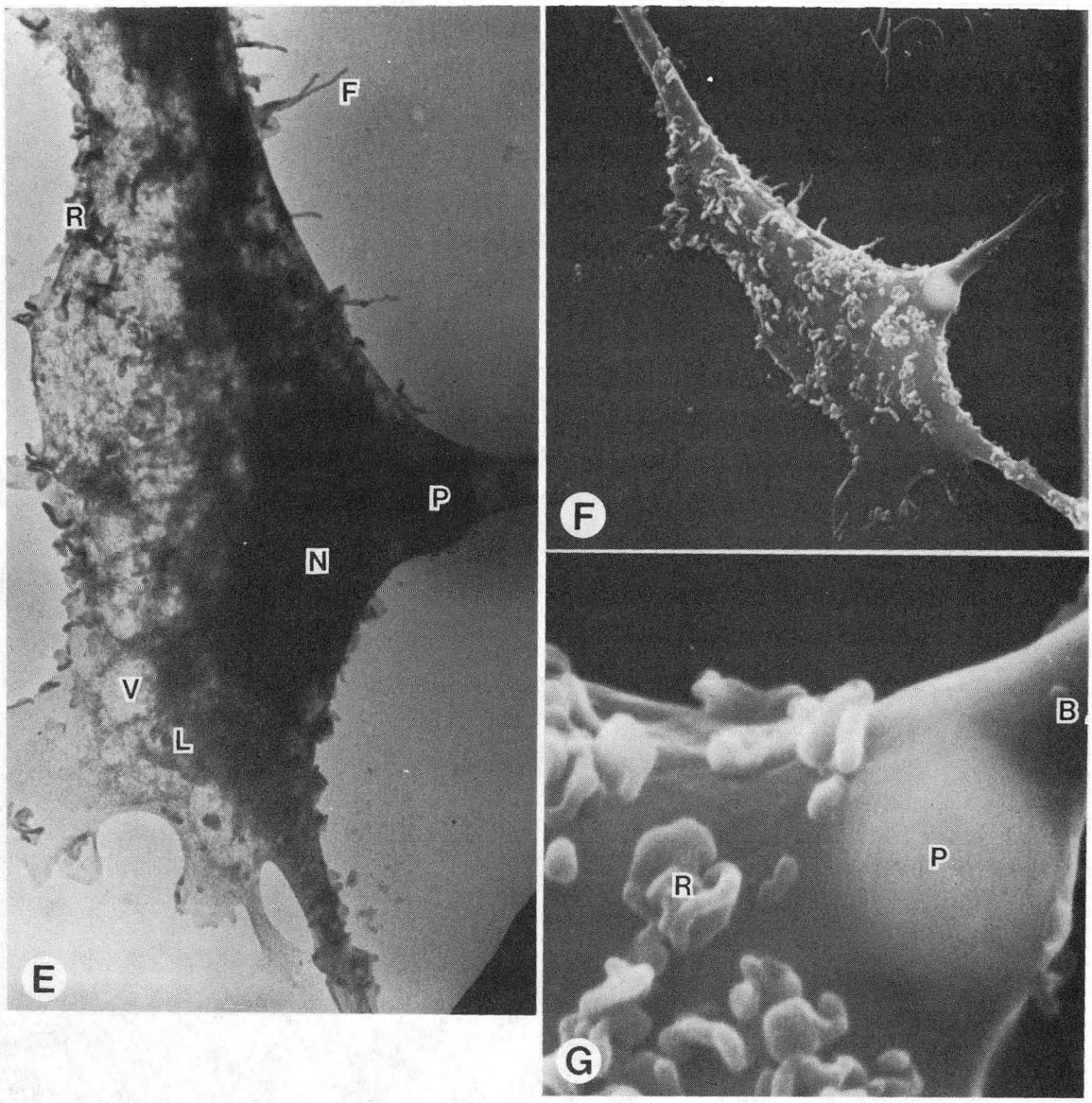

Figure IV.1 (cont'd) E. TEM of above cell with nucleus (N), particle (P), vacuoles (V), ruffles (R), filopodia (F), and electron-dense lysosomes (L). Thicker, ruffled area appear out of focus; the fine microtrabecular lattice is not evident at this relatively low magnification; original magnification = 4,000X, print magnification = 8,000X. F. SEM of same cell following Pt coating; surface features are more clearly resolved; magnification = 3,000X. G. High magnification SEM of cell/particle interaction; the cell membrane is continuous over the particle (P), other features include ruffles (R) and small blebs (B) not evident at lower magnification; magnification = 20,000X.

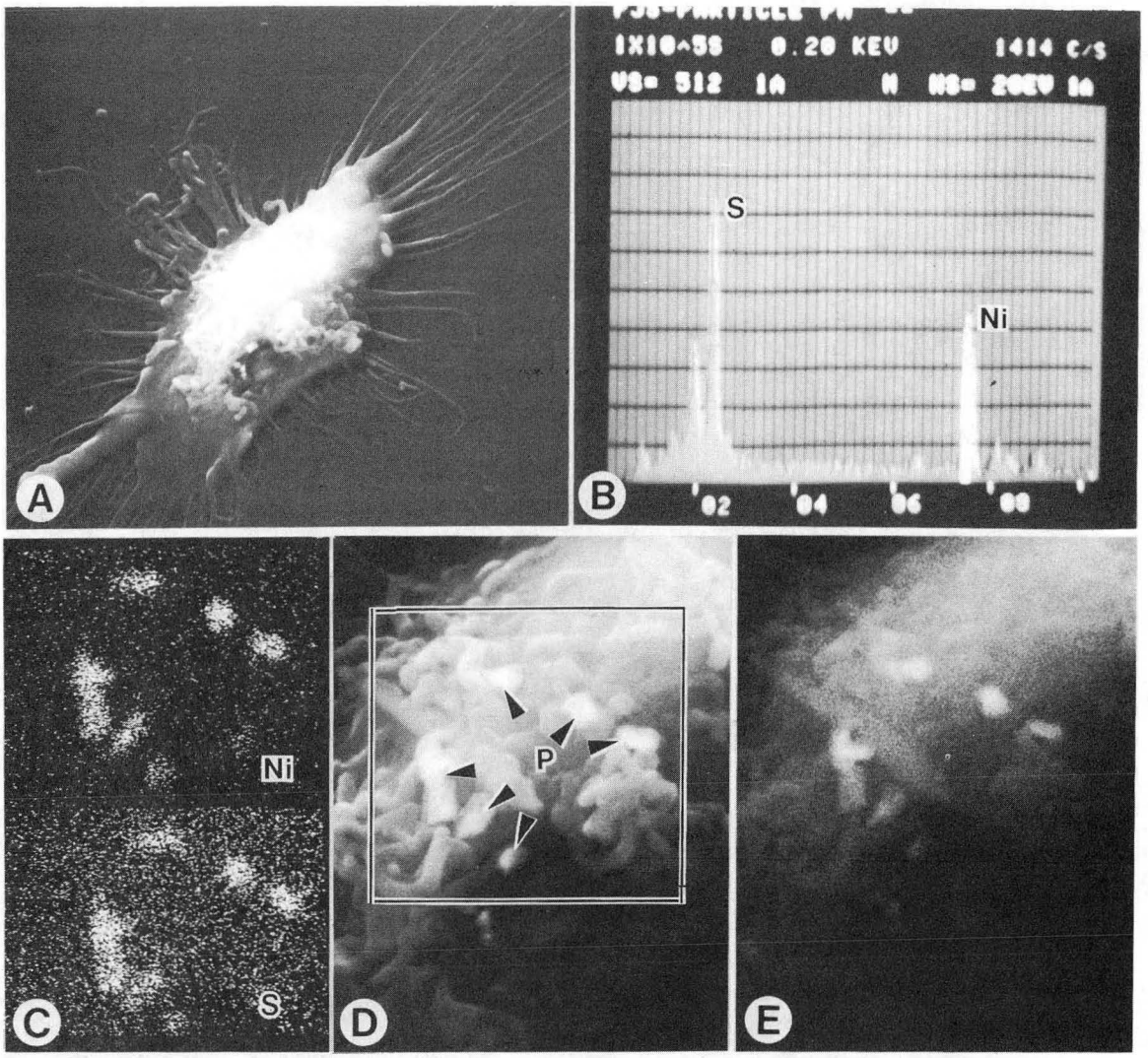

Figure IV.2 Illustration of techniques used in particle identification. A. SEM of carbon-coated Ni_3S_2-containing AM, intermediately spread, with surface ruffles and filopodia. Particles are difficult to distinguish; magnification = 3,600X. B. Photograph of spectrometer display obtained by placing beam directly on a particle; Ni and S K_α lines are present. C. X-ray mapping used in examining cell/particle interactions. X-ray map (left) is for Ni K_α (top, energy mapped 7.42-7.58 KeV) and S K_α (bottom, energy range 2.26-2.40 KeV). Background noise is present, however, particles are easily identified; both Ni and S appear identically distributed within the resoving power of the mapping technique; magnification = 9,200X. D. Higher magnification SEM of central area containing particles (P); a large vacuole (V) is evident; box encloses area used for x-ray mapping; magnification = 9,200X. E. Pseudo-backscattered electron image derived from switching off collector cage voltage; particles appear brighter than the surrounding cell body; magnification = 9,200X.

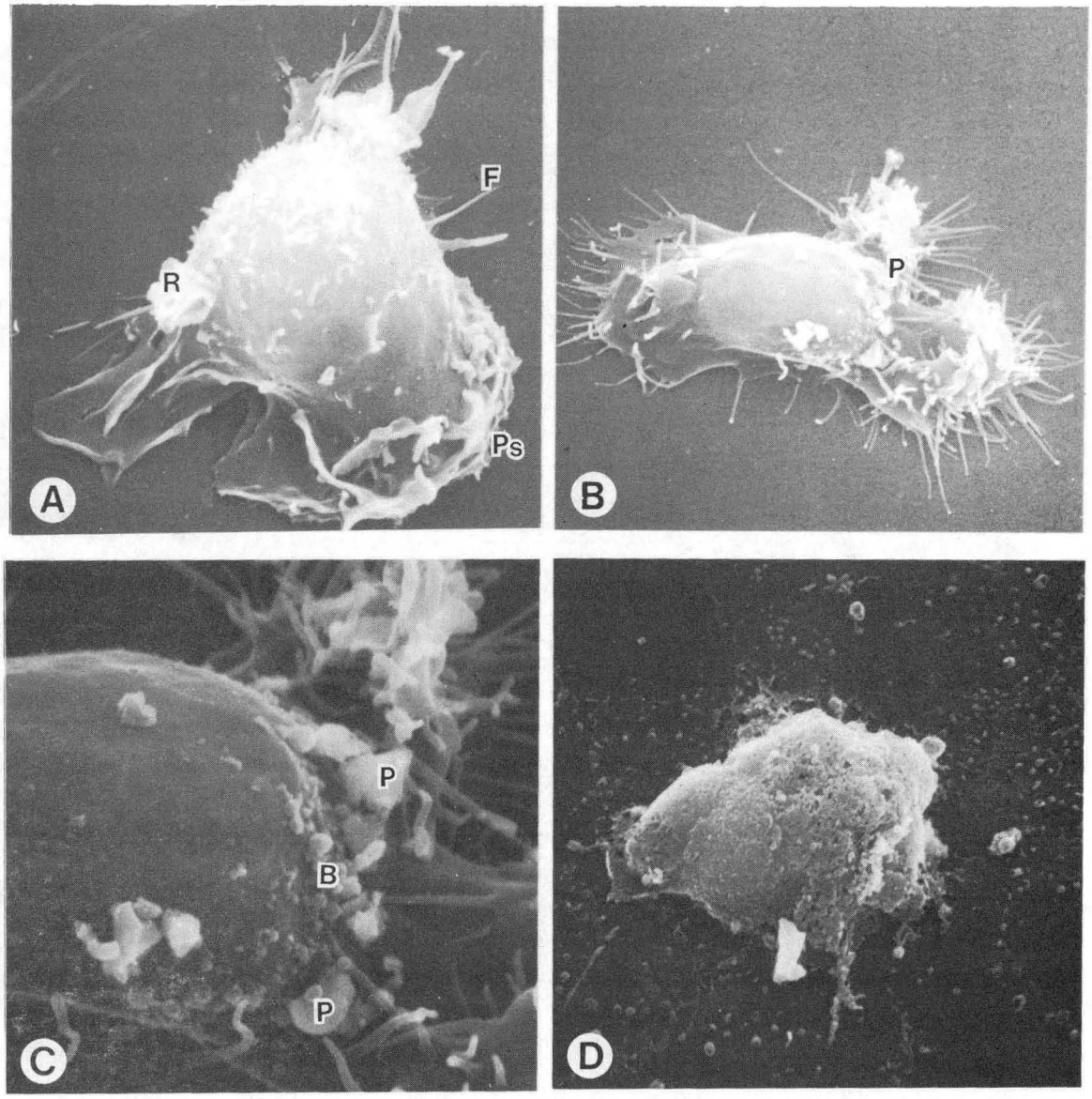

Figure IV.3 Scanning electron micrographs (SEM) illustrating degenerative alterations to cultured alveolar macrophages (AM). A. Typical intact cell displaying surface ruffles (R), threadlike filopodia (F), and pseudopodia (Ps); magnification = 5,000X. B. Intermediately spread AM with numerous filopodia, ruffled pseudopodia, and Ni_3S_2 particles (P) associated with a bleb cluster; magnification = 3,500X. C. Higher magnification of cell in (B) clearly displaying blebs (B) in close conjunction with particles (P); magnification = 8,100X. D. Ni_3S_2 exposed cell with widespread membrane mottling and blebs sloughed onto the substrates; magnification = 5,000X.

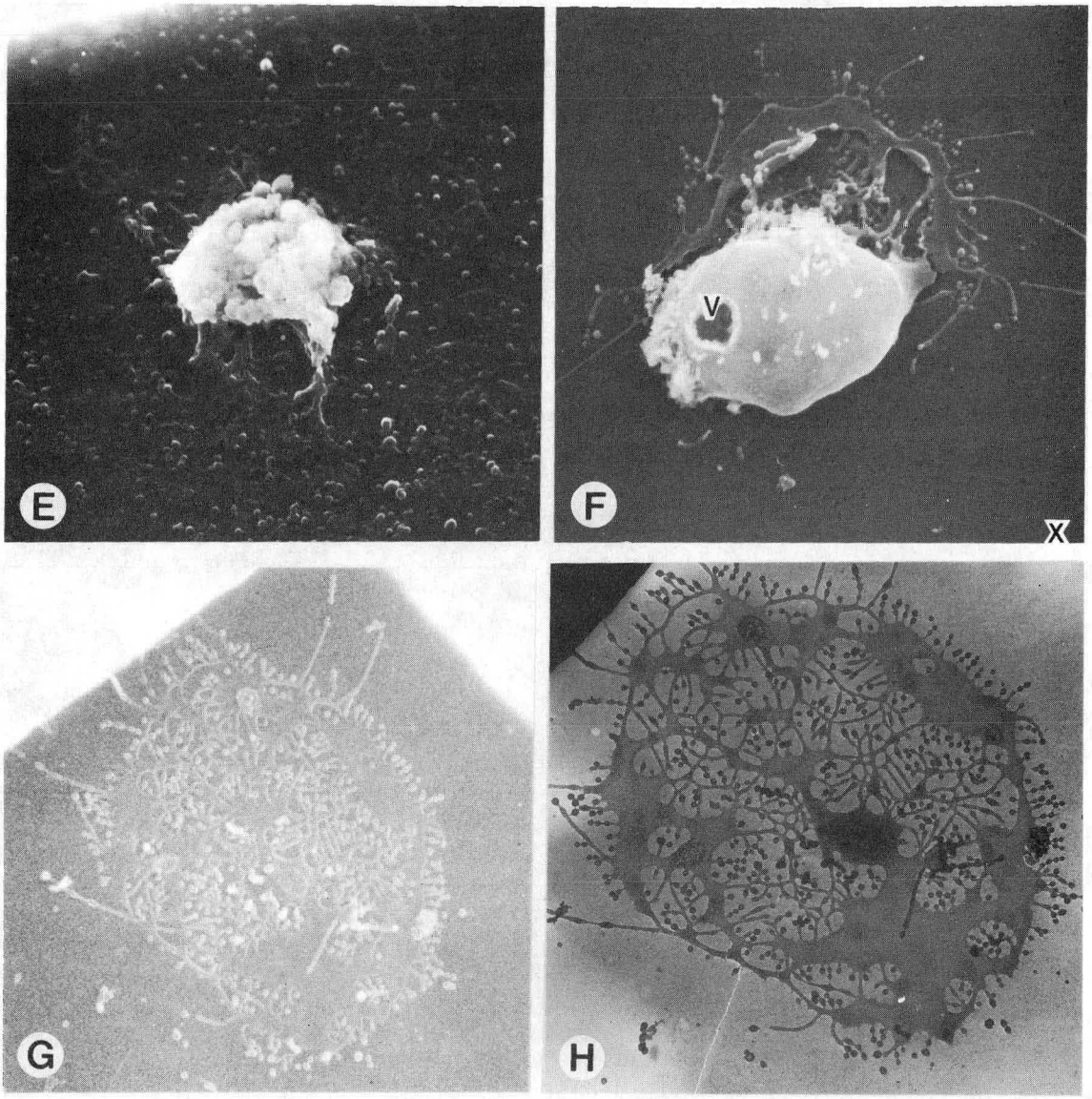

Figure IV.3 (cont'd) E. Cell which has lost normal surface features, consisting of spherical clusters of cytoplasm with numerous sloughed blebs; magnifcation = 3,400X. F. AM cell partially lysed, with a rounded, smooth central area, degranulated pseudopodia, and an emptied vacoule (V); magnification = 5,000X. G. Cell remnant with no nucleus or cytoplasm; magnification = 5,000X. H. Transmission electron micrograph (TEM) of cell in (G) showing little internal structure; 80 kV, magnification = 6,000X.

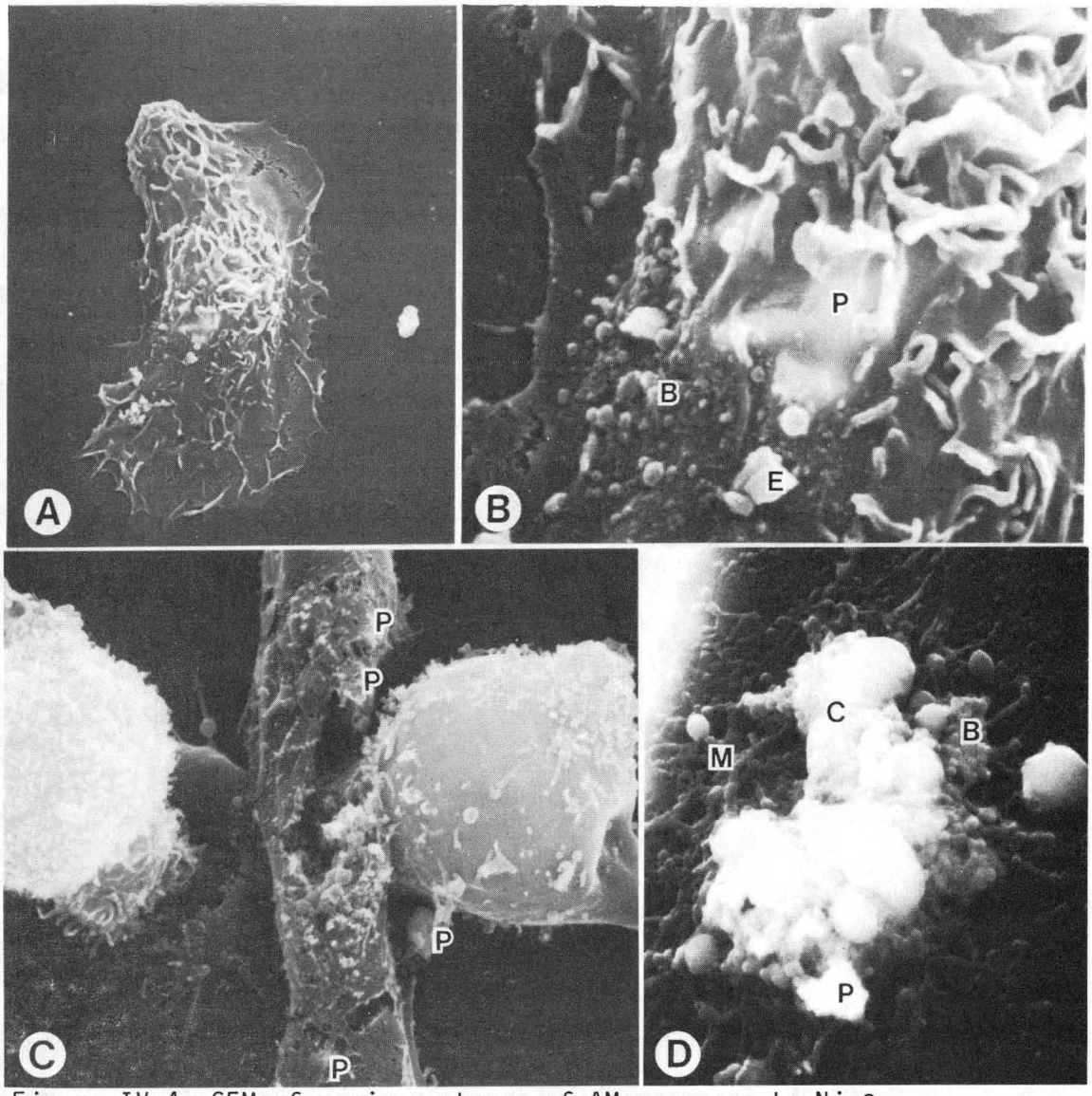

Figure IV.4 SEM of various stages of AM response to Ni_3S_2. A. Intermediately spread AM displaying ruffles and pseudopodia; 2 hours exposure to Ni_3S_2; magnification = 2,800X. B. High magnification of enclosed area from above cell. Phagocytized N_3S_2 particles (P) appear as indistinct bright spots beneath the ruffled membrane; an external particle (E) is also present. Numerous blebs (B) appear to be resting upon or emanating from the cell membrane; magnification = 20,000X. C. Cells from a 20 hour Ni_3S_2 exposure with four particles present (P). Center AM, dead at the time of fixation, is clearly breaking apart. The other two cells were both identified as live; the cell at left is intact, with a covering of ruffles and microvilli, and the cell at right displays a focal bleb cluster on the upper right; magnification = 5,000X. D. Severely damaged AM with one Ni_3S_2 particle (P). Cell constituents are spread onto the substrate, no normal external membrane is evident, and the cell body consists of blebs (B) and larger cytoplasmic granules (C), with a meshwork of thickened filaments (M) also observed; magnification = 5,000X.

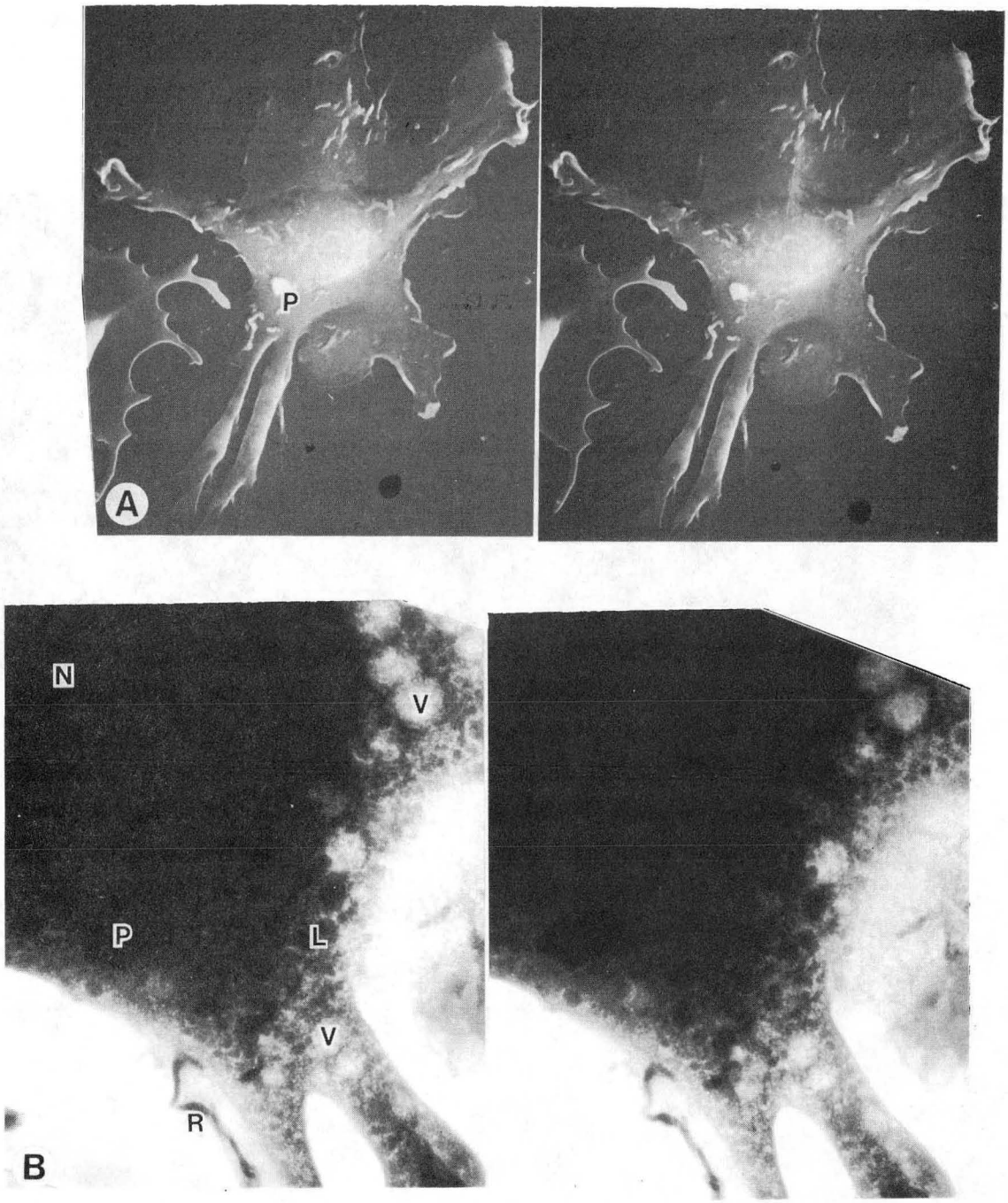

Figure IV.5 Intact, intermediately spread live AM with extensive pseudopodia; Ni_3S_2 exposed, 2 hours culture. A. Stereo SEM, one external Ni_3S_2 particle (P) is present. The cell is quite flat except for the raised central area; the external membrane is continuous, smooth, and relatively featureless; magnification = 2,000X. B. Stereo TEM; the nucleus (N) is present in the dense central area, and the external particle (P) can be seen. Several features are observed in the more spread periphery, including vacuoles (V), lysosomes (L), ruffles (R), and elongated mitochondria (M); original magnification = 4,000X, print magnification = 7,400X XBB 8411-8661

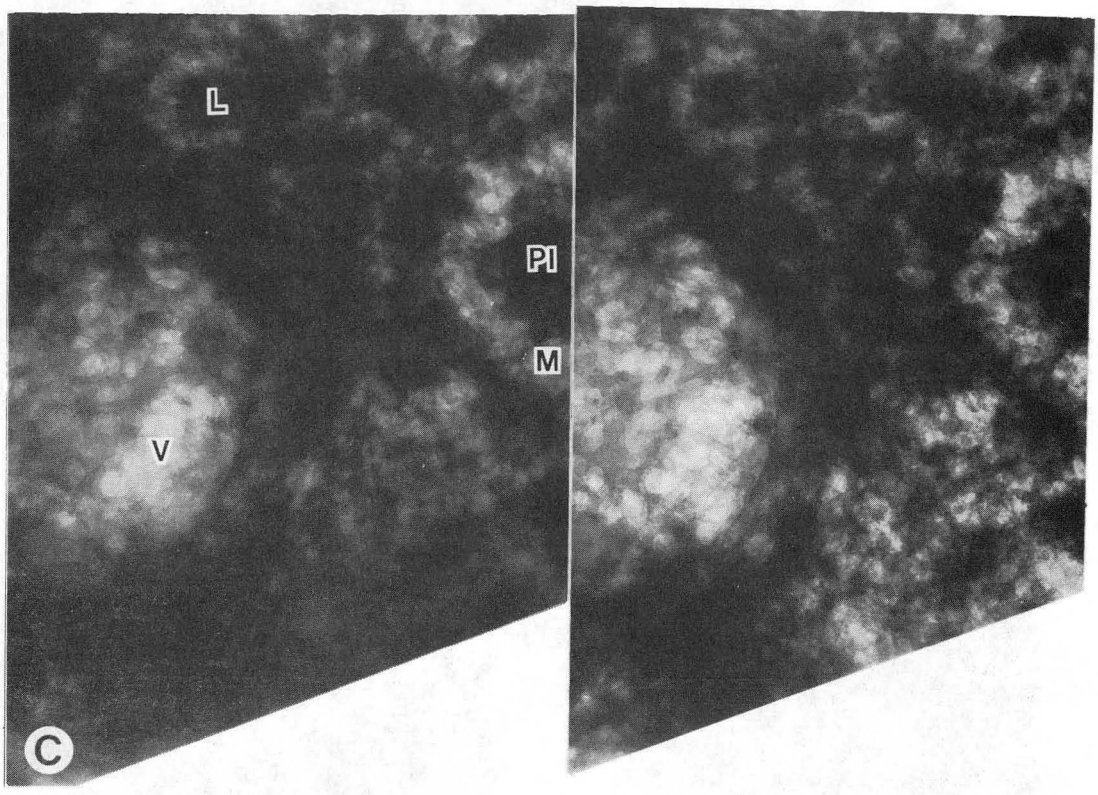

Figure IV.5 (cont'd) C. Higher magnification stereo TEM of area enclosed by box above; features include vacuoles (V), lysosomes (L), a possible phagolysosome (P1), and a fine filamentous meshwork (M) often described as the microtrabecular lattice; original magnification = 31,000X, print magnification = 57,000X. XBB 8411-8662

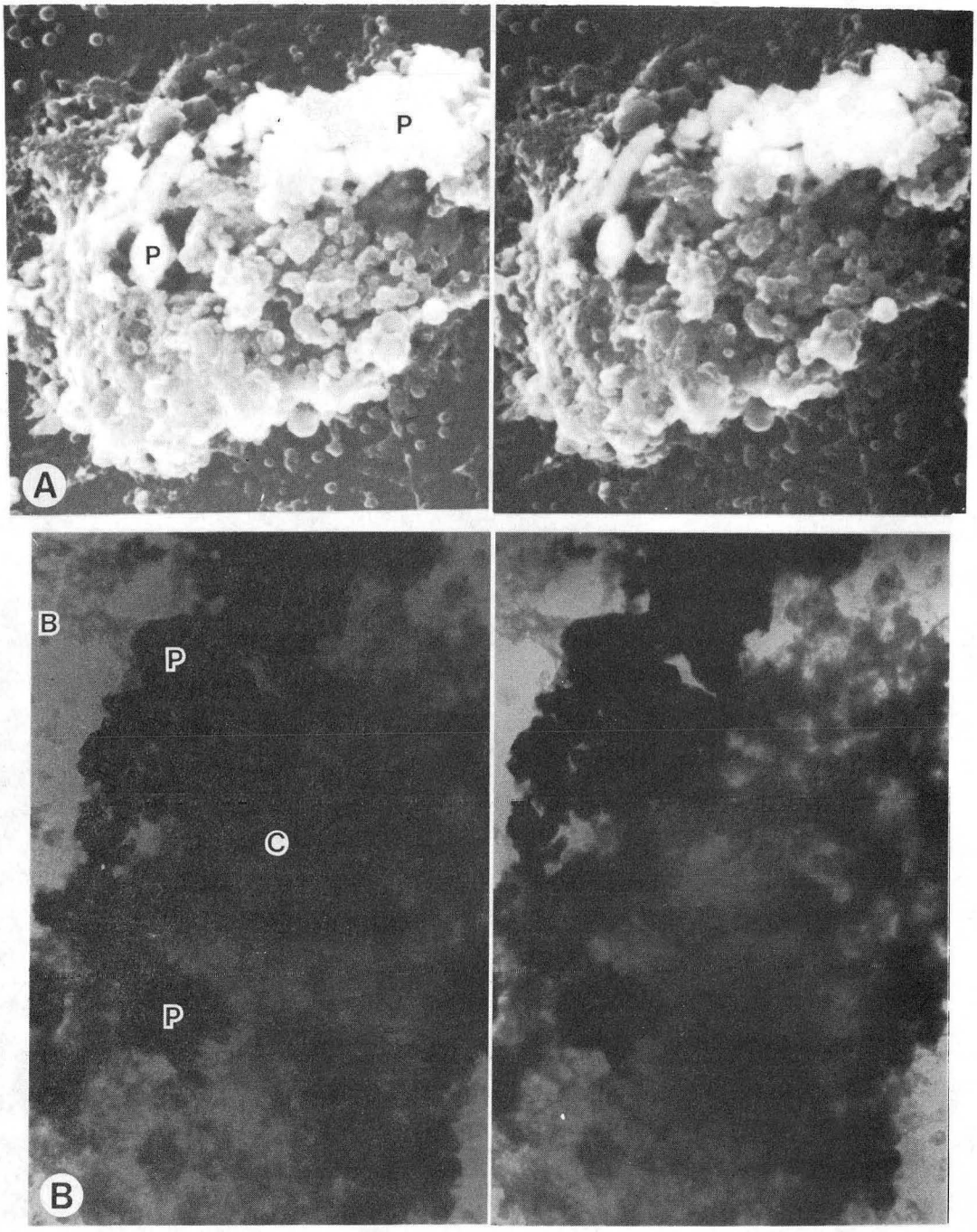

Figure IV.6 Severely damaged AM; TiO_2 exposed, 20 hour culture. Although more strongly associated with Ni_3S_2 internalization, AM damage is also correlated with TiO_2 internalization. A. Stereo SEM; several particles are present (P), blebs have been sloughed to the substrate, the cytoplasm appears to be degranulating, and little if any normal membrane is present; magnification = 8,000X. B. Stereo TEM of above, with particle (P), blebs (B), and cytoplasm (C). No nucleus is present, and the cytoplasm is abnormal in appearance; original magnification = 6,300X, print magnification = 11,600X. XBB 8411-8663

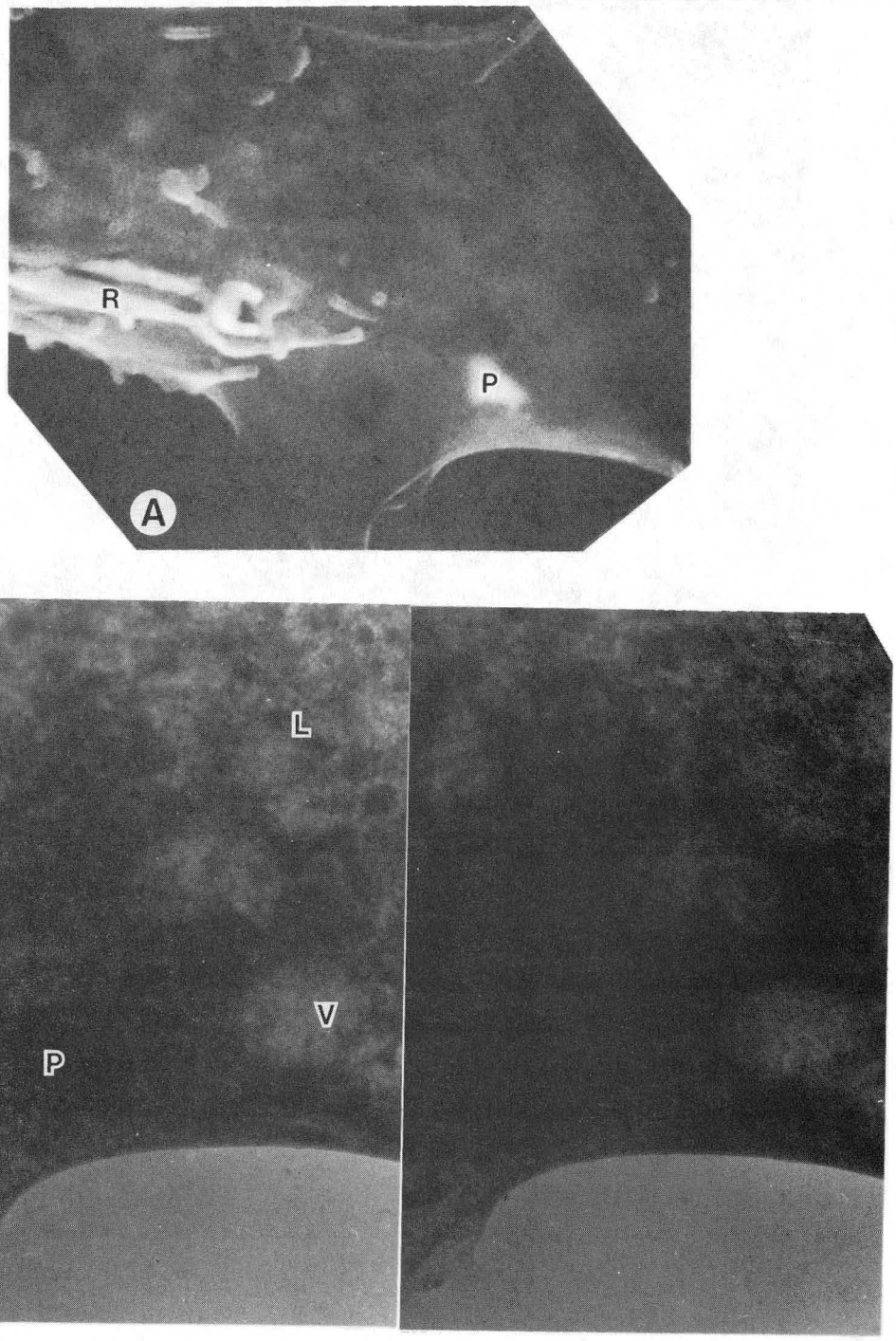

Figure IV.7 High magnification SEM and TEM showing AM interactions with TiO_2 particles, both 20 hours culture. A. Spread periphery of cell, displaying ruffles (R) and a particle (P). The particle edges appear indistinct suggesting that it is internal to the cell; magnification = 10,000X. B. Stereo TEM of above, with vacuoles (V), particle (P), and lysosomes (L). The three dimensional view shows that the particle is internal to a vacuole; the fine meshlike framework of the cell is visible in thin areas; original magnification = 8,000X; print magnification = 15,000X. XBB 8411-8664

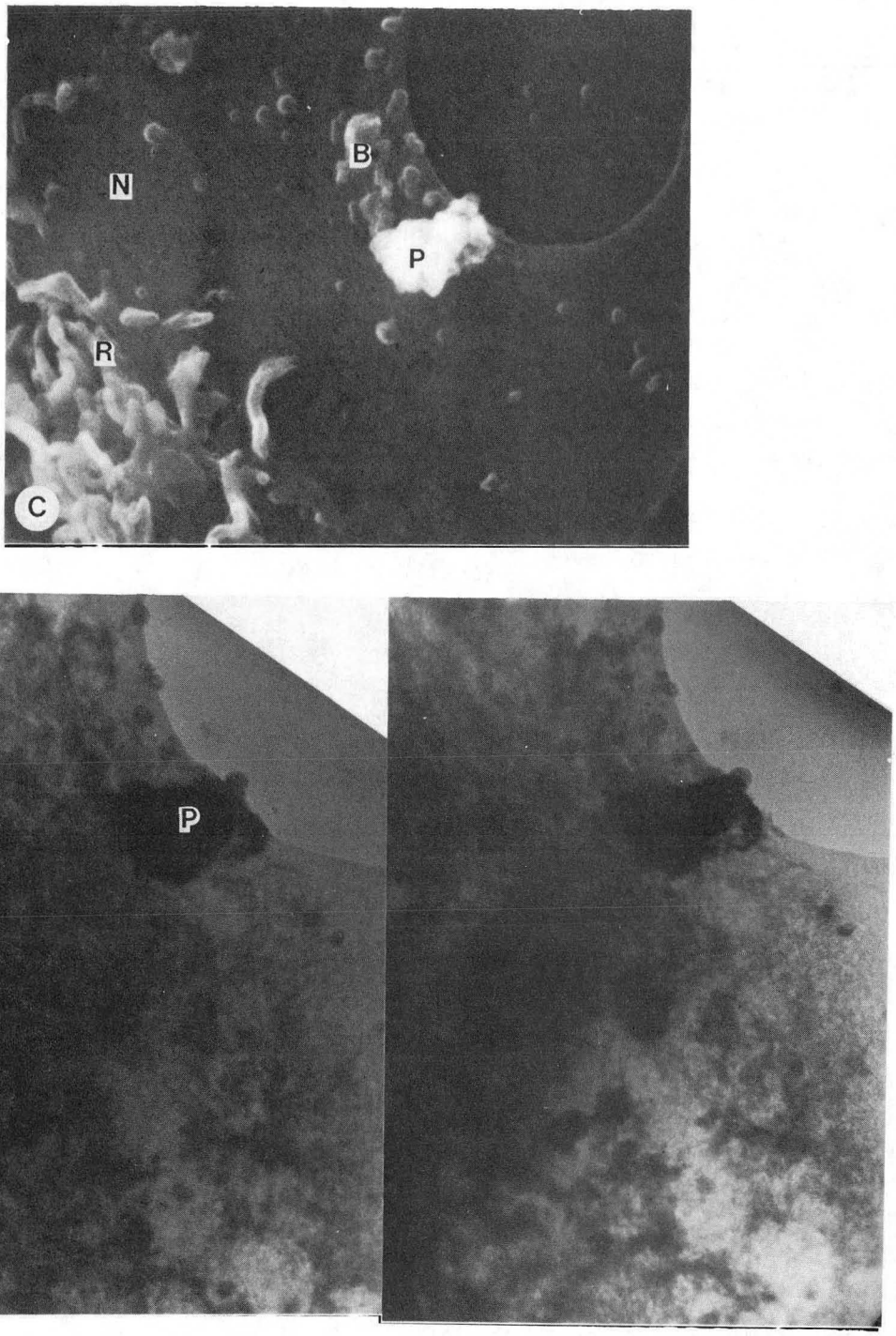

Figure IV.7 (cont'd) C. TiO_2 particle (P) present along with surface blebs (B); also evident are ruffles (R), and the cell nucleus (N) can also be resolved in this carbon-coated specimen; SEM, original magnification = 10,000X. D. Stereo TEM corresponding to (C); the particle (P) is clearly above the body of the cell; original magnification = 10,000X; print magnification = 18,000X XBB 8411-8665

CHAPTER V

MORPHOLOGICAL STUDIES OF FROZEN HYDRATED LUNG: INTERACTIONS BETWEEN PULMONARY TISSUE AND RESPIRABLE PARTICLES

V.1 INTRODUCTION

Inflated frozen hydrated mouse lungs were examined using low temperature scanning electron microscopy (SEM) following bulk fracture and surface etching by radiant heating. Various aspects of pulmonary architecture were identified and correlated with structures revealed by conventional SEM fixation and preparation techniques. Condensed cytoplasmic and nuclear lattice patterns due to ice crystal formation during freezing were evident in cells after surface etching, but features such as nuclear membranes and secretory granules were identifiable, and such etch patterns actually aided in identifying intra- versus extracellular spaces. Pulmonary fluids such as mucus and surfactant could be identified. Respirably-sized iron oxide particles were introduced into some lungs by the method of intratracheal instillation and were subsequently identified in frozen hydrated lung tissue using characteristic x-ray mapping and other analytic techniques. Particles were observed both intra- and extracellularly and were commonly found in large deposits. These observations confirm that etched frozen hydrated lung specimens can be used to examine particles within pulmonary tissue, and suggest that particle exposure by intratracheal instillation may result in different distributional patterns when compared with inhalation exposure.

V.2 MATERIALS AND METHODS

Lungs were obtained from male Strain A/J mice (Jackson Laboratories, Bar Harbor, Maine; 10 - 15 weeks of age, 22 - 30 gm. body weights). After cervical dislocation, animals were pinned then

opened and the trachea cannulated with polyethylene tubing (outside diameter = 0.05 in., Clay-Adams, New York) hooked up to a pressure system designed to inflate the lungs and provide excess air at constant pressure when required. The rib cage was opened then lungs excised, taking care not to nick or puncture any lung lobe. Lungs were gradually inflated to 20 cm water pressure while being gently massaged on a moistened glass surface to promote complete and uniform inflation of airspaces, then plunged into melting nitrogen slush. Excess air at 20 cm water pressure was provided to the lungs to avoid the partial collapse during freezing due to air volume shrinkage observed both here and by other researchers (Manabe, 1979). Samples thus obtained were held under liquid nitrogen until used. Some animals were exposed to respirable-sized iron oxide particles (Fe_2O_3; 0.4 - 3.7 μm; 2 mg per animal; Particle Information Services, Grants Pass, OR) by intratracheal instillation (Ho and Furst, 1973). Particles were suspended in phosphate-buffered saline (PBS, Grand Island Biological Co., Grand Island, NY) and sonicated and vortexed immediately before use; a 20 μl bolus of suspension was then gently instilled through a 23 ga. blunt needle into the tracheas of ether or pentobarbitol anethesized animals held upright. At various times postexposure (15 min. to 18 hrs) frozen lungs were collected as described above.

Portions of frozen lungs were prepared for the SEM by methods described by Hook et al. (1980) with a few modifications. In recent experiments a pre-cooled copper stub with a sliding clamp was used to

secure rectangular pieces of either right or left lobes trimmed using a small high-speed circular saw under liquid nitrogen. The sample was transferred through an airlock into the high vacuum of the AMRay Biochamber (AMRay Corp., New Bedford, MA), where samples were fractured using a cold knife, then viewed through a dissecting microscope for fracture face suitability. Samples were refractured if contaminants such as ice chunks or debris from the knife were widespread, if no alveolar ducts were evident, or if no cross-sectioned ciliated airway epithelium was present in the fracture face. A radiant heat etch unit was routinely employed (etch duration ca. 1.5-2 minutes) to sublime surface water and reveal cellular detail in the fracture face. Occasionally light microscopic or uncoated SEM examination revealed that an additional 2 minute etch period was required. Finally, samples were lightly coated with evapoarated gold and transferred to the cold stage of an AMRay 1000A SEM with equipped anticontamination cold shroud and Kevex 5100C energy-dispersive x-ray spectrometer (Kevex, Foster City, CA). For a comlete description of the system, see Pawley and Norton (1978), Pawley and Hayes (1977), and Pawley et al. (1980). Samples were first imaged with secondary electrons at an accelerating voltage of 20 KeV to orient the fracture face towards the x-ray detector, then beam current was increased (ca. 0.1 - 1.0 nA) and x-ray maps of the Fe K_{α} peak (width used = 160 eV) were made of the entire fracture face. Areas of interest such as airways and observed particle agglomerations were mapped at higher magnification. Morphological

investigations of frozen hydrated lung structure and cell/particle interactions were routinely conducted at 10 to 15 KeV and low beam currents (ca. 0.01 nA) to reduce charging effects. Selected specimens freeze-dried by warming on a large copper LN_2 reservoir under high vacuum overnight were reexamined after another gold coating.

V.3 RESULTS

Mouse lungs were successfully inflated at 20 cm water pressure; quick-frozen in melting nitrogen slush, fractured to present an entire lung lobe in cross-section, etched, coated, then viewed in the frozen-hydrated state using the low temperature AMRay Biochamber and 1000A SEM. Lung structures observed were well-correlated with the morphology of airway fixed lung tissue as seen in the literature (Kessel and Kardon, 1979; Kuhn, 1974) and in our laboratory (Bastacky et al., 1983a, 1983b).

V.3.A Lung Morphology

A low magnification stereopair image (Figure V.1) proved essential for understanding the convoluted fracture face presented to the electron beam. Varying amounts of ice crystals (frost) were present but usually did not hinder morphological examination. Conducting airways were located adjacent to blood vessels; smaller airways were seen in both cross-sectional and longitudinal fracture. Away from these areas alveolar spaces appeared as rounded or polyhedrally-shaped air sacs bounded by thin alveolar walls. Airway epithelium consisted largely of columnar ciliated and nonciliated cells.

In cross-section, etching revealed surface detail enabling distinctions between intra- and extracellular spaces. Cells had fine residual cytoplasmic and nuclear matrices resulting from ice crystal damage compared with airway mucus or submucosal spaces, which exhibited a coarser granular structure (Figure V.2A). Close inspection of fractured epithelial cells revealed the presence of nuclear membranes and presumptive mucus secretory granules. Occasional wandering cells, probably phagocytes, were observed resting atop the epithelium. The bilayered basement membrane could often be identified immediately below epithelial cells separating epithelium from the submucosal spaces which contained occasional cells (identified by the fine reticular etch pattern), blood capillaries with or without erythrocytes, and connective fibers which appeared as bundles of elongated hollow tubes most frequently seen immediately below the basement membrane. Erythrocytes were not observed to exhibit cellular etch patterns as described above. When viewed en face, airway mucus linings appeared smooth (little or no etch) or cracked (regular etch); stereopair examination revealed gently rounded cell projections into the lumen, with cilia apparent as lacy patterns present within the mucus blanket (Figure V.2B), in marked contrast to the free-standing cilia typically seen in airway fixed lungs.

In the mouse there is a rather sharp transition between terminal conducting airways, lined predominantly with gently rounded nonciliated cells, and alveolar ducts, with flatter squamous epithelium commonly

displaying a finely wrinkled appearance (Figure V.3). Epithelium-lining fluids appeared continuous across this transition zone and distally, alveolar ducts with relatively smooth surfaces gave rise to a shallow alveoli along the ducts as well as deeper, more spherical alveoli farther along the airpath. The morphology of alveoli in the frozen-hydrated state, alterations in alveolar shape related to position in the respiratory path, and characterization of alveolar surfactant are topics of great interet in pulmonary research and are examined in detail elsewhere (Bastacky et al., 1984, in preparation). Briefly, alveoli appear relatively smooth with few pores evident (Figure V.4A), in contrast to airway fixed samples. Smooth surfaces of presumed surfactant are evident, as are adjacent wrinkled areas representing finely attenuated epithelium. Often capillary networks can be seen bulging into the alveolar lumen; in cross-section, thin epithelium, interstitial spaces, and thin-walled capillaries are seen. Lymphatic spaces are difficult to identify. The parietal pleura consists of a dense network of cells (Figure V.4B) with extremely fine ice crystal lattices.

Etching of large blood vessels revealed apparently crenated erythrocytes (Figure V.5A), indicating that relatively slow freezing rates were encountered in central portions of the lung (Kuhn, 1974). However, ice crystal damage patterns in cells, a function of freezing rate (Echlin, 1978), were consistently on the order of a few tenths micrometer and actually aided in the identification of intracellular spaces. Such profiles were clearly revealed by surface sublimation of

water due to the etching process. In unetched samples identification of structures was rendered more difficult since the flat, fully hydrated fracture faces presented less structural information (Figure V.5B and C).

Following freeze drying overnight lung pieces shrank an undetermined amount; however, little change in the morphology of fracture faces was evident. Cracking of the original gold coating and wrinkling of epithelium, particulary in alveoli, confirms observations described by Hook et al. (1980) and was probably responsible for increased charging effects, resulting in a need for recoating. The dense network of condensed cytoplasm due to ice crystal damage observed after etching from the frozen hydrated state was similar to the appearance after freeze drying. The greatest morphological alterations were in airway and alveolar fluids and blood vessels which were markedly cracked and buckled (Figure V.5D).

V.3.B Interactions Between Cells and Particles

For Fe_2O_3-exposed animals, x-ray maps were made of the frozen hydrated lung surface at low magnifications (50 - 100 X) to locate deposits of particles. Occasionally no particles were observed in exposed animals and samples were refractured, re-etched, and recoated. At higher magnifications, observed particles were either mapped or identified as Fe-containing by placing a reduced raster on appropriate volumes. Particles were observed in various locations within the pulmonary system. In conducting airway cross-sections, particle agglomerations were either embedded within mucus or within presumptive

phagocytes residing upon the epithelial surface. When observed within phagocytes, particles invariably appeared within the cytoplasm and never within the nucleus (Figure V.6A and B). Occasionally, extracellular particles appeared to be wedging between two adjacent epithelial cells (Figure V.6C); however, no particles were observed within epithelial cells. En face, airway particles were generally clustered, were embedded in mucus, and were usually located preferentially around cell borders between rounded apical cell surfaces (Figure V.2B). Occasional large particle agglomerates were seen. Greater difficulty was encountered in identifying suspected phagocytes and in characterizing particle deposits as intra- versus extra cellular when viewing airway surfaces (Figure V.7 and 8). Large particle agglomerates were more commonly observed in large airways when compared with small airways and alveoli. Particles were observed both proximally and distally to the conducting airway/alveolar duct transition zone (Figure V.7). Distally, particle clusters were scattered throughout the alveolar ducts and first few alveoli in the respiratory path, and were preferentially associated with smooth, presumably fluid patches in more distal alveolar spaces. Occasionally particle deposits were correlated with presumptive macrophages (Figure V.8).

V.3.C Comments on Methodology

In early experiments occasional incomplete inflation near the pleura was observed; this problem was reduced by gently massaging the diaphramatic lung surface at 20 cm water pressure before quick-freezing.

Another problem encountered was distortion in structures near the entering lobar bronchus, which was reduced by orienting the lung so that the trachea entered the melting nitrogen slush first. Imaging problems due to charging were variable but usually significant due to the highly convoluted topography of the lung which made charge dissipation more difficult, the application of relatively light gold coatings, and the relatively high beam currents required for x-ray maps. Best SE results were obtained by interrupting specimen exposure to the beam for about 10 minutes after x-ray imaging then conducting subsequent SE imaging at 10 to 15 KeV with relatively low beam currents. This substantially reduced but did not eliminate charging phenomena.

V.4. DISCUSSION

V.4.A Frozen-Hydrated Lung Morphology

Various approaches have been used to examine lung tissue in as nearly natural a state as possible. Vascular perfusion fixations are reported to preserve mucus and surfactant (Kuhn, 1974), but questions exist concerning possible alterations in particle distribution or to fluid compartments (Manabe, 1979; Holma, 1969). In freeze-fracture studies, the morphology of successfully preserved surfactant has been examined (Untersee, 1971; Manabe, 1979), yet there are many drawbacks to the use of freeze fracture replicas when compared with bulk frozen tissue (Hayes, 1982).

The morphology of inflated bulk-fractured frozen lung tissue observed in this study confirms previous descriptions (Hook et al.,

1980; Bastacky et al., 1983, 1983b). Most features were easily correlated with known histological (Weiss and Greep, 1978) and SEM appearances (Kessel and Kardon, 1979; Kuhn, 1974; Greenwood and Holland, 1972; Bastacky et al., 1983, 1983b). En face examination of airways revealed a mucus blanket whose continuity was related to the amount of water content which in turn affected by surface etch. Cells were gently rounded into the lumen and wavy patterns represented cilia, which were occasionally observed through cracks in the mucus. Cross-sectional fractures revealed epithelial cell features (subcellular organelles), basement membrane, and various features of the interstitial and vascular networks. Connective tissue in the lamina propria was revealed by etching to have a tube-like ice crystal lattice; interstitial cells, large blood vessels, and capillaries could also be identified. Zones of transition between terminal bronchioles and alveolar ducts were apparent as were the alveolar spaces, which contained surfactant, the continuity of which again was related to etch. Several artifacts of freezing and preparation were noted; most notably, (1) ice crystal lattice patterns, (2) crenation of centrally-located erythrocytes, (3) large-scale cracks from bulk fracture, and (4) occasional surface accumulation of debris consisting of both tissue (fragments from knife) and ice crystals.

Samples were freeze dried overnight in the high vacuum environment of the SEM then reexamined at room temperature. Recoating was necessary to reduce charging which was more severe than in the frozen hydrated state under identical SEM conditions. Causes for this

breakdown in charge conduction may include cracks formed in the coating during drying (Hook et al., 1980) and a decreased ability of specimen ions and electrolytes to carry away charge (Echlin, 1978). Morphology of the unfixed lung after freeze drying is similar to the frozen hydrated state except for widely dispersed cracking of former primarily aqueous compartments (mucus, surfactant) and dimensional shrinkage due to drying.

V.4.B Particle Distribution

Particle administration to lung tissue by intratracheal instillation is commonly used in toxicologic studies due to ease of exposure, reduction of experimental time involved, ability to give large doses in short times, and lack of expense when compared with inhalation exposure (Brain et al., 1976). However, this exposure route is reported to result in nonuniform distributions dependent on anatomic location within the lung (Brain et al., 1976, 1979; Cember, 1964; R. Valentine and D. McNeill, personal communication). In this study we demonstrate the ability to instill Fe_2O_3 into mice and subsequently locate test particles in frozen hydrated lung. Quick-freezing is considered to be an optimal approach towards preserving the lung in its natural state given the need to avoid fluid and particle washout or translation (Manabe, 1979; Kuhn, 1974). Particles were observed in various portions of the pulmonary system including conducting airways (within the mucus blanket wedged between domed epithelial cells and within plagocytes), the transition zone between terminal brochioles and alveolar ducts, in alveolar spaces,

and within interstitial cells. Particles were commonly grouped in large clusters and aggregations of suspected phagocytes were seen as early as one hour post-exposure. Internalized particles were within the the cytoplasm of phagocytes, as seen in cross-section, and suspected phagocyte clusters en face could be correlated with particle burdens both in respiratory and in conducting airway luminal spaces. Although particles were observed in contact with the columnar epithelium of conducting airways, thus presumably increasing chances of endocytosis, no internalization by or transport between epithelial cells was evident.

In some particle-exposed mice entire fracture faces were frequently particle-free. Thus, particle distribution can be described as nonhomogeneous both globally (between respiratory airpaths) and within a single airpath. Global nonhomogeneity in instilled particle distribution is to be expected on the basis of the literature cited above, and may also exist to some extent in inhalation exposures due to variations in local ventilation (Holma, 1969). However, it is not clear to what extent particle deposition is variable within an individual unit airway in instillation versus inhalation exposure regimes. After instillation, we find many clumps of particles present in various portions of the airspaces including alveoli. Holma (1969) examined by SEM the distribution of inhaled polystyrene particles after lung fixation by paraformaldehyde vapor inhalation, and found nonuniform distributions of particles within airways. Particles were observed at bifurcations as reported here

(see Figure V.2B). Holma (1969) observed only a few particles in any one alveolus; here, some alveoli are loaded with many particles and clusters of phagocytes appear evident. Differences between the deposition of particles by inhalation versus instillation may therefore exist, and frozen hydrated lung imaging appears to be a useful technique in such investigations. If different deposition patterns exist, problems of interpreting biological responses using instillations for pulmonary toxicologic research may result. For example, Schlesinger and Lippmann (1978) saw a close correspondence between relative particle deposition efficiency and frequency of bronchial cancers at specific sites, and Hayes et al. (1980) suggested that the exposure to a single cell or group of cells may be crucial in determining responses such as mutation or neoplasia.

V.4.C Frozen-Hydrated SEM Techniques

Artifacts caused by the freezing of biological tissues preparatory to SEM examination have been of interest for some time due to the popularity of freeze drying techniques (Boyde, 1978). Low temperature SEM methods avoid attendant drying artifacts (such as shrinkage) and preserve tissue fluids as a solid within the specimen. Fewer preparative steps can reduce specimen shrinkage, preserve spatial relationships, and reduce extraction and diffusion artifacts (Hayes, 1982). Rapid freezing followed by frozen hydrated SEM is of great value in x-ray microanalytic work since it reduces intracellular ionic diffusion, and has been used in studies of elemental distributions in differentiating root tips (Echlin et al., 1979, 1980b, and 1982).

Morphological studies of various mammalian tissues have also been conducted using frozen hydrated SEM; these include studies of mouse intestine (Carr et al., 1983) and lung tissue. Hook et al (1980) described the morphology of frozen hydrated mouse lung and alterations caused by shrinkage during freeze drying; subsequent studies by these investigators examined the accumulation of fluid in edematous dog lungs (Hook et al., 1982). Albertine et al. (1983) studied morphological relationships and pulmonary fluid in pleural spaces of sheep lung. Bastacky et al. (1983, 1983b; 1984, in preparation) examined the architecture of alveolar spaces with intact surfactant in mice. Studies such as these are dependent on retaining tissue fluids during SEM imaging.

Cryoprotectants are used in some studies (Echlin, 1978; Echlin et al., 1980b, 1982) to reduce ultrastructural deformation due to water translocation during freezing. However, the convoluted topography of the lung, the desire to precisely control pulmonary inflation pressure, and the need to avoid particle washout or translocation, made the infiltration of cryoprotectants inadvisable in this study. Rejection of cryoprotectants necessitated the acceptance of widespread freezing artifacts in the etched frozen hydrated lung. Perhaps foremost were artifacts due to intracellular ice crystal damage. The freezing of cells and biological tissue is an extremely complex process (Mazur, 1970; Plattner and Bachman, 1982) and the freezing rate of cells and tissues is critically related to observed intracellular morphology (Nei, 1978; Echlin, 1978). It is generally

agreed that ultra-rapid cooling is essential to reduce the size of ice crystals formed (Nei, 1978; Kuhn, 1974); the rate at which tissue can be frozen is a complicated function of the temperature gradient, thermal constants and size of the tissue, and the rate of heat transfer to the coolant (Kuhn, 1974; Bald and Crowley, 1979; Plattner and Bachman, 1982). In the case of relatively large bulk frozen tissues it is therefore not surprising that variations in the quality of morphological preservation within tissues are observed (Bald and Crowley, 1979). Elder et al. (1982) found maximum ice crystal profiles at a depth of 40 to 50 μm from the tissue surface, with smaller, more uniform profiles at increasing depths; however, Weibel et al. (1982) report variations in preservation that render frozen lung specimens unsuitable for quantitative ultrastructural morphology. A slurry of melting solid/liquid nitrogen slush was used in our study to freeze lungs rather than liquid nitrogen alone, in order to increase cooling rates (Elder et al., 1982).

Variations in morphological preservation were observed in our investigations of frozen hydrated mouse lungs. In all cases after etching, a reticular matrix of condensed cellular material caused by ice crystal formation was seen. The dimensions of spaces thus formed were dependent on location within the lung. Larger spaces were seen in etched, cross-sectioned airway epithelium, compared with the fine pattern observed in pleural cells (see Figure V.4B). This is not surprising since the pleural surface is in direct contact with the coolant and was thus expected to have more rapid cooling rates

(Kuhn, 1974; Elder et al., 1982). Also, erythrocytes were seen in various states of preservation. In alveolar capillaries, especially near the pleura, the characteristic erythrocyte biconcave shape was well-preserved. However, in large blood vessels, etching revealed obviously crenated cells (Figure V.5A) suggesting that intracellular transfer of water occurred due to the relatively slower freezing rates (Kuhn, 1974). In this study, the variable preservation and ice crystal damage observed was not considered to be a problem in evaluating interactions between particles and cells, and indeed was of value in allowing easy identification of intra- versus extracellular spaces.

As noted by many researchers (e.g., Echlin, 1978), the use of radiant heat etching is important in interpreting the morphology of frozen hydrated material. This was confirmed in our work; the interpretation of structural relationships between fully-hydrated cells and the extracellular matrix was difficult if not impossible in complex areas such as cross-sectioned large airways containing cells, blood capillaries, and connective fibers (Figure 3B). Although etching times were usually held constant, varying degrees of surface ice sublimation were observed. The mechanisms of this variation include geometry between fracture face and etcher, vacuum conditions, temperature, and the "etchability" of the specimen (Echlin et al., 1979), but to our knowledge have not been critically evaluated for a variety of cell and tissue specimens. Here, etch variability was not a crucial problem, except as it, but it is of great importance in

quantitative x-ray microanalytic investigations of bulk frozen hydrated material where the degree of specimen hydration must be known and controlled, since peak-to-background ratio calculations of cellular elemental components require knowledge of specimen mass (Echlin, 1978; Echlin et al., 1980b, 1982; and Fuchs and Fuchs, 1980). It should be noted that the observed etch patterns may be due in part to other factors such as ice sublimation during coating or while under the electron beam (Goldstein et al., 1981).

As an example of the unique capabilities of low temperature SEM we have examined particle interactions with inflated lung tissue preserved by quick freezing. Techniques described here eliminated many preparative steps in conventional EM in an attempt to avoid particle translocation. Particles were identified and the nature of cell/particle interactions could generally be characterized. Correlative microscopic techniques would be of value in further characterizing such interactions. For example, after freeze drying selected areas of interest can be excised by microdissection (Bastacky et al., 1983) and embedded in appropriate materials for histological or TEM examinations as described by Carr et al. (1983).

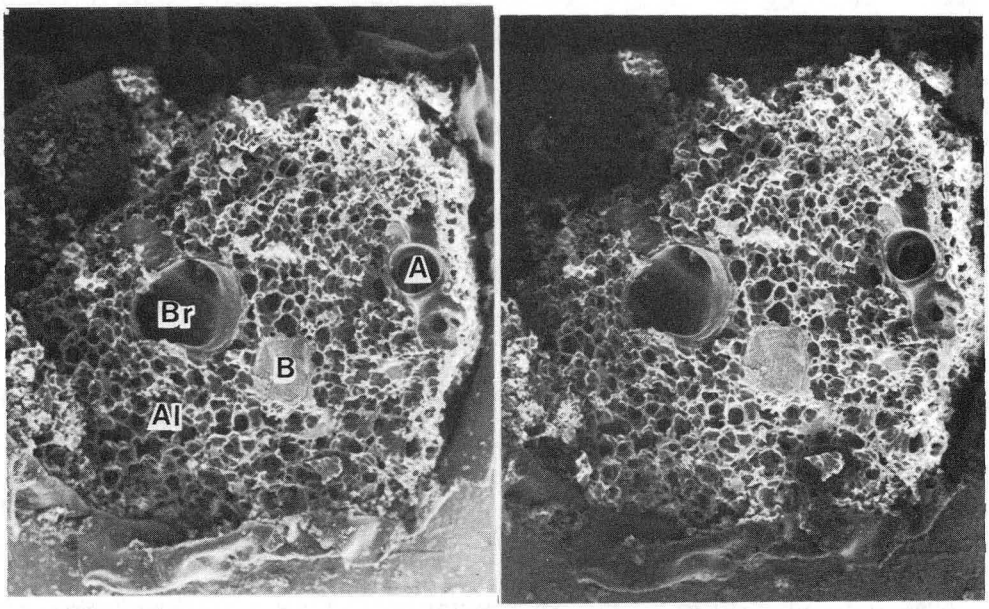

Figure V.1 Low magnification stereopair scanning electron micrograph (SEM) of fracture face of frozen-hydrated, etched, gold-coated mouse lung. Evident are blood vessels (B), lobar bronchus (Br), airway (A), and alveolar spaces (A1). Magnification = 20X, tilt separation = 8°.

XBB 845-3382A

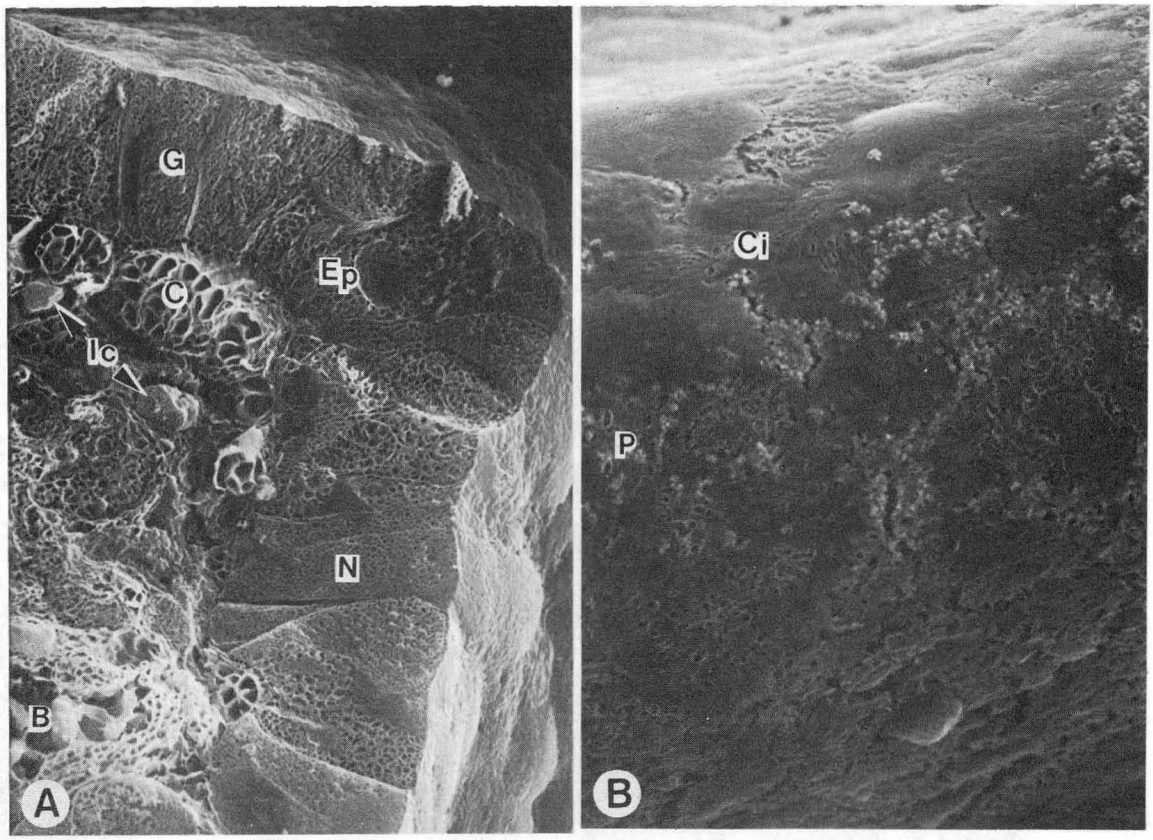

Figure V.2 SEM of frozen-hydrated, etched airway. A. In cross-section, surface etching allows the visualization of an ice crystal lattice pattern. Features include epithelial cells (Ep) with internal granules (G) and nuclei (N), connective fibers (C) of the lamina propria, blood vessels (B), and interstitial cells (Ic). Magnification = 2,000X. XBB 841-323. B. View from the airway lumen of the epithelial surface at a bifurcation; cracks in the mucus blanket result from surface etching. Gently rounded cells are seen, as are cilia embedded wihin the mucus (Ci) and particles (P) in this Fe_2O_3-exposed mouse (one hour post-exposure). Magnification = 2,000X. XBB 841-310A

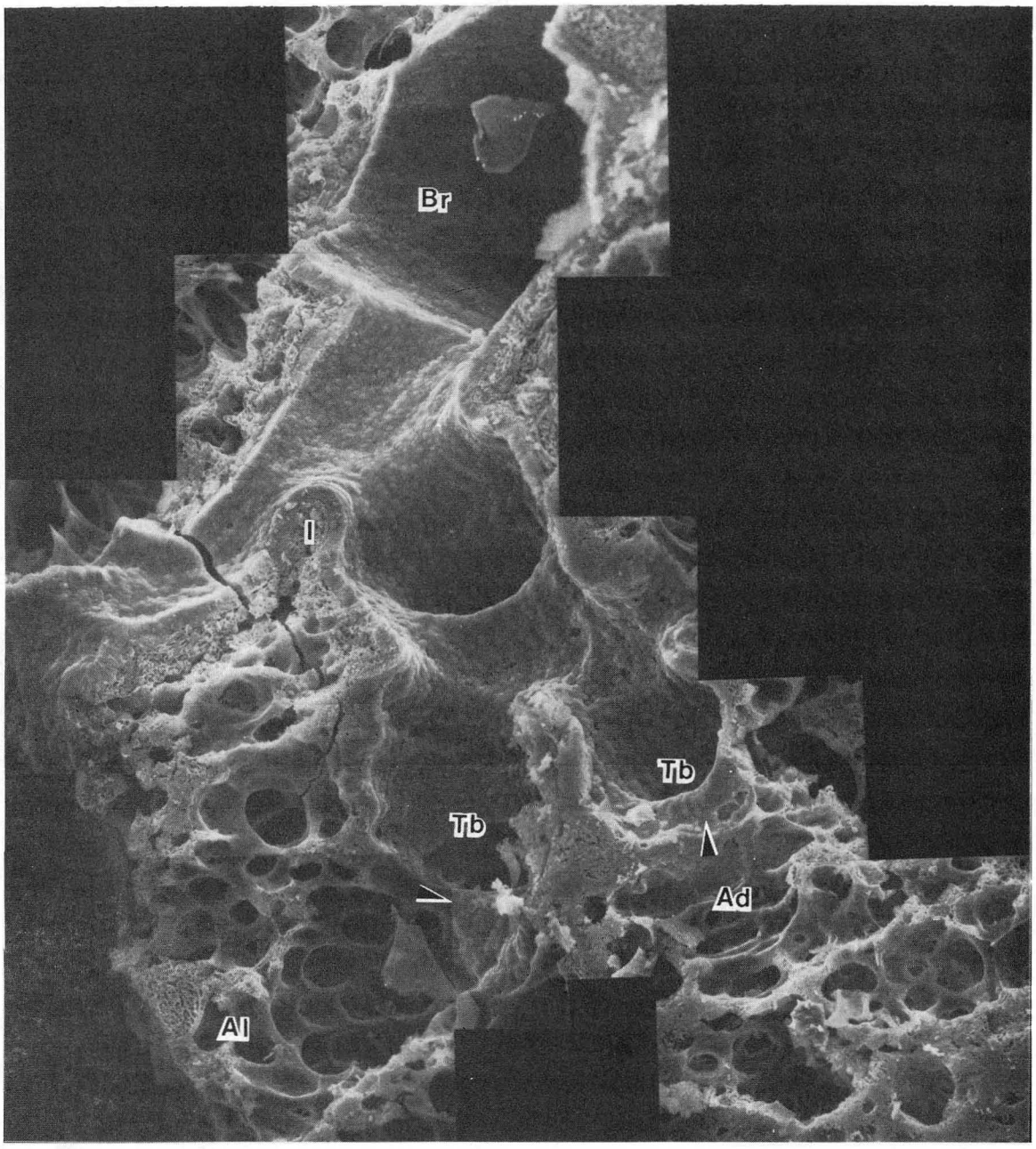

Figure V.3 SEM photomontage of frozen-hydrated, etched airpath. A large bronchus (Br) branches into smaller bronchi, terminal bronchioles (Tb), alveolar ducts (Ad), and finally alevoli (Al). A thicknened interstitium is evident around larger airways (I), and sharp transition zones (arrowheads) are evident between terminal bronchioles and alveolar ducts. Magnification = 250X. XBB 841-606A

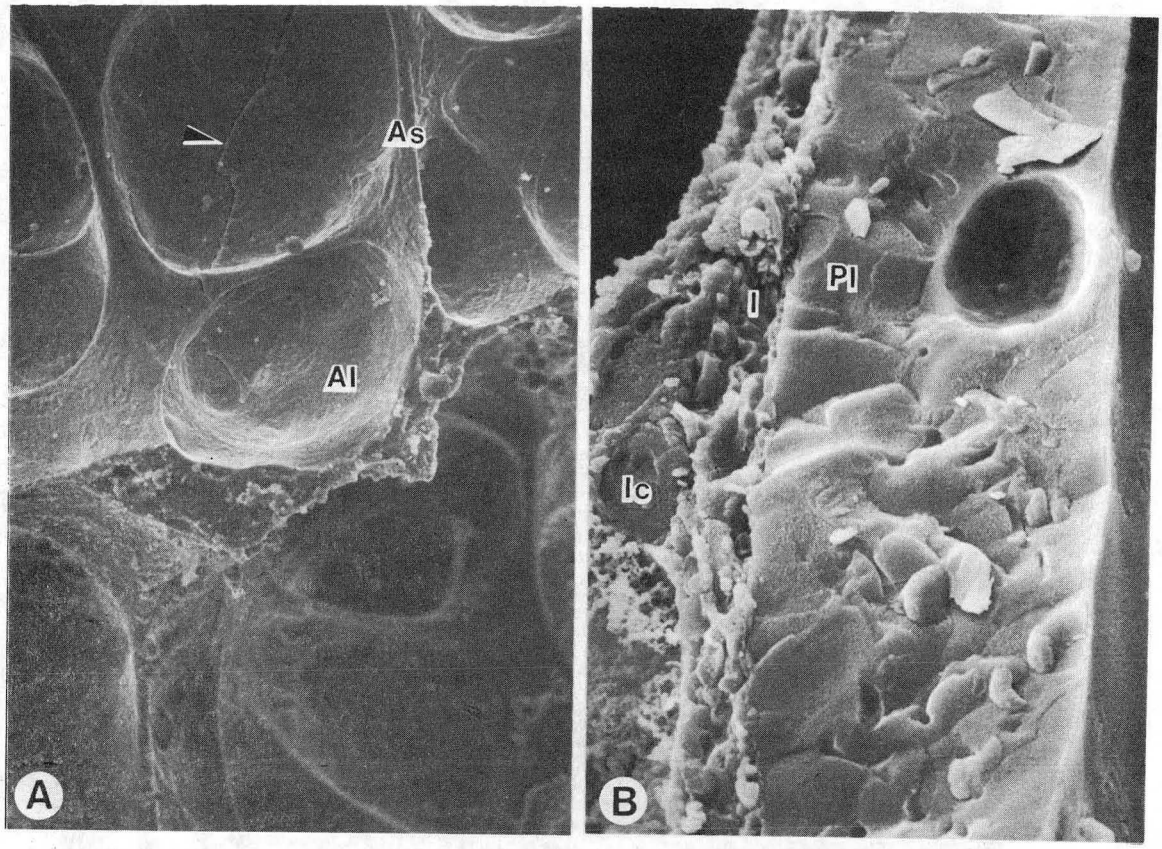

Figure V.4 Frozen-hydrated SEM of fractured, etched mouse lung. A. Alveoli (Al) and alveolar septa (As) are evident. In the frozen-hydrated state, few pores are observed. A stress fracture (arrowhead) is evident from the fracturing process. Magnification = 500X. XBB 841-349. B. Cells of the parietal pleura (Pl) have a very fine ice crystal lattice pattern indicative of rapid freezing rates. Also evident are interstitial spaces (I) and cells of the interstitium (Ic). Magnification = 2,000X. XBB 841-343A

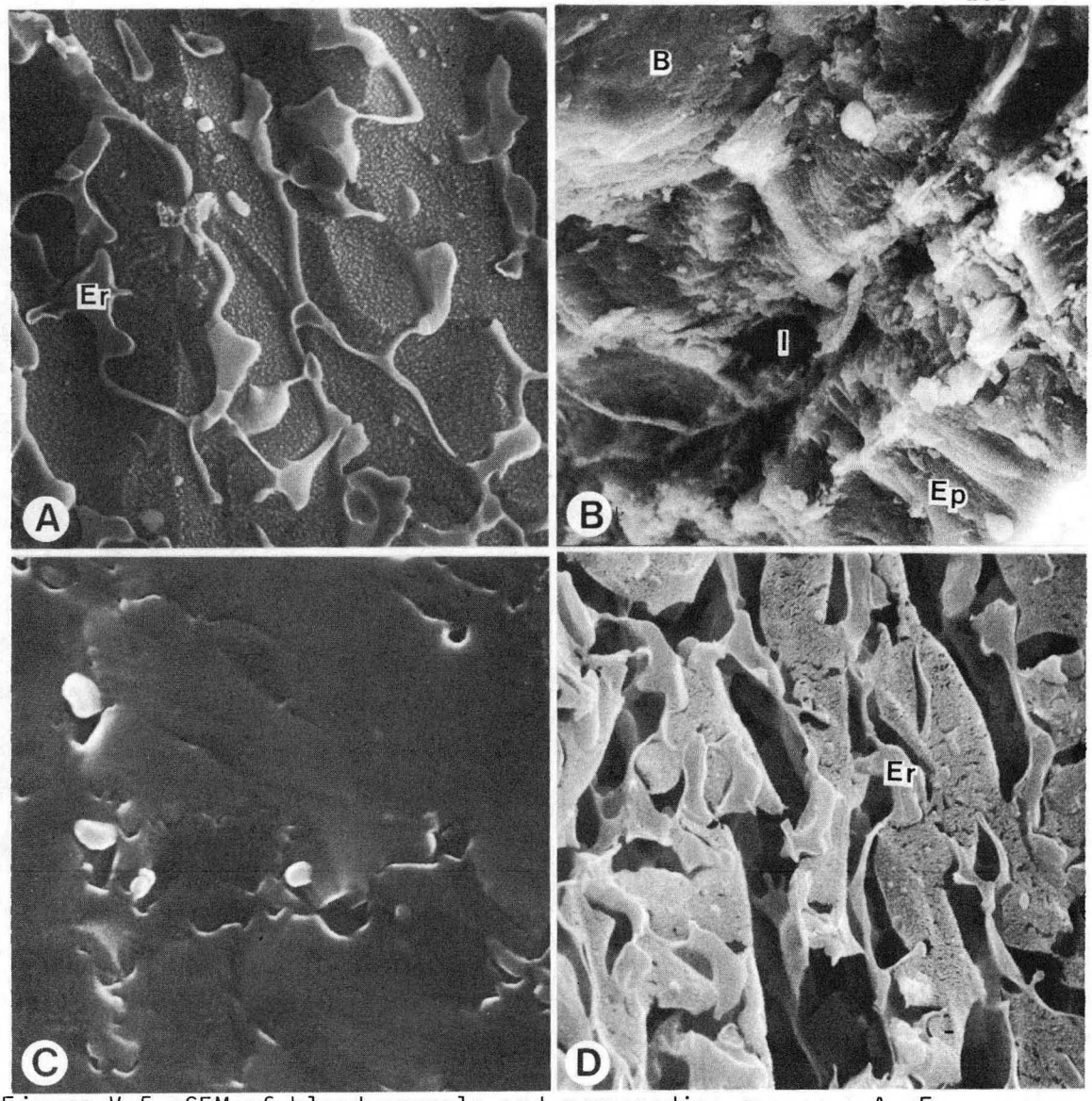

Figure V.5 SEM of blood vessels and surrounding spaces. A. Frozen-hydrated, fractured, etched blood vessel. The crenation of erythrocytes (Er) is evident, and the blood plasma exhibits a granular appearance. Magnification = 5,300X. XBB 841-288. B. Fully hydrated, unetched cross-sectional area roughly corresponding to that seen in Figure V.2A. Identification of features is difficult due to the lack of ice crystal lattice patterns; evident is a blood vessel (B), epithelium (Ep), and interstitium (I). Magnification = 1,000X. XBB 841-316. C. Higher magnification of blood vessel seen in B. Identification of erythrocytes is difficult. Magnification = 5,000X. XBB 841-306. D. Blood vessel after freeze-drying overnight. The water is no longer present; erythrocytes (Er) can be identified. Magnification = 5,000X. XBB 841-339A

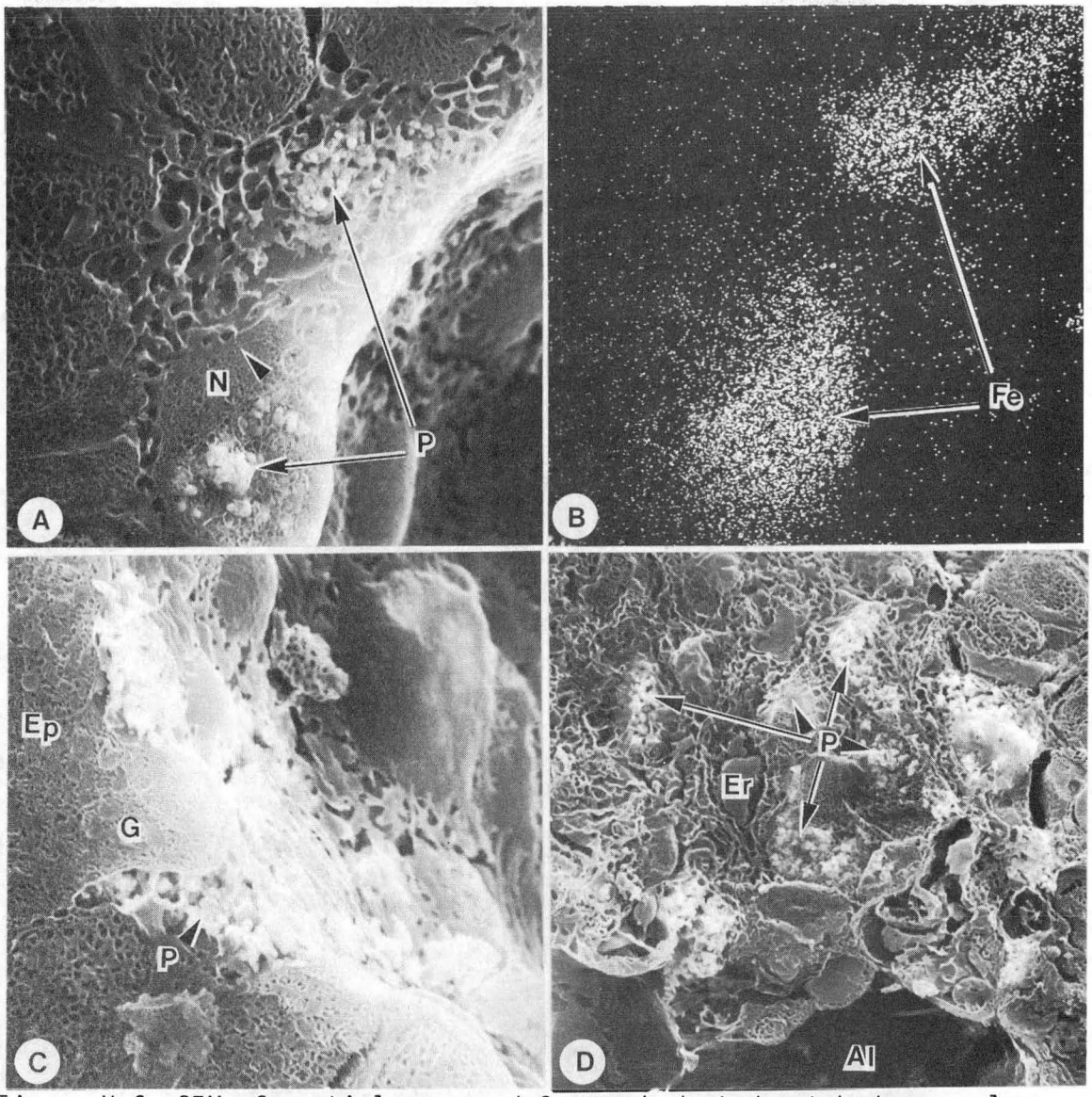

Figure V.6 SEM of particle-exposed frozen-hydrated, etched mouse lung. A. Two particle deposits (P) are observed atop the epithelium (Ep). The lower particle cluster is within a cell not continuous with the epithelium, probably a macrophage. The nucleus (N) and nuclear membrane (arrowheads) are evident, and particles are sequestered strictly to the cytoplasm. The top particle cluster is associated with the larger grained lattice pattern characteristic of mucus. One hour post-exposure. Magnification = 5,000X. XBB 841-356. B. X-ray map for the Fe Kα line corresponding to the field of view seen in A, clearly defining the two particle clusters. Magnification = 5,000X. XBB 841-355. C. Another area of cross-sectioned epithelium (Ep), showing particle deposits (P) located in a trough between rounded epithelial cells. Granules (G) are observed within the epithelium. One hour post-exposure. Magnification = 5,000X. XBB 841-358. D. A cluster of cells containing particles (P). Also observed are erythrocytes (Er) within capillaries, and alveolar spaces (Al) relatively free of particles or phagocytes. Four hours post-exposure. Magnification = 2,000X. XBB 841-321A

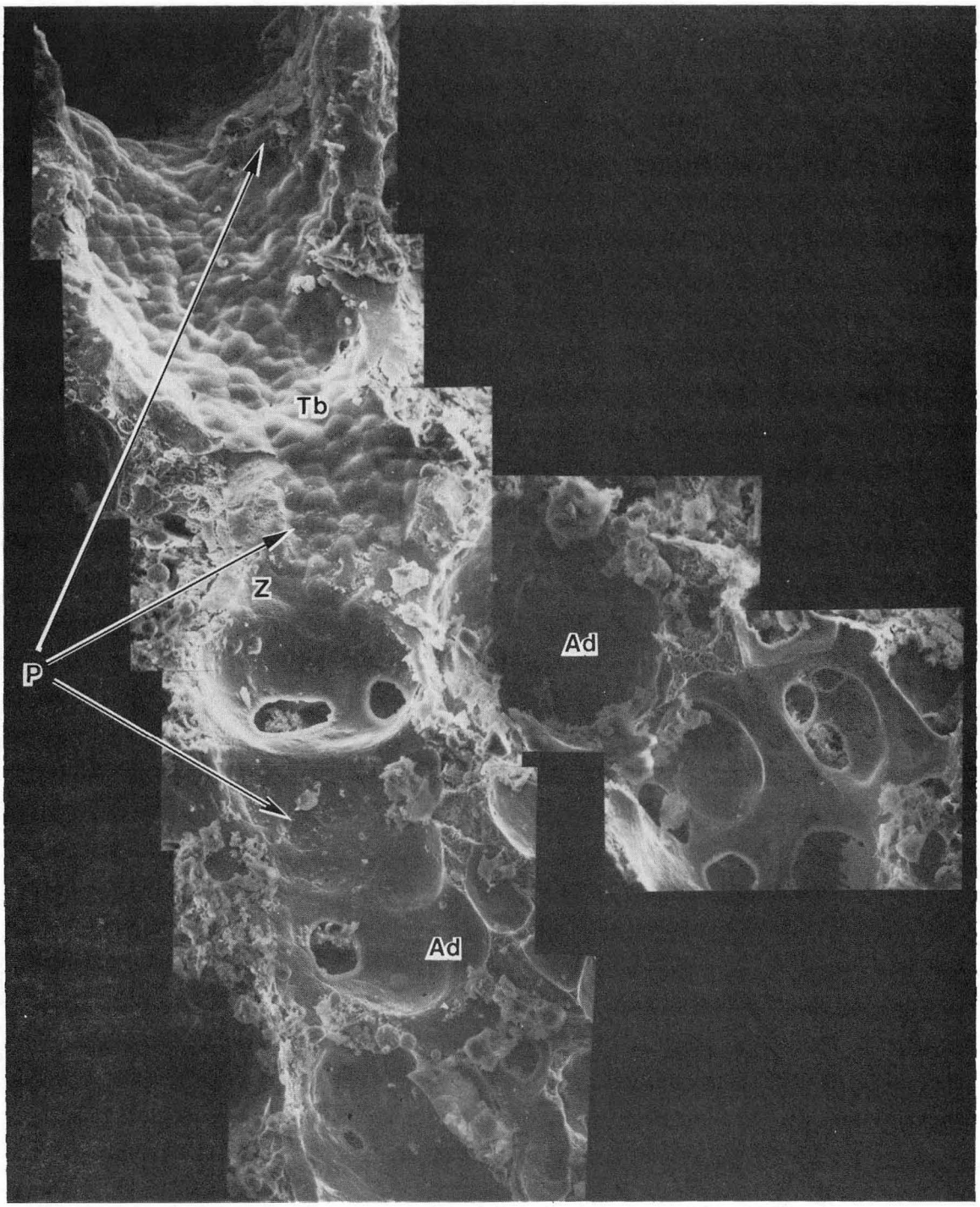

Figure V.7 SEM photomontage of frozen-hydrated, etched, particle-exposed mouse lung, one hour post-exposure. A terminal bronchiole (Tb) leads into two alveolar ducts (Ad). Particle deposits (P) are evident both proximal and distal to the sharp zone of transition (Z) between the terminal bronchiole and the alveolar ducts. Magnification = 500X. XBB 841-607A

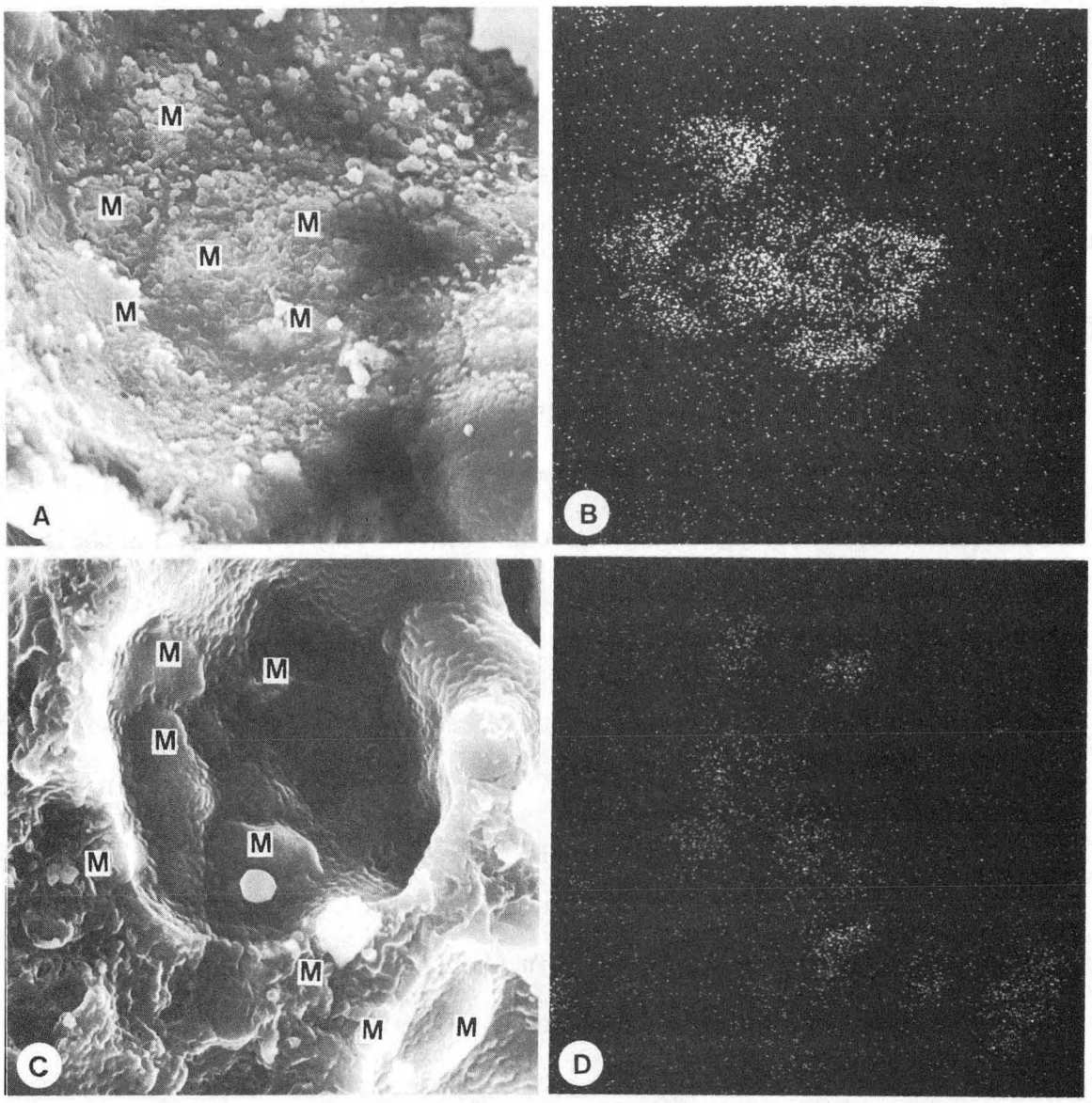

Figure V.8 SEM of frozen-hydrated mouse lung, showing particles sequestered within phagocytes (presumptive macrophages). One hour post exposure. A. Airway lumen just proximal to the terminal bronchiole/ alveolar duct transition zone; in this unetched sample, the fluid blanket appears continuous and ice crystals are present, but it is difficult to identify particle-containing cells (M). Magnification = 1,000X. SBB 841-352. B. X-ray map for Fe Kα corresponding to A. A cluster of particles is evident; furthermore, comparison with the secondary electron image suggests these particles are associated with a group of cells, possibly representing particle-laden macrophages entering a pulmonary airway. Eighteen hours post-exposure. Magnification = 1,000X. XBB 841-351. C. Several cells (M) appear to be gently rounded into the alveolar lumen. One hour post exposure. Magnification = 2,000X. XBB 841-302. D. X-ray map for the Fe Kα line corresponding to A; the localization of Fe_2O_3 corresponds with the identified cells. Magnification = 2,000X. XBB 841-301A

VI. CONCLUSIONS

An examination of the potential health effects of inhaled, deposited particulate material on the pulmonary system is of interest in toxicological research. The work described herein forms a coordinated study of the differential pulmonary effects of toxic (Ni_3S_2) versus nontoxic (TiO_2, glass beads, and Fe_2O_3) particles. The studies endeavor to provide quantitative morphological characterizations of cell/particle interactions at the tissue, cell, and ultrastructural level, under the operating assumption that morphological evaluations can help to elucidate mechanisms at work. Throughout, the examination of low doses at short timepoints post-exposure were employed. Low doses were used to avoid acute systemic toxicity and the potential non-specific effects of high particle loadings. Short timeperiods were examined in order to investigate early physiologic and morphologic alterations resulting from particulate exposure.

The *in vivo* experiments in Chapter II served to validate the model systems and compounds examined. Differential biological effects were expressed by mice after intratracheal instillation of low doses (approximately 0.5 mg/kg) of Ni_3S_2 and TiO_2. Clinical symptoms and the increase of lavageable PMN cells observed in the Ni_3S_2-exposed mice indicated that this compound is toxic, whereas the response of animals to TiO_2 was indistinguishable from PBS control groups. The pulmonary clearance of ^{63}Ni and Ti was examined, as was the metabolism of ^{63}Ni. Nickel was cleared more rapidly than Ti,

resulting in a significantly lower lung Ni burden at 3 and 7 days post-exposure; when clearance data were fitted to a biexponential clearance curve, the longer-term clearance rate constant was significantly greater than that for Ti. These results are most probably explained on the basis of differences in compound solubility; TiO_2 is relatively insoluble in biological fluids, whereas Ni_3S_2 is somewhat more soluble, especially in the presence of serum and oxygen, conditions which exist in the Ni_3S_2-exposed lung. Further evidence for ^{63}Ni solubilization was provided by the rapidity with which ^{63}Ni was found in the blood and kidneys. Maximum levels were observed one hour post-exposure, and the longer term clearance rate constants were similar for the lung, kidney and blood.

Various observations were made in Chapters II and V describing the unphysiological nature of the intratracheal instillation technique used to introduce particles to mouse lungs. Upon instillation of a 20 µl suspension to upright, deep-breathing anesthesized mice, induced coughing often resulted in the formation of bubbles which rapidly transported particles from the trachea to the GI tract. In studies employing Fe_2O_3 (Chapter V), the rust color of the bubbles demonstrated that particles were translocated in this manner. In Chapter II, rapid clearance of ^{63}Ni to the GI tract was observed; 20 percent of the instilled dose was in the GI tract only 15 minutes post-exposure, and pulmonary recoveries of ^{63}Ni and Ti were only 74 and 65 percent, respectively, 15 minutes post-exposure. Therefore, the instilled dose does not accurately reflect the dose administered

to the lungs, and in studies where specific pulmonary dosages are desired, this rapid regurgitation of particles must be evaluated.

The nonuniform deposition of particles instilled into lungs, observed by many researchers, was confirmed in Chapter V. The frozen-hydrated SEM approach used eliminated particle translocation and washout by fluids which are involved in conventional EM preparatory techniques. Multifocal particle clusters were encountered, as were occasional entire fracture faces without particles. The interactions between clusters of particles and frozen-hydrated lung structures were characterized, and differences in particle deposition within individual respiratory airpaths were hypothesized for the instillation versus inhalation exposure route. The extent to which instillation can serve as an appropriate model for inhalation exposure should therefore be critically examined in any proposed experiments.

The toxic effects of Ni_3S_2 particles to cultured hamster tracheal explants were examined using quantitative SEM analytical techniques in Chapter III. Explant sections were maintained in vitro using an appropriate culture medium, and they presented a number of cell types preserved in a physiological arrangement. A one hour exposure of 20 µg Ni_3S_2 per ml culture medium caused a rapid sloughing of differentiated columnar epithelial cells. From immediately after to one hour post-exposure, most 2000X fields of view exhibited varying degrees of focal or complete desquamation. By 4 hours post-exposure, the initial desquamation appeared complete, and

elongated, interdigitating basal cells were present. Replacement of these basal cells led to recolonization of the epithelium, the stages of which included coverage by large, polyhedrally-shaped squamous cells, the reappearance of ciliated cells, and many fields of view similar to controls by 7 days in culture. The role of ciliated cells is of interest in assessing the expression of toxic effects since such cells are considered end-stage in development, are important in maintaining mucus flow in vivo, and have been considered to be specially sensitive to damage in the literature. In this study Ni_3S_2 particles were often found trapped in clumps of cilia, suggesting that ciliated cells may have a greater chance for exposure to particles compared with nonciliated cells, a hypothesis which could account for heightened susceptibility to damage. Another interesting question raised by this research concerns the mechanism(s) of epithelial toxicity. Generally, few particles per field of view were located, yet complete desquamation occurred, and many sloughing cells were not observed to be particle burdened.

A major portion of the in vitro experiments concerned the exposure of lavaged, cultured AM cells to Ni_3S_2, TiO_2, and glass beads. Pulmonary AM are of importance in response to particulate challenge and are therefore of interest in health effects assessment. Cells were exposed, prepared for electron microscopy, then examined using quantitative microscopic techniques. A correlative microscopic technique was developed that allowed cell exposure, identification of individual cell viability (by trypan dye exclusion), then EM analyses

of previously identified AM, including SEM surface morphology, x-ray microanalytic evaluation of particle content, and whole cell mount TEM of cell interior ultrastructure. It was possible to examine the correlations between individual cell viability, particle content, and morphologic alterations. Many stages of AM disruption were described, including bleb formation and sloughing, cell rounding and the loss of normal surface architecture, degeneration of the external cell membrane, and complete cell degranulation. Quantitative examinations demonstrated that Ni_3S_2 and TiO_2, but not GB, particle content was correlated with AM alteration. Furthermore, Ni_3S_2 and TiO_2 internalization was correlated with AM death, while GB appeared to be nontoxic. In the case of TiO_2, particle content (either internal or external) was not significantly associated with cell death; however, the association between TiO_2 internalization and death was statistically significant. This finding demonstrated that individual cell analytic techniques coupled with correlative microscopy were invaluable in characterizing sensitive indicators of AM damage, by providing increased amounts of information about individual cells.

Although bleb formation and sloughing occurs in unexposed control AM, this study suggests that increased bleb incidence results from particle exposure (especially toxic Ni_3S_2). These increases are also evident in AM lavaged from Ni_3S_2-instilled mice. In the literature, increased enzyme secretion is observed in AM populations after exposure to various particle types; it is possible that the blebs observed here may correspond to excreted cytoplasmic packets.

If so, it is interesting to speculate on the mechanism of bleb formation and release; bleb clusters are not always associated with particles, and particles are often found without bleb clusters. A defect in the external membrane, often observed near the site of Ni_3S_2, may or may not be a requirement for bleb formation. It is also not clear to what extent bleb cluster formation necessarily leads to AM disruption, since blebs are also found in control cultures, or at which stage morphological alteration irreversibly leads to either cell lysis and death or the disruption of normal cell function.

VII. BIBLIOGRAPHY

Abbracchio, M. P., J. D. Heck, and M. Costa. The Phagocytosis and Transforming Activity of Crystalline Metal Sulfide Particles are Related to their Negative Surface Charge. Carcinogenesis 3: 175-180, 1982.

Adalis, D., D. E. Gardner, F. J. Miller, and D. L. Coffin. Toxic Effects of Cadmium on Ciliary Activity Using a Tracheal Ring Model System. Environ. Res. 13: 111-120, 1977.

Adler, K. B., G. S. Davis, C W. Woodworth, and A. R. Brody. The Human Pulmonary Macrophage: Two Distinct Morphological Populations. SEM/1979/III, SEM Inc., AMF O'Hare, Chicago, IL, p. 921-927, 1979.

Albert, D. M., J. R. Gonder, J. Papale, J. L. Craft, H. G. Dohlman, M. C. Reid, and F. W. Sunderman, Jr. Induction of Ocular Neoplasms in Fischer Rats by Intraocular Injection of Nickel Subsulfide. Invest. Ophthalmol. Visual Sci. 22: 768-782, 1982.

Albertine, K. H., J. P. Wiener-Kronish, J. Bastacky, N. C. Staub. The Structure of Pleural Spaces in Sheep. Fed. Proc., submitted, 1983.

Anderson, T. R. Techniques for Preservation of Three-Dimensional Structures in Preparing Specimens for Electron Microscopy. Trans. N. Y. Acad. Sci. (Ser. II), 13: 130, 1951.

Asmundsson, T., K. H. Kilburn, and W. N. McKenzie. Injury and Metaplasia of Airway Cells due to SO_2. Lab. Invest. 29: 41-53, 1973.

Bald, W. B. and A. B. Crowley. On Defining the Thermal History of Cells During the Freezing of Biological Materials. J. Microsc. 117: 395-409, 1979.

Barhad, B., N. Manoleseu, N. Siminescu, and V. Ciocnitu. Changes Concerning the External Structure of Peritoneal Macrophages due to the DQ-12 Standard Dust. Environ. Res. 31: 256-265, 1983.

Bastacky, J., T. L. Hayes, and B. von Schmidt. Lung Structure as Revealed by Microdissection: Positional Morphology of Human Lung. Am. Rev. Resirp. Dis. 128: S7-S13, 1983.

Bastacky, J., T. L. Hayes, B. VonSchmidt, S. B. Klein, J. Barr J, G. L. Finch, M. McKoon, L. Baskin, G. R. Hook. Correlative Microscopy of Native Surfaces of Human Lung: Color Macrophotography, SEM, LM, TEM, HVEM and Low-Temperature Scanning Electron Microscopy. 41st EMSA Proc., Bailey GW, ed., San Francisco Press, Inc., p 500-503, 1983a.

Bastacky, J. et al. Scanning Electron Microscopy Investigations of Frozen Hydrated Mouse Lungs. In Preparation, 1984.

Becci, P. J., E. M. McDowell, B. F. Trump. The Respiratory Epithelium. II. Hamster Trachea, Bronchus, and Bronchioles. J. Nat. Cancer Inst. 61: 551-561, 1978.

Bell, P. B. The Application of Scanning Electron Microscopy to the Study of the Cytoskeleton of Cells in Culture. Scanning Electron Microscopy/1981/II, p. 139-157, SEM Inc., AMF O'Hare, Chicago, IL, 1981.

Bell, S. W., S. K. Masters, P. Ingram, M. Waters and J. D. Shelburne. Ultrastructure and X-Ray Microanalysis of Macrophages Exposed to Cadmium Chloride. Scanning Electron Microscopy/1979/III, p. 111-121, AMF O'Hare, Chicago, IL, 1979.

Boyde, A. Pros and Cons of Critical Point Drying and Freeze Drying for SEM. Scanning Electron Microscopy Inc. 1978/II, AMF O'Hare, Chicago, p. 303-314, 1978.

Brain, J. D., D. E. Knudson, S. P. Sorokin and M. A. Davis. Pulmonary Distribution of Particles Given by Intratracheal Instillation or by Aerosol Inhalation. Environ. Res. 11: 13-33, 1976.

Brain, J. D. and P. A. Valberg. Deposition of Aerosol in the Respiratory Tract. Am. Rev. Respir. Dis. 120: 1325-1373, 1979.

Brody, A. R. and G. S. Davis. Alveolar Macrophage Toxicology. In: Mechanisms in Respiratory Toxicology, H. Witschi and P. Nettesheim, eds., CRC Press, Inc., Boca Raton, FL, p. 3-28, 1982.

Brody, A. R. and M. W. Roe. Deposition Pattern of Inorganic Particles at the Alveolar Level in the Lungs of Rats and Mice. Am. Rev. Respir. Dis. 128: 724-729, 1983.

Buckley, I. K. and K. R. Porter. Electron Microscopy of Critical Point Dried Whole Cultured Cells. J. Microsc. 104: 107-120, 1975.

Carr, K. E., T. L. Hayes, M. McKoon, M. Sprague and S. J. Bastacky. Low Temperature Scanning Electron Microscopic Studies of Mouse Small Intestine. J. Microsc. 132: 209-217, 1983.

Carvalho, S. M. M. and P. L. Ziemer. Distribution and Clearance of ^{63}Ni Administered as $^{63}NiCl_2$ in the Rat: Intratracheal Study. Arch. Environ. Contam. Toxicol. 11: 245-248, 1982.

Casarett, L. J. The Vital Sacs: Alveolar Clearance Mechanisms in Inhalation Toxicology. In Essays in Toxicology, Vol. 3, Academic Press, New York, p. 1-36, 1972.

Cember, H. Empirical Establishment of Cancer-Associated Dose to the Lung from ^{144}Ce. Health Phys. 10: 1177-1180, 1964.

Charles, J. M., S. J. Williams, and D. B. Menzel. Nickel Chloride: Kinetics of Removal from the Airway and Potential Accumulation in the Rat Lung. Toxicol. Appl. Pharmacol. 45: 302, 1978.

Christie, H., R. J. MacKay, and A. M. Fisher. Pulmonary Effects of Inhalation of Titanium Dioxide by Rats. J. Am. Ind. Hyg. Assoc. 24: 42-46, 1963.

Clamon, G. H., M. B, Sporn, J. M. Smith, and U. Saffiotti. Alpha- and beta-Retinyl acetate Reverse Metaplasias of Vitamin A Deficiency in Hamater Trachea in Organ Culture. Nature 250: 64-66, 1974.

Clary, J. J. Nickel Chloride-Induced Metabolic Changes in the Rat and Guinea Pig. Toxicol. Appl. Pharmacol. 31: 55-65, 1975.

Cline, M. J. The White Cell. Harvard Univ. Press, Cambridge, MA, p. 459, 1975.

Cohen, A. B. Potential Adverse Effects of Lung Macrophages and Neutrophils. Fed. Proc. 38: 2644-2647, 1979.

Collier, A. M. Injury of Respiratory Epithelium. Environ. Hlth. Perspect. 35: 83-87, 1980.

Costa, M., M. P. Abbracchio, and J. Simmons-Hansen. Factors Influencing the Phagocytosis, Neoplastic Transformation, and Cytotoxicity of Particulate Nickel Compounds in Tissue Culture Systems. Toxicol. Appl. Pharmacol. 60: 313-323, 1981.

Costa, M. and H. H. Mollenhauer. Phagocytosis of Nickel Subsulfide Particles during the Early Stages of Neoplastic Transformation in Tissue Culture. Cancer Res. 40: 2688-2694, 1980a.

Costa, M., and H. N. Mollenhauer. Carcinogenic Activity of Particulate Nickel Compounds is Proportional to Their Celluar Uptake. Science 209: 515-517, 1980.

Costa, M., Nye, J. S., F. W. Sunderman, Jr., P. R. Allpass, and B. Gondos. Induction of Sarcomas in Nude Mice by Implantation of Syrian Hamster Fetal Cells Exposed in vitro to Nickel Subsulfide. Cancer Res. 39: 3591-3597, 1979.

Costa, M., J. Simmons-Hansen, C. W. M. Bedrossian, J. Bonura, and R. M. Caprioli. Phagocytosis, Cellular Distribution, and Carcinogenic Activity of Particulate Nickel Compounds in Tissue Culture. Cancer Res. 41: 2868-2876, 1981b.

Dale, K. Early Effects of Quartz and Titanium Dioxide on Pulmonary Function and Tissue. Scand. J. Respir. Dis. 54: 168-184, 1973.

Damjanov, I., F. W. Sunderman, Jr., J. M. Mitchell and P. R. Allpass. Induction of Testicular Sarcomas in Fischer Rats by Intratesticular Injection of Nickel Subsulfide. Cancer Res. 38: 268-276, 1978.

DeVries, C. R., P. Ingram, S. R. Walker, R. W. Linton, W. F. Gutknecht, and J. D. Shelburne. Acute Toxicity of Lead Particulates on Pulmonary Alveolar Macrophages. Lab. Invest. 48: 35-44, 1983.

DiPaolo, J. A. and B. C. Casto. Quantitative Studies of In Vitro Morphological Transformation of Syrian Hamster Cells by Inorganic Metal Salts. Cancer Res. 39: 1008-1013, 1979.

Dodson, R. F., M. G. Williams, Jr., and G. A. Hurst. Acute Lung Response to Amosite Asbestos: A Morphological Study. Environ. Res. 32: 80-90, 1983.

Echlin, P. Low Temperature Scanning Electron Microscopy: A Review. J. Microsc. 112: 47-61, 1978.

Echlin, P., C. E. Lai and T. L. Hayes. Low-Temperature X-ray Microanalysis of the Differentiating Vascular Tissue on Root Tips of Lemna Minor L. J. Microsc. 126: 285-306, 1982.

Echlin, P., C. Lai, T. L. Hayes, A. Saubermann. Cryofixation of Lemna Minor Roots for Morphological and Analaytical Studies. Cryoletters 1: 289-292, 1980a.

Echlin, P., C. E. Lai, T. L. Hayes, G. Hook. Elemental Analysis of Frozen-Hydrated Differentiating Phloem Parenchyma in Roots of Lemna Minor L. Scanning Electron Microscopy Inc. 1980/II, AMF O'Hare, Chicago, p. 383-394, 1980b.

Echlin, P., J. B. Pawley and T. L. Hayes. Freeze-Fracture Scanning Electron Microscopy of Lemna Minor L. (Duckweed). Scanning Electron Microscopy Inc. 1979/III, AMF O'Hare, Chicago, p. 69-76, 1979.

Elder, H. Y., C. C. Gray, A. G. Jardine, J. N. Chapman, W. H. Biddlecombe. Optimum conditions for Cryoquenching of Small Tissue Blocks on Liquid Coolants. J. Microsc. 126: 45-61, 1982.

English, J. C., R. D. R. Parker, R. P. Sharma, and S. G. Oberg. Toxicokinetics of Nickel in Rats After Intratracheal Administration of a Soluble and Insoluble Form. J. Am. Ind. Hyg. Assoc. 42: 486-493, 1981.

Erickson, C. A. and J. P. Trinkaus. Microvilli and Blebs as Sources of Reserve Surface Membrane During Cell Spreading. Exp. Cell Res. 99: 375-384, 1976.

Evans, R. M., P. J. A. Davies, and M. Costa. Video Time-Lapse Microscopy of Phagocytosis and Intracellular Fate of Crystalline Nickel Sulfide Particles in Cultured Mammalian Cells. Cancer Res. 42: 2729-2735, 1982.

Ferin, J. Papain-Induced Emphysema and the Elimiation of TiO_2 Particulates from the Lung. J. Am. Ind. Hyg. Assoc. 32: 157-162, 1971.

Ferin, J. Emphysema in Rats and Clearance of Dust Particles. In Inhaled Particles III, W. H. Walton, ed., Vol. 1, p. 283-291, Greshmam Press, Old Woking, 1971b.

Ferin, J. Lung Clearance of Particles. in Air Pollution and the Lung, Proc. 20th Ann. OHOLO Ciological Conf., Israel, John Wiley and Sons, New York, p. 64-78, 1976.

Ferin, J. Pulmonary Alveolar Pores and Alveolar Macrophage-Mediated Particle Clearance. Anat. Record 203: 265-272, 1982.

Ferin, J. and M. L. Feldstein. Pulmonary Clearance and Hilar Lymph Node Content in Rats after Particle Exposure. Environ. Res. 16: 342-352, 1978.

Finch, G. L., T. L. Hayes, G. L. Fisher and K. L. McNeill. Scanning Electron Microscopic Investigations of Interactions Between Pulmonary Macrophages and Toxic Particles," in Biology and Medicine Division Annual Report, LBL-13501, p. 130-132, Lawrence Berkeley Laboratory, University of California, Berkeley, 1982.

Finch, G. L., G. L. Fisher, T L. Hayes, and D. W. Golde. Morphological Studies of Cultured Human Pulmonary Macrophages. In SEM Inc./1980/III, O. Johari, ed., AMF O'Hare, IL, p. 315-326, 1980.

Finch, G. L., G. L. Fisher, T. L. Hayes and D. W. Golde. Surface Morphology and Functional Studies of Human Alveolar Macrophages from Cigarette Smokers and Nonsmokers. J. Reticuloendothel. Soc. 32: 1-23, 1982.

Fisher, G. L., C. E. Chrisp, K. L. McNeill, D. A. McNeill, C. Democko, and G. L. Finch. Mechanistic Evaluation of the Pulmonary Toxicity of Nickel Subsulfide. In The Toxicology of Petroleum Hydrocarbons, H. N. MacFarland et al., eds., American Petroleum Institute, Washington, D.C., p. 87-96, 1982.

Fisher, G. L., K. L. McNeill, C. B. Whaley, and J. Fong. Attachment and Phagocytosis Studies with Murine Pulmonary Alveolar Macrophages. J. Reticuloendothel. Soc. 24: 243-252, 1978.

Frank, A. L. Asbestos-Induced Changes in Hamster Trachea Organ Culture, in The In Vitro Effects of Mineral Dusts, R. L. Brown et al., Academic Press, London, p. 235-240, 1980.

Fuchs, W., H. Fuchs. The Use of Frozen-Hydrated Bulk Specimens for X-ray Microanalysis. Scanning Electron Microscopy Inc. 1980/II, AMF O'Hare, Chicago, p. 371-382, 1080.

Gabridge, M. G., C. C. Agee, and A. M. Cameron. Differential Distribution of Ciliated Epithelial Cells in the Trachea of Hamsters: Implications for Studies of Pathogenesis. J. Infect. Dis. 135: 9-19, 1977.

Gabridge, M. G. Hamster Tracheal Organ Cultures as Models for Infection and Toxicology Studies. Prog. Exp. Tumor Res. 24: 85-95, 1979.

Garrett, N. E., J. A Campbell, H. F. Stack, M. D. Waters, and J. Lewtas. The Utilization of the Rabbit Alveolar Marcrophage and Chinese Hamster Ovary Cell for Evaluation of the Toxicity of Particulate Materials. 1. Model Compounds and Metal-Coated Fly Ash. Environ. Res. 24: 345-365, 1981.

Goldstein, B., I. Webster and H. S. Sichel. Evaluation of Experimental Methods in the Determination of the Fibrogenic Action of Dusts. Br. J. Exp. Pathol. 43: 38-43, 1962.

Goldstein, J. I., D. E. Newbury, P. Echlin, D. C. Joy, C. Fiori, E. Lifshin. Scanning Electron Microscopy and X-Ray Microanalysis, Plenum Press, New York, p. 586, 1981.

Gordon, R. E., and B. P. Lane Regeneration of Rat Tracheal Epithelium after Mechanical Injury. II. Restoration of Surface Integraty during the Early Hours of Injury. Am. Rev. Resp. Dis. 113: 799-807, 1976.

Grandjean, E., H. Turrian, and J. L. Nicod. The Fibrogenic Actions of Quartz Dusts. A. M. A. Arch. Ind. Hlth. 14: 426-441, 1956.

Green, G. M., G. J. Jakab, R. B. Low and G. S. Davis. Defense Mechanisms of the Respiratory Membrane. Am. Rev. Resp. Dis. 115: 479-514, 1977.

Greenwood, M. F., P. Holland. The Mammalian Respiratory Tract Surface: A Scanning Electron Microscopic Study. Lab. Invest. 27: 296-304, 1972.

Hansell, M. M. and R. L. Moretti; Ultrastructure of the Mouse Tracheal Epithelium. J. Morphol. 128: 159-170, 1969.

Hayes, T. L. Low Temperature Bulk SEM Technique in Biology. A Review. 2nd International Conference on Low Temperature Biological Microscoy and X-Ray Microanalysis. (Abstr.), RMS Proc. 16: Suppl., 1982.

Hayes, T. L., J. B. Pawley, G. L. Fisher and M. Goldman. A Model for the Exposure of Individual Lung Cells to the Foreign Elements Contained in Fly Ash. Environ. Res. 22: 499-509, 1980.

Henson, P. M. The Immunologic Release of Constituents from Neutrophil Leukocytes. J. Immunol. 107: 1535-1546, 1971.

Hill, J. O., R. H. Gray, P. B. DeNee, and G. J. Newton. Comparative Damage to Alveolar Macrophages after Phagocytosis of Respirable Particles. Environ. Res. 27: 95-109, 1982.

Ho, W. and A. Furst. Intratracheal Instillation Method for Mouse Lungs. Oncology 27: 385-393, 1973.

Ho, W. and A. Furst. Nickel Excretion by Rats Following a Single Treatment. Proc. West. Pharmacol. Soc. 16: 245-248, 1975.

Hocking, W. G. and D. W. Golde. The Pulmonary Alveolar Macrophage. N. Engl. J. Med., 304: 580 and 639 (2 parts), 1979.

Holma, B. Scanning Electron Microscopic Observations of Particles Deposited in the Lung. Arch. Environ. Health 18: 330-339, 1969.

Holt, P. F. Dust Elimination from Pulmonary Alveoli. Environ. Res. 23: 224-227, 1980.

Holt, P. F. Translocation of Inhaled Dust to the Pleura. Environ. Res. 31: 212-220, 1983.

Hook, G., C. Lai, J. Bastacky and T. Hayes. Conductive Coatings Studied on Inflated Lung in the Frozen-Hydrated and Freeze-Dried States. Scanning Electron Microscopy Inc 1980/IV, AMF O'Hare, Chicago, p. 27-32, 1980.

Hook, G., J. Bastacky, T. Hayes, R. Conhaion and N. Staub. Frozen-Hydrated Lung Preparation for Low Temperature Scanning Electron Microscopy, 40th Electron Microscope Society of America Proc, Bailey GW, Ed., Claitors Publishing, Baton Rouge, p. 372-373, 1982.

Hunninghake, G. W., J. E. Gadek, O. Kawanami, V. J. Ferrans, and R. G. Crystal. Inflammatory and Immune Processes in the Human Lung in Health and Disease: Evaluation by Bronchoalveolar Lavage. Am. J. Pathol. 97: 149-206, 1979.

Hunt, J., F. D. Pooley and R. J. Richards. Biological Reactivity of Calcium Silicate Composites—In Vitro Studies. Environ. Res. 26: 51-68, 1981.

Johansson, A., P. Camner, C. Jarstrand, and A. Wiernik. Rabbit Alveolar Macrophages after Inhalation of Soluble Cadmium, Cobalt, and Copper. A Comparison with the Effects of Soluble Nickel. Environ. Res. 31: 340-354, 1983.

Kang, K-Y., D. Bice, R. D'Amato, M. Ziskind, and J. Salvaggio. Effects of Asbestos and Beryllium on Release of Alveolar Macrophage Enzymes. Arch. Environ. Hlth. 34: 133-140, 1979.

Kasprzak, K. S. and F. W. Sunderman, Jr. Mechanisms of Dissolution of Nickel Subsulfide in Rat Serum. Res. Comm. Chem. Path. Pharmacol. 16: 95-108, 1977.

Kasprzak, K. S. and F. W. Sunderman, Jr. Radioactive ^{63}Ni in Biological Research. Pure Appl. Chem. 51: 1375-1389, 1979.

Kennedy, A. R. and J. B. Little. The Transport and Localization of Benzo(a)Pyrene-Hematite and Hematite-^{210}Po in the Hamster Lung following Intratracheal Instillaton. Canc. Res. 34: 1344-1352, 1974.

Kennedy, J. R. and P. L. Allen. Effects of Cigarette Smoke Residue on Rabbit Tracheal Epithelium in Organ Culture. Arch. Environ. Hlth. 34: 5-11, 1979.

Kessel, R. G., R. H. Kardon. Tissues and Organs: A Text-Atlas of Scanning Electron Microscopy. WH Freeman CO, San Francisco p. 203-217, 1979.

Kuehn, K., C. B. Fraser, and F. W. Sunderman, Jr. Phagocytosis of Particulate Nickel Compounds by Rat Peritoneal Macrophages In Vitro. Carcinogenesis 3: 321-326, 1982.

Kuhn, C. Lung, in Principles and Techniques of Structure, Vol 2, Hyatt MA, ed., Van Nostrand, New York, 111-122, 1974.

Kumon, H., Y. Nasu, Y. Matsumura, H. Ohmori, and T. Tanaka. A Combined Light and Scanning Electron Microscopy on Human Urinary Cytology. J. Electron Microsc. 32: 27-37, 1983.

LaBelle, C. W. and H. Brieger. Patterns and Mechanisms in the Elimination of Dust from the Lung. In Inhaled Particles and Vapours, Vol. 1; C. N. Davies, ed., Pergamon Press, p. 356-368, 1961.

Lane, B. P., S. L. Miller, E. J. Drummond. Use of Tracheal Organ Cultures in Toxicity Testing. Environ. Hlth. Perspect. 16: 89-98, 1976.

Lauweryns, J. M. and J. H. Baert. Alveolar Clearance and the Role of the Pulmonary Lymphatics. Am. Rev. Respir. Dis. 115: 625-683, 1977.

Lee, J. E., R. B. Ciccarelli and K. W. Jennette. Solubilization of the Carcinogen Nickel Subsulfide and its Interaction with Deoxyribonucleic Acid and Protein. Biochemistry 21: 771-778, 1982.

Lewis, J. C., T. Prater, R. G. Taylor and M. S. White. The Use of Correlative SEM and TEM to Study Thrombocyte and Platelet Adhesion to Artificial Surfaces. Scanning Electron Microscopy/1980/III, p. 189-202, SEM Inc., AMF O'Hare, Chicago, IL, 1980.

Lippmann, M., D. B. Yeates and R. E. Albert. Deposition, Retention, and Clearance of Inhaled Particles. Br. J. Ind. Med 37: 337-362, 1980.

Manabe, T. Freeze-Fracture Study of Alveolar Lining Layer in Adult Rat Lung. J. Ultrastruct. Res. 69: 86-97, 1979.

Mazur, P. Cryobiology: The Freezing of Biological Systems. Science 168: 939-949, 1971.

McDowell, E. M., L. A. Barrett, F. Glavin, C. C. Harris and B. F. Trump. The Respiratory Epithelium. I. Human Bronchus. J. Nat. Cancer Inst. 61: 539-549, 1978.

McDowell, E. M., P. J. Becci, W. Schurch and B. F. Trump. The Respiratory Epithelium. VII. Epidermoid Metaplasia of Hamster Tracheal Epithelium During Regeneration Following Mechanical Injury. J. Nat. Cancer Inst. 62: 995-1008, 1979.

McDowell, E. M., J. W. Combs, and C. Newkirk. A Quantitative Light and Electron Microscopic Study of Hamster Tracheal Epithelium with Special Attention to So-Called Intermeidate Cells. Exp. Lung Res. 4: 205-226, 1983.

McDowell, E. M., F. G. Hess, Jr., and B. F. Trump. Epidermoid Metaplasia, Carcinoma in situ, and Carcinomas of the Lung. In Diagnostic Electron Microscopy, B. F. Trump and R. J. Jones, eds., John Wiley and Sons Publishing, New York, pp. 37-96, 1980.

Miller, K. Alterations in the Surface-Related Phenomena of Alveolar Macrophages following Inhalation of Crocidilite Asbestos and Quartz Dusts: An Overview. Environ. Res. 20: 162-182, 1979.

Miller, K., R. I. M. Handfield, and E. Kagan. The Effect of Different Mineral Dusts on the Mechanism of Phagocytosis: A Scanning Electron Microscope Study. Environ. Res. 15: 139-154, 1978.

Miller, K. and E. Kagan. The In Vivo Effects of Asbestos on Macrophage Membrane Structure and Population Characteristics of Macrophages: A Scanning Electron Microscopic Study. J. Reticuloendothel. Soc. 20: 159-171, 1976.

Miller, K. and E. Kagan. The In Vivo Effect of Quartz and Alveolar Macrophage Membrane Topography and on the Characteristics of the Intrapulmonary Cell Population. J. Reticuloendothel. Soc. 21: 307-316, 1977.

Moores, S. R., S. E. Sykes, A. Morgan, N. Evans, J. C. Evans, and A. Holmes. The Short-Term Cellular and Biochemical Response of the Lung to Toxic Dusts: An In Vivo Cytotoxic Test. In The In Vitro Effects of Mineral Dusts, R. C. Brown et al., eds., Academic Press, London, p. 297-303, 1980.

Mossman, B. T., K. B. Adler, and J. E. Craighead. Interaction of Carbon Particles with Tracheal Epithelium in Organ Culture. Environ. Res. 16: 110-122, 1978.

Mossman, B. T., K. B. Adler, and J. E. Craighead. Cytotoxic and Proliferative Changes in Trachel Organ and Cell Cultures After Exposure to Mineral Dusts, in The In Vitro Effects of Mineral Dusts, R. C. Brown et al., eds., Academic Press, London, p. 241-250, 1980.

Mossman, B. T. and J. E. Craighead. Use of Hamster Tracheal Organ Cultures for Assessing the Cocarcinogenic Effects of Inorganic Particulates of the Respiratory Epithelium. Prog. Exp. Tumor Res. 24: 36-47, 1979.

Mossman, B. T., and J. E. Craighead. Mechanisms of Asbestos Carcinogenesis. Environ. Res. 25: 269-280, 1981.

Mossman, B. T., J. B. Kessler, B. W. Ley, and J. E. Craighead. Interaction of Crocidolite Asbestos with Hamster Respiratory Mucosa in Organ Culture. Lab. Invest. 36: 131-139, 1977.

Mossman, B., W. Light, and E. Wei. Asbestos: Mechanisms of Toxicity and Carcinogenicity in the Respiratory Tract. Ann. Rev. Pharmacol. Toxicol. 23: 595-615, 1983.

Myrvik, Q. N., E. S. Leake and B. Fariss. Studies on Pulmonary Alveolar Macrophages from the Normal Rabbit: A Technique to Procure them in a High Stage of Purity. J. Immunol. 86: 128, 1961.

Nei, T. Structure and Function of Frozen Cells: Freezing Patterns and Post-Thaw Survival. J. Microsc. 112: 197-204, 1978.

Oskarsson, A., Y. Anderson and H. Tjalve. Fate of Nickel Subsulfide during Carcinogenesis Studies by Autoradiography and X-Ray Powder Diffraction. Cancer Res. 39: 4175-4182, 1979.

Ottolenghi, A. D., J. K. Haseman, W. W. Payne, H. L. Falk and H. N. MacFarland. Inhalation Studies of Nickel Sulfide in Pulmonary Carcinogenesis of Rats. J. Nat. Canc. Inst. 54: 1165-1172, 1974.

Pawley, J. B., T. L. Hayes. A Freeze Fracture Preparation Chamber Attached to the SEM. 35th Electron Microscope Society of America Proc., Claitor's Publishing, Baton Rouge, p. 588-589, 1977.

Pawley, J. B., G. Hook, T. L. Hayes and C. Lai. Direct Scanning Electron Microscopy of Frozen-Hydrated Yeast. Scanning 3: 219-226, 1980.

Pawley, J. B., J. T. Norton. A Chamber Attached to the SEM for Fracturing and Coating Frozen Biological Samples. J. Microsc. 112: 169-182, 1978.

Plattner, H. and L. Bachmann. Cryofixation: A Tool in Biological Ultrastructural Research. Int. Rev. Cytol. 79: 237-304, 1982.

Plopper, C. G., D. M. Hyde and A. J. Weir. Centriacinar Alterations in Lungs of Cats Chronically Exposed to Diesel Exhaust. Lab. Invest. 49: 391-399, 1983.

Porter, K. R. and M. E. Stearns. Stereomicroscopy of Whole Cells. Methods Cell Biol. 22: 51-75, 1981.

Pudney, J. and R. H. Singer. Electron Microscopic Visualization of the Filamentous Reticulum in Whole Cultured Presumptive Chick Myoblasts. Am. J. Anat. 156: 321-336, 1979.

Reed, S. E., and A. Boyde. Organ Cultures of Respiratory Epithelium Infected with Rhinovirus or Parainfluenza Virus Studied in a Scanning Electron Microscope. Infect. Immun. 6: 68-76, 1972.

Remington, R. D. and M. A. Schork. Statistics with Applications to the Biological and Health Sciences. Prentice-Hall, Inc., Englewood Cliffs, N.J, 1970.

Rylander, R., M. Sjostrand, and R. Bergstrom. Free Lung Cell Response after Combined Exposure to Cigarette Smoke and Industrial Dusts. Toxicology 12: 211-220, 1979.

Saxholm, H. J. K., A. Reith and A. Brogger. Oncogenic Transformation and Cell Lysis in C3H/10$T_{1/2}$ Cells and Increased Sister Chromatid Exchange in Human Lymphocytes by Nickel Subsulfide. Cancer Res. 41: 4136-4139, 1981.

Schiff, L. J., M. M. Byrne, S. F. Elliott, S. J. Moore, K. V. Ketels, and J. A. Graham. Response of Hamster Trachea in Organ Culture to Mount St. Helens Volcano Ash. Scanning Electron Microscopy/1981/II, SEM Inc., AMF O'Hare, IL, 1981b.

Schiff, L. J., M. M. Byrne, J. D. Fenters, J. A. Graham, and D. E. Gardner. Cytotoxic Effects of Sulfuric Acid Mist, Carbon Particulates, and Their Mixtures on Hamster Tracheal Epithelium. Environ. Res. 19: 330-354, 1979.

Schiff, L. J., M. M. Byrne, and J. A. Graham. Fly-Ash Induced Changes in Hamster Tracheal Epithelium In Vivo and In Vitro. J. Toxicol. Environ. Hlth. 8: 431-448, 1981.

Schiff, L. J., M. M. Byrne, K. V. Ketels, W. T. Brown and J. A. Graham. A Scanning Electron Microscope Study of Developing Hamster Tracheal Epithelium in Organ Culture. Differentiation 15: 49-55, 1979b.

Schlesinger, R. B. Defense Mechanisms of the Respiratory System. Bioscience 32: 45-50, 1982.

Schlesinger, R. B., M. Lippmann. Selective Particle Deposition and Bronchogenic Carcinoma. Environ. Res. 15: 424-431, 1978.

Smith, J. C. and B. Hackley. Distribution and Excretion of Nickel-63 Administered Intravenously to Rats. J. Nutr. 95: 541-546, 1968.

Snipes, M. B. and M. F. Clem. Retention of Microspheres in the Rat Lung after Intratracheal Instillation. Environ. Res. 24: 33-41, 1981.

Soestbergen, M V. and F. W. Sunderman, Jr. ^{63}Ni Complexes in Rabbit Serum and Urine after Injection of $^{63}NiCl_2$. Clin. Chem. 18: 1478-1484, 1972.

Sorokin, S. P. and J. D. Brain. Pathways of Clearance in Mouse Lungs Exposed to Iron Oxide Aerosols. Anat. Rec. 181: 581-626, 1975.

Stenback, F., J. Rowland, and A. Sellakumar. Carcinogenicity of Benzo(a)Pyrene and Dusts in the Hamster Lung. Oncology 33: 29-34, 1976.

Stirling, C. and G. Patrick. The Localization of Particles Retained in the Trachea of the Rat. J. Pathol. 131: 309-320, 1980.

Stossel, T. P. Phagocytosis: Recognition and Ingestion. Semin. Hematol. 12: 83-116, 1975.

Stossel, T. P. The Mechanisms of Phagocytosis. J. Reticuloendothel. Soc. 19: 237-245, 1976.

Stuart, B. O. Deposition of Inhaled Aerosols. Arch. Intern. Med. 131: 60, 1973.

Sunderman, F. W., Jr. The Current Status of Nickel Carcinogenesis. Ann. Clin. Lab. Sci. 3: 156-180, 1973.

Sunderman, F. W., Jr. Metal Carcinogenesis. In Advances in Modern Toxicology, Vol. 2, R. A. Goyer and M. A. Mehlam, eds., Hemisphere Pub. Co., Washington, D. C., p. 257-295, 1977.

Sunderman, F. W., Jr. Recent Research on Nickel Carcinogenesis. Environ. Hlth. Perspect. 40: 131-141, 1981.

Sunderman, F. W., Jr., K. S. Kasprzak, T. J. Lau, P. P. Minghetti, R. M. Maenza, N. Becker, C. Onkelinx, and P. J. Goldblatt. Effects of Manganese on Carcinogenicity and Metabolism of Nickel Subsulfide. Cancer Res. 36: 1790-1800, 1976.

Sunderman, F. W., Jr., R. M. Maenza, S. M. Hopfer, J. M. Mitchell, P. R. Allpass, and I. Damjanov. Induction of Renal Cancers in Rats by Intrarenal Injection of Nickel Subsulfide. J. Environ. Pathol. Toxicol. 2: 1511-1527, 1979.

Sykes, S. E., A. Morgan, J. C. Evans, N. Evans, A. Holmes, and S. R. Moores. Use of an In Vivo Test System to Investigate the Acute and Sub-acute Responses of the Rat Lung to Mineral Dusts. Ann. Occup. Hyg. 26: 593-605, 1982.

Task Force on Lung Dynamics. Deposition and Retention Models for Internal Dosimetry of the Human Respiratory Tract. Health Phys. 12: 173-207, 1966.

Thoren, S. A. and B. Holma. Identification of Viable and Nonviable Cells in Scanning Electron Microscopy. J. Toxicol. and Environ. Hlth. 12: 21-25, 1983.

Untersee, P., J. Gil, E. R. Weibel. Visualization of extracellular lining layer of lung alveoli by freeze-etching. J. Appl. Physiol. 13: 171-185, 1971.

Valentine, R., M. J. W. Chang, R. W. Hart, G. L. Finch, and G. L. Fisher. Thermal Modification of Chrysotile Asbestos: Evidence for Decreased Cytotoxity. Environ. Hlth. Perspect. 51: 357-368, 1983.

Waters, M. D., D. E. Gardner, C. Aranyi, and D. L. Coffin. Metal Toxicity for Rabbit Alveolar Macrophages In Vitro. Environ. Res. 9: 32-47, 1975.

Watson, J. A., J. A. Auld and A. S. Spritzer. Upper Respiratory Tract Clearance in Rats after Thoracic Irradiation. Radiation Res. 37: 57-70, 1969b.

Watson, J. A., A. A. Spritzer, J. A. Auld and M. A. Guetthoff. Deposition and Clearance Following Inhalation and Intratracheal Injection of Particles. Arch. Environ. Hlth. 19: 51-58, 1969.

Weibel, E. R., W. Limacher, H. Bachofen. Electron Microscopy of Rapidly Frozen Lungs: Evaluation on the Basis of Standard Criteria. J. Appl. Physiol: 53: 516-527, 1982.

Weiss, L. and R. O. Greep. Histology. McGraw-Hill Co., New York, NY, p. 778-783, 1977.

Wolosewick, J. J. and K. R. Porter. Observations on the Morphological Heterogeneity of WI-38 Cells. Am. J. Anat. 149: 197-226, 1976.

Wolosewick, J. J., and K. R. Porter. Microtrabecular Lattice of the Cytoplasmic Ground Substance. J. Cell Biol. 82: 114-139, 1979.

Woodworth, C. D., B. T. Mossman, and J. E. Craighead. Squamous Metaplasia of the Respiratory Tract. Lab. Invest. 48: 578-584, 1983.

World Health Organization, International Agency for Research on Cancer. IARC Monographs of the Evaluation of Carcinogenic Risk of Chemicals to Man: Some Inorganic and Organometallic Compounds, Vol. 2, Lyon, 1973.

World Health Organization. Titanium. Environmental Health Criteria 24, Geneva, 1982.

Wozniak, A., E. Wiecek, Goscicki, J. Wojtezak, S. Szendzikowski, A. Rozycki and G. Bielichowska. (Experimental Silicosis. Pneumoconiotic Properties of Silica Dust in the Mixture with Titanium Dioxide). Polish. Med. Prac. 27: 201-214, 1976.

Yarita, T. and P. Nettesheim. Carcinogenicity of Nickel Subsulfide for Respiratory Tract Mucosa. Cancer Res. 38: 3140-3145, 1978.

Yeh, H. C., R. F. Phalen and O. G. Raabe. Factors Influencing the Deposition of Inhaled Particles. Environ. Hlth. Perspect. 15: 147-156, 1966.

Zitting, A., E. Skytta, Biological Activity of Titanium Dioxides. Int. Arch. Occup. Environ. Hlth. 43: 93-97, 1979.

VIII. APPENDIX. A TECHNIQUE PERMITTING CORRELATIVE MICROSCOPY (LM, SEM, TEM, AND HVEM) OF CULTURED ALVEOLAR MACROPHAGE CELLS

INTRODUCTION

Increased understanding of biological structure results from the use of correlative microscopic techniques. Our group is interested in characterizing interactions between particles and alveolar macrophage cells (AM) which are important in pulmonary defense. In this letter, we report an integrated system permitting cell culturing, particle exposure, characterization of AM viability using light microscopy (LM), and subsequent scanning, transmission, and high voltage electron microscopy (SEM, TEM, and HVEM).

MATERIALS AND METHODS

Alveolar macrophages are obtained by lavage from intact bovine lung lobes (for techniques see Fisher et al., 1982) and are cultured on formvar-coated finder grids. A film of 0.7 to 1.0 percent formvar in ethylene dichloride (Ted Pella, Tustin, CA), is floated onto water then acetone-cleaned 135 mesh Cu finder grids (HF15, Ernest Fullam, Schnectady, NY) are placed upside-down to the film. Grids plus film are picked up with cleaned microverslips (35 x 10-1/2 mm, Bellco Glass, Vineland, NJ) to form a sandwich of coverslip, grids, then formvar. Coverslips are rinsed in ethanol, dried under uv light, then placed inside sterile Leighton tubes (Bellco). Cells are seeded into the tubes, allowed to attach for one hour, then exposed to test substances (Ni_3S_2, TiO_2, glass beads, and unexposed controls) at 37°C for varying periods. After exposure cultures are inverted into

room temperature 0.4 percent trypan blue dye in phosphate buffered saline (PBS; both Grand Island Biolocial Co., Grand Island, NY) in a concave micro-culture slide (Arthur Thomas, Philadelphia, PA). Grids are located and photographed (Polaroid Type 108 film, Carbridge, MA) at approximately 130 X in a Nikon LM with attached photographic head (Nikon, New York, NY; see Fig. VIII.1A). The dye stains dead cell nuclei which are identified on the photograph with a pinprick. Cultures are left in the stain for at most 10 minutes, rinsed in PBS, then plunged into room temperature fixative consisting of 2.3 percent glutaradehyde in 0.05M cacodylate buffer (both Electron Microscopic Services, Fort Washington, PA) at pH = 7.4 and 360 (±10) milliosmoles. Converslips are fixed at least overnight then placed in a mesh basket, rinsed twice in fresh buffer (0.05M cacodylate with sucrose, 360 mOsm), postfixed three minutes in 1 percent OsO_4 (Ted Pella) in 0.05M cacodylate, dehydrated through a graded ethanol series (25, 50, 75, 90, 95 (2X), and 100 (3X) percent ethanol in distilled, deionized water), transferred to a critical point dryer (Polaron, Wateford, England), then rinsed and dried through CO_2. After drying grids are removed from the coverslips then carbon coated by evaporation (Denton DV-502, Cherry Hill, NJ) with sample rotation. Grids are viewed at 10 to 30 KeV in a SEM (AMRay 1000A, Bedford, MA) with attached energy-dispersive x-ray spectrometer (Kevex 5100C, Foster City, CA). A low magnification SEM micrograph (Fig. VIII.1B) allows previously identified AM to be located then examined at higher magnification (Fig. VIII.1C) for cell morphology and particle content as revealed by

x-ray microanalysis and/or mapping. Selected cells are then examined by convetional TEM (Zeiss EM-10A, New York, NY) at 80 to 100 KeV and by HVEM (Kratos EM1500, England) at 1.2 to 1.5 MeV (Fig. VIII.1D). Stereopair micrographs are employed to interpret cellular structure.

DISCUSSION

Techniques described here permit the examination of interactions between particles and individual AM cells using vital staining LM, SEM, TEM, and HVEM. The morphological characteristics of AM populations appear independent of glass versus formvar attachment, and no differences are evident between trypan exposed versus unexposed cultures. We have successfully observed cultures using these techniques and have correlated cell morphology, viability, and particle content (Finch et al., in preparation).

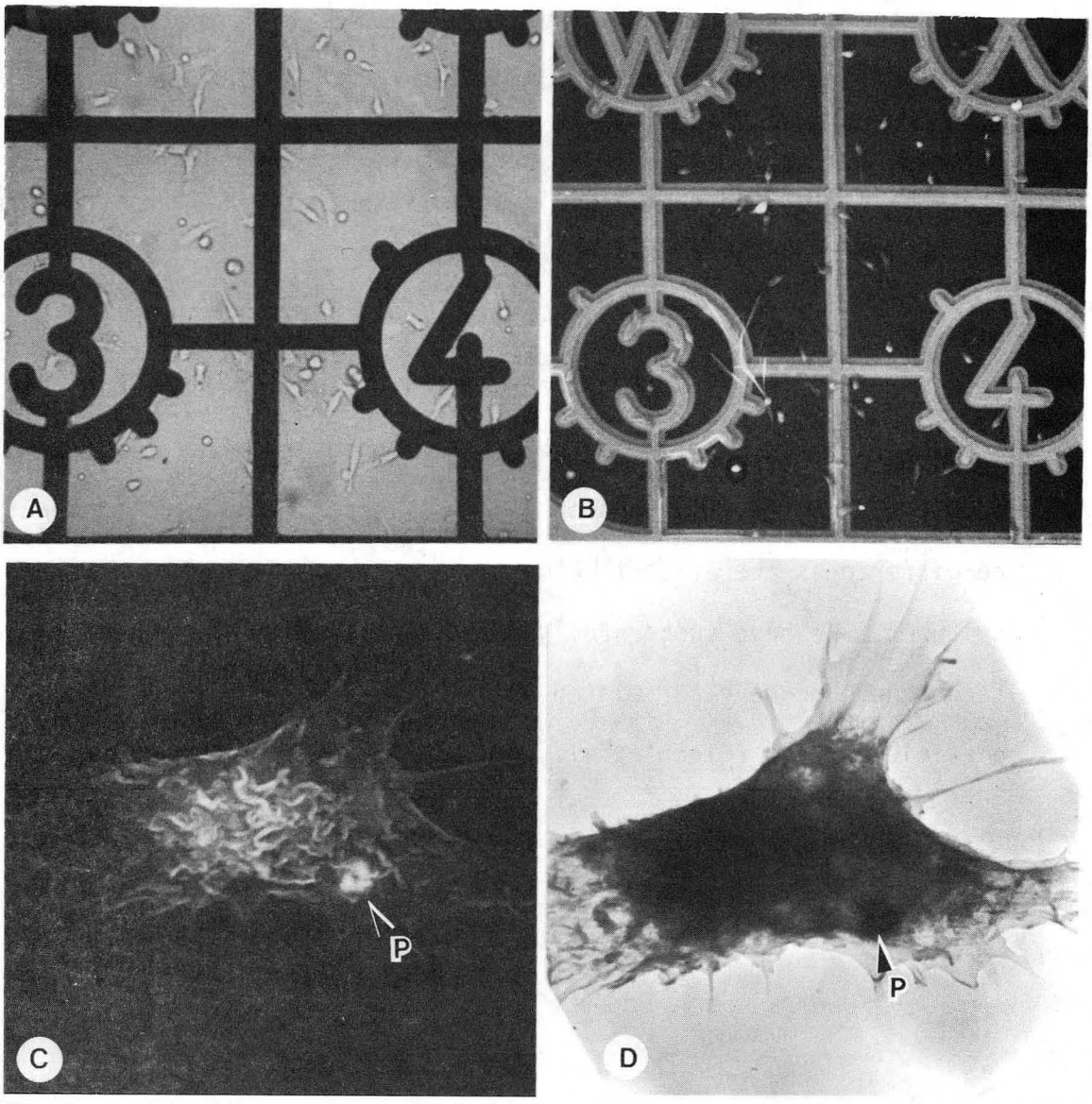

Figure VIII.1 Correlative microscopic images of AM exposed to Ni_3S_2 particles. A. LM of formvar-attached cells under trypan blue stain; magnification = 130X. B. Same area as seen by SEM; circle encloses a cell live at fixation, shown below; magnification = 120X. C. Individual AM by SEM with particles evident (arrow); magnification = 4,000X. D. HVEM of above cell; arrow identifies particles; N = Nucleus; magnification = 4,000X XBB 8411-8666

This report was done with support from the Department of Energy. Any conclusions or opinions expressed in this report represent solely those of the author(s) and not necessarily those of The Regents of the University of California, the Lawrence Berkeley Laboratory or the Department of Energy.

Reference to a company or product name does not imply approval or recommendation of the product by the University of California or the U.S. Department of Energy to the exclusion of others that may be suitable.

TECHNICAL INFORMATION DEPARTMENT
LAWRENCE BERKELEY LABORATORY
UNIVERSITY OF CALIFORNIA
BERKELEY, CALIFORNIA 94720